DESIGN AND ANALYSIS OF DUAL-LINEARLY POLARIZED DIELECTRIC RESONATOR ANTENNA ARRAY

A Thesis submitted with partial fulfillment of Requirements for the degree of

Master of Technology

(By Research)

in

Electronics and Communication Engineering

by

Ayaskanta Panigrahi

Roll No: 613EC6001

Under the guidance of

Dr. Santanu Kumar Behera

Department of Electronics and Communication Engineering

National Institute of Technology Rourkela

Rourkela-769008, Odisha, India

September 2015

DESIGN AND ANALYSIS OF DUAL-LINEARLY POLARIZED DIELECTRIC RESONATOR ANTENNA ARRAY

A Thesis submitted with partial fulfillment of Requirements for the degree of

Master of Technology

(By Research)

in

Electronics and Communication Engineering

by

Ayaskanta Panigrahi

Roll No: 613EC6001

Under the guidance of

Dr. Santanu Kumar Behera

Department of Electronics and Communication Engineering

National Institute of Technology Rourkela

Rourkela-769008, Odisha, India

September 2015

Dedicated to my Parents without whom none of my success would be possible…

DEPARTMENT OF ELECTRONICS AND COMMUNICATION ENGINEERING

NATIONAL INSTITUTE OF TECHNOLOGY ROURKELA-769008, ODISHA, INDIA

CERTIFICATE

This is to certify that the work in this thesis titled "**DESIGN AND ANALYSIS OF DUAL-LINEARLY POLARIZED DIELECTRIC RESONATOR ANTENNA ARRAY"** by Mr. **AYASKANTA PANIGRAHI** is a record of an original research work carried out by him during 2015-2016 under my supervision and guidance in partial fulfilment of the requirement for the award of the degree of Master of Technology by research in Electronics and Communication Engineering, National Institute of Technology Rourkela. Neither this thesis nor any part of it, to the best of my knowledge, has been submitted for any degree or diploma elsewhere.

Place: NIT Rourkela

Date:

Dr. Santanu Kumar Behera

Associate Professor

DEPARTMENT OF ELECTRONICS AND COMMUNICATION ENGINEERING

NATIONAL INSTITUTE OF TECHNOLOGY ROURKELA-769008, ODISHA, INDIA

Declaration

I certify that

a) The work comprised in the thesis is original and is done by myself under the supervision of my supervisor.

b) The work has not been submitted to any other institute for any degree or diploma.

c) I have followed the guidelines provided by the Institute in writing the thesis.

d) Whenever I have used materials (data, theoretical analysis, and text) from other sources, I have given due credit to them in the text of the thesis and giving their details in the references.

e) Whenever I have quoted written materials from other sources, I have put them under quotation marks and given due credit to the sources by citing them and giving required details in the references.

(Ayaskanta Panigrahi)

Roll No. 613EC6001

Acknowledgements

My intellectual debts are many and could not possibly be covered in the amount of space available here. I apologize for my oversight if I have missed some people who are deserving of public acknowledgement.

First and foremost, my greatest debts are to my ever encouraging, patient and supportive supervisor, mentor as well as moral supporter Prof. S. K. Behera whose warmth, understanding and support I have been continually grateful for. Prof. Behera pushed, prodded and poked my brain on numerous occasions, and generally kept my intellectual stamina going. I have benefitted from his insightful comments and suggestions throughout this study, and I am deeply indebted to him for so readily and generously giving of his precious time and energy out of his busy schedule, for which I sincerely thank him. His guidance, patience and spiritual support have directed me throughout my postgraduate life. Without his encouragement, I would have embarked on a topic much less meaningful.

I am grateful to Prof. S. K. Sarangi, Director, NIT Rourkela for providing me adequate infrastructure to carry out the present investigations. I would like to express my heartfelt thankfulness to my MSC members Prof. S. Meher, Prof. S. K. Patra, Prof. Deepti Patra and Prof. P. K. Sahu who have been giving me general encouragement and warm support in my electronic endeavours. I have benefitted greatly from their suggestions.

I might want to reveal a profound feeling of appreciation to admirable Prof. K. K. Mahapatra, Head of the Department of Electronics and Communication Engineering for furnishing us with best facilities and his auspicious recommendations. I need to thank all

other faculties of Department of Electronics and Communication Engineering for their consistent backing and consolation amid my examination.

I would like to send my deepest gratitude to Shri Rajeev Jyoti, Head, Satellite Communication Antenna Division, SAC, ISRO, Ahmedabad for his support during my JRF Position in the respond project.

I would also like to express my sincere thanks to Mr. B. Pandey, Senior scientist of SAC, ISRO, Ahmedabad for his sophisticated insights and reference sources on my chosen theme. Despite the fact the designs included in this dissertation are reflections of my work and desperate experiments, several individuals have had a remarkable effect on the results. In particular, Ph.D. researcher Biswajit Dwivedy deserve special gratitude for giving his time, expertise and experience as well as his invaluable specialist perceptions on various issues of this work. Many thanks should be given to Ph.D. Research scholar Debakanta Behera for providing perceptions for analysis in my study and morally supporting me.

I am grateful to a number of colleagues who have given their friendship and collaboration over the years. Thanks should go to them for making the darker times of my study more bearable and celebrating good times with me. This list includes but is not limited to Dr. Yogesh K Choukiker, Dr. Natarajamani S and Dr. Runa Kumari.

Finally and most importantly, I extend my deepest sense of gratitude to my family for their resolute love and backing for the duration of my life. I wish to pay the highest tribute to my parents and sisters for their endless love and all the hardship that they went through to support me in every way.

(Ayasknata Panigrahi)

Abstract

Dielectric resonators have been widely used as narrowband shielded circuit components. The dielectric resonator antenna is an implementation of using an unshielded dielectric structure in order to extract the radiation of electric fields. Dielectric materials can have low dielectric loss and the absence of metallic surfaces also reduces conduction losses. A dielectric resonator antenna can have efficiencies above 95% for several hundred megahertz. The versatility in choice of shape, relative permittivity and size enables a whole spectrum of operating frequency ranges (1GHz-40GHz), sizes, radiation patterns and bandwidths. The far field radiation pattern is a characteristic of the resonating modes. In this project the investigation of dielectric resonator antennas was quantitatively realized by the design and evaluation of one omni-directional wideband dielectric resonator antenna with operating frequency range 3.9GHz to 6.2GHz and two dual linearly polarized broadside antenna arrays in L, S and C band applications. Transverse modes with rotational symmetry are preferred for an omni-directional radiation pattern, whereas a hybrid mode is suitable for a broadside radiation pattern. The modes can be excited by feeding from microstrip lines and coaxial probes. The location of the excitation determines what mode is excited.

The resonant frequency is controlled by size, shape and permittivity of the DR element. Dual polarization is achieved by exciting two orthogonal modes simultaneously in the resonator. The cross coupling between the feeding networks and the matching of these becomes a crucial step in the design of a dielectric resonator antenna. The broadside antenna elements have been arranged in a linear as well as planar array to increase the directivity.

Contents

List of Figures

List of Tables

List of Abbreviations

AR	Axial Ratio
AUT	Antenna Under Test
BW	Bandwidth
CAD	Computer Aided Design
CDR	Cylindrical Dielectric Resonator antenna
CPW	Coplanar Waveguide
CP	Circular Polarization
CST	Computer Simulation Technology
DCS	Defense Communication System
DOF	Degree Of Freedom
DR	Dielectric Resonator
DRA	Dielectric Resonator Antenna
DTV	Direct Television
dB	Decibel
dBi	Decibel isotropic
EBG	Electromagnetic Band-Gap
EIRP	Effective Isotropic Radiated Power
EM	Electromagnetic
EHF	Extremely High Frequency
F/B	ratio Front to Back ratio
FCC	Federal Communication Commission
FDTD	Finite Differentiation Time Domain
FEM	Finite Element Method
FIT	Finite Integration Technique
GaAs	Gallium Arsenide
GPS	Global Position System
GPRS	General Packet Radio Services
GSM	Global System for Mobile Communication
IE	Integral Equations

LHCP	Left Hand Circular Polarization
LPDRA	Log Periodic Dielectric Resonator Antenna
MIC	Microwave Integrated Circuit
MIMO	Multiple Input Multiple Output
MMIC	Millimeter-wave Monolithic Integrated Circuit
MPA	Microstrip Patch Antenna
PCB	Printed Circuit Board
PCS	Personal Communication System
PDA	Personal Digital Assistant
RADAR	RAdio Detection And Ranging
RF	Radio Frequency
RHCP	Right Hand Circular Polarization
RL	Return Loss
RSGB	Radio Society of Great Britain
SAP	Shorted Annular Patch
SLL	Side Lobe Level
T/R	Transmitter and Receiver
TSDR	Two-Segments Dielectric Resonator antenna
UHF	Ultra High Frequency
UMTS	Universal Mobile Telecommunication System
UWB	Ultra Wide Band
VSWR	Voltage Standing Wave Ratio
WLAN	Wireless Local Area Network

List of Symbols

ε_s	Dielectric constant of substrate
ε_r	Dielectric constant of resonator
ρ_e	Envelope correlation coefficient
λ	Wavelength
λ_0	Free-space Wavelength
λ_g	Guided Wavelength
$\tan\delta$	Loss tangent
γ	Propagation Constant
α	Attenuation Constant
β	Phase Constant
k	Free space wave number
k_c	Cut-off wave number
ψ_r	Envelope correction coefficient
$\vec{E}$	Electric field intensity
$\vec{H}$	Magnetic field intensity
$\vec{D}$	Electric flux density
$\vec{B}$	Magnetic flux density
f_c	Centre frequency
G_t	Gain of the transmitting antenna
G_r	Gain of the receiving antenna
P_t	Transmitted power
P_r	Received power

Chapter 1
INTRODUCTION

In the heterogeneous world of communications and radar systems, significant advances in antenna technology have been brought by the phenomenal growth in the wireless industry. This development has put more demand for compact size and low energy consumption for the equipment. Base stations powered by solar cells are a reality, considering low energy consumption. Low loss in the antenna is also crucial for the operation of such a network. High energy efficiency is a key for obtaining higher signal strengths and increasing the capacity of existing networks [1].

Satellite communication systems provide flexibility as well as high speed data transfer at high frequencies. With the increasing demand to support satellite communication system for simultaneous transmission and reception of high quality data, both wideband and dual band antennas are in boom. In all communication systems, antenna is the most vital component. Recently dual-band and dual polarized antenna arrays have been widely studied for satellite and wireless communication applications, particularly for synthetic aperture radar (SAR) applications. Today's patch antennas have many advantages with drawbacks such as conduction losses due to the skin effect, narrow operating frequency bandwidth, low gain etc.

In the last two decades, much research has been performed on the dielectric resonator antenna (DRA) which also regained a wider interest in recent years. Its small volume and low profile, together with its lack of metallic surfaces make it interesting for low conduction losses. The dielectric resonator is widely used in microwave circuits for filters and oscillators, where as its resonant modes are confined and narrowband.

1.1 Wideband Dielectric Resonator Antennas

Many applications such as direct digital broadcast, video conferencing, satellite communications, wireless and radar applications require wide bandwidth. In a DRA, wideband is achieved for low values of a dielectric constant as the bandwidth of the DRA is inversely proportional to the dielectric constant [2-3]. Various enhancement techniques have been proposed to broaden the bandwidth of the DRA such as notched DRA, multilayer multipermittivity DRA, and parasitic DRA [34-35]. The bandwidth of a DRA can also be enhanced by adapting new feeding techniques.

1.2 Dual Linear Polarized Antennas

Dual-polarized antenna combines two sets of antennas with mutually orthogonal polarization directions (+45° and -45°) and works in the duplex model of transmitting and receiving signals. Therefore, its outstanding advantage is that it saves antennas for directional applications. Normally the directional BTS (three-sector) of GSM digital mobile communication network needs to use nine antennas; each of its sectors uses three (for space diversity, one for transmitting, and two for receiving signals). If dual-polarized antenna is adopted, each sector needs only one antenna [50-58]. In the meantime, the orthogonality of ±45° polarization can ensure that the isolation between the two sets of antennas (+45° and -45°) meets the requirement from intermodulation (≥ 30dB), therefore the space interval between dual-polarized antenna is just 20-30cm. Besides, dual-polarized antenna also possesses advantages like reducing call loss and interference and improving the whole network quality, which are the same as those of electrical antennas. There is no specific requirement for installing dual-polarized antenna and no need to acquire land for building antenna tower. Just a metal pole with 20 cm diameter is needed. Then antenna can be fixed on the pole in the corresponding coverage direction. In this way, basic construction cost is saved.

1.3 Dual Linear Polarized Dielectric Resonator Antennas

The polarization-diversity antennas have been an important area for antenna designers. There have been significant works on different feeding methods, different shapes of DRA with linearly polarized or circularly polarized radiation patterns. The number of designs of dual polarized DRA are however very less in currently available open literature. The study of DRA has been increasing in the last decade for their inherent merits of small size, low cost and no conductor loss as an efficient radiator. In general the dual-polarized radiation has practical applications in wireless communication systems [6-7]. With the capability of dual polarization, the antenna can combat the multipath effects and optimize the system performance with increased information rate [43-45]. This technique combines two feed ports with mutually orthogonal polarization directions and works in the duplex model of transmitting and receiving signals in the meantime.

1.4 DRA Array

In many applications it is necessary to design antennas with very directive characteristics (very high gains) to meet the demands of long distance communication. This can only be

accomplished by increasing the electrical size of the antenna. Enlarging the dimensions of single element, often lead to more directive characteristics. Another way to enlarge the dimensions of the antenna, without necessarily increasing the size of the individual elements, is to form an assembly of radiating elements in an electrical and geometrical configuration. This new antenna, formed by multi elements, is referred to as an array.

DRA elements of proper geometry can be assembled and fed in a suitable way to modify their gain, bandwidth and radiation performances and hence can be advantageous over a single element [59-64]. These DRA array finds applications in terrestrial applications as well as radars. The performance of an array depends on the geometry and dimensions of individual elements, number of elements, their spacing, mode of operation and feeding techniques implemented. The DRA elements can also be phased to form adaptive arrays or functional arrays with beam-steering capability. Linearly or circularly polarised DRAs can also be implemented to construct circularly polarised arrays for applications in telecommunications via satellites.

The experimental study of a dielectric waveguide-fed series DRA array for millimetre wave applications by Birand and Gelsthorpe [8] at ERA Technology Ltd, UK in early 1980s fascinated the antenna designers to study on DRA arrays.

1.5 Motivation

The rapid increase in the demand for wireless applications in the microwave range has led the research community to focus their attention on highly efficient antennas, which exhibit wide bandwidth, good radiation characteristics and low metallic losses with small size. For these reasons, DRAs are preferred over microstrip and conventional antennas. The DRA could be useful for the above applications due to their many inherent features like small size, low cost and no conductor losses. In recent few decades, researchers have developed several techniques to increase the bandwidth and obtain a wideband response for the DRA which will accomplish high data rates to facilitate information sharing with equipment mobility in short-range communications.

The advancements in wireless communication industry, especially the area of mobile communication, wireless data communication and satellite communication have led to the increased demand for information rate for which polarization-diversity antennas have been an important subject for antenna designers. With the capability of dual polarization the system performance can be optimized with increased information rate. It is relatively easy to realize a dual-polarized structure by making use of two ports in conjunction with

a circular, square or annular microstrip antenna, but it is a challenge to design a structure that can support dual-band and dual-polarized operation

1.6 Problem Statement

With the motivation mentioned above, we decided to take up a problem for the Master in research programme, which is stated below.

To design and develop,

- Wideband Dielectric Resonator Antenna (DRA) for WLAN applications,
- Dual-Linearly polarized Dielectric Resonator Antenna array for L and S band Applications,
- Dual- linearly Polarized Dielectric Resonator Antenna array for C-Band applications.

1.7 Thesis Organization

The **FIRST** chapter of this thesis presents a brief introduction of the wideband DRA, DRA array and the Dual linear polarized DRA array. The motivation and problem statement of the research work are stated in this chapter. At the end, the chapter wise presentation of the thesis is included in summary.

The **SECOND** chapter dedicates the historical overview and development of DRA. Both theoretical and mathematical descriptions with focus on describing resonances are presented. Numerous examples of different antennas, modes and excitation techniques, polarizations, DRA array and its parameters have been described.

The **THIRD** chapter is based on design and analysis of the wideband DRA with square ring shape. The design methodology taking U-shaped microstrip feed; to excite a hybrid mode in square ring dielectric resonator has been stated. The proposed antenna is suitable candidate for WLAN applications.

In the **FOURTH** chapter, a 2×2 cylindrical dielectric resonator antenna (DRA) array, where each element is excited by a slot orthogonally placed to a strip fed probe is presented. The proposed design is showing dual linear polarization with high isolation in L-band and S-band operations. The isolation, reflection coefficients and co-cross polarization levels have been studied. The dual band and dual polarization performance of the antenna is a suitable candidate to reduce multipath effects, while increasing the data rate.

The **FIFTH** chapter contributes a slot coupled Dual-Polarized Dielectric Resonator Antenna for C-Band applications. The excitation technique applied here is to achieve high isolation, which reduces the surface wave losses. This antenna seeks promising applications in the satellite and radar communication systems operating in C-band.

Finally, the **SIXTH** chapter outlines the overall contributions of the thesis. The achievements and limitations of the results are also discussed. The details of further research work in this area are also included in this chapter.

1.8 Summary

In this chapter, a brief introduction on wideband DRA, dual polarized DRA, and DRA array are discussed. The wideband antennas have many applications in direct digital broadcast, satellite communications and radar applications. The antennas with dual polarized radiation patterns can combat the multipath effect while increasing the information rate. This chapter also systematically outlines the research motivation with the problem statement of the thesis. A chapter wise concise presentation of the research work has been presented. In essence, this chapter provides an overview of the thesis in a comprehensive manner.

Chapter 2

DIELECTRIC RESONATOR ANTENNAS: AN OVERVIEW

2.1 History of the Dielectric Resonator Antennas

Resonance cavities of simple shapes with a metallic coating have been analysed for a long time as a special case of waveguides. There exist explicit expressions for calculating the resonant frequencies and electromagnetic fields in a resonance cavity. In 1939, Richtmeyer at Stanford University showed that dielectric objects shaped like toroids could be used as microwave resonators [9]. The DR as a practical resonator was reported in the early 1960s by Okaya and Barash at Columbia University [10]. This first ever dielectric resonator was made from a single crystal TiO_2. The first extensive theoretical and experimental evaluations of the dielectric resonator were carried out by Cohn et al. at Rantec Corporation in the mid-1960s. A breakthrough came in 1971, when Masse et al presented the first temperature-stable low loss ceramic of barium tetratitanate [11]. In 1975, a report of Van Bladel, Ghent University, Belgium described a detailed analysis of various modes in the dielectric resonator of arbitrary shape [12]. The usage of narrow-band dielectric resonators and resonance cavities with high *Q*-factors exploded in microwave applications as oscillators and filters, especially as low-loss dielectric materials were developed. In these circuits, oscillators are made of high-permittivity materials and are usually shielded to avoid radiation and maintain high *Q*-factors.

The idea of using dielectric resonators as antennas first came from Long et al. as a way of creating a microstrip antenna by replacing the leaky conducting patch and substrate. This investigation took place at the US Army, Harry Diamond Laboratories during the summer of 1981. The theory was based on perfectly conducting magnetic wall boundary approximations. The investigated shape was cylindrical in shape. The first result was possible to achieve a radiation pattern similar to that of an electric dipole parallel to the ground plane, originating from the HE_{11} mode. Also, the impedance bandwidth was better compared to the microstrip antenna. A sketch of this single polarized antenna and feeding is shown in Figure 2.1. S. A Long along with McAllister and Shen investigated

systematically different shapes and sizes, as well as materials, at the University of Houston, which resulted in the first publications [13-16] starting from 1983. The term dielectric resonator antenna was used for the first time in their first publication. In these works the feeding was made by coaxial lines with probes extending into the resonators through drilled holes.

In the second half of the 1980s several publications were made by different research groups, the first from outside of Houston being a paper by Haneishi et al at the Saitama University of Japan [17]. Pioneers in the area were three research groups situated in the University of Mississippi, the Communications Research Center in Ottawa and the City University of Hong Kong. The first group contained Kishk, Junker, Glisson and Kajfez. The second group contained Petosa, Ittpiboon, Mongia and Barthia among others and the third group mentioned was led by Luk and Leung. In the mid-1990s more emphasis was laid on dielectric resonator antenna arrays, both linear and planar with as many as *300* elements with beam control. Also ferrite resonator antennas came during this period, together with antennas operating in the millimeter frequency band and wideband antennas.

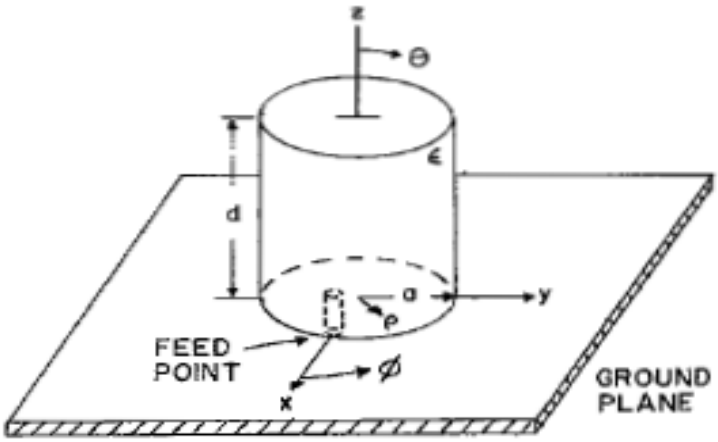

Fig. 2.1 Illustration of the first dielectric resonator antenna

Fig. 2. 1 Sample of different shapes of dielectric resonator antennas [3]

2.2 Advantages of Dielectric Resonator Antennas

The dielectric resonator has been studied extensively in recent years for different applications from low frequencies to high frequencies. The dielectric resonator antenna has a high flexibility and versatility in adopting a shape over a wide frequency range, which allows the designer to achieve the desired requirement. Some of the major advantages or characteristics of the dielectric resonator antenna are as follows [2-3]:

1. The size of the dielectric resonator antenna is proportional to $\lambda_0/\sqrt{\varepsilon_r}$, where λ_o is the free space wavelength of the resonant frequency and ε_r is the dielectric constant of the dielectric resonator. This means that the size of the dielectric resonator antenna can be reduced by just increasing the dielectric constant.
2. The dielectric constant ε_r can be from a range of below 3 upto 100, which allows for a great deal of flexibility while controlling the size and bandwidth.

3. A millimetre-wave frequency operation can be achieved by choosing a low-loss characteristic dielectric material due to absence of surface waves and minimal conductor losses associated with the dielectric resonator antenna. At these frequencies high radiation efficiency can be achieved.
4. Many modes can be excited within the dielectric resonator antenna element depending on the shape of the resonator. Different modes give different radiation patterns for various coverage requirements.
5. The radiation *Q*-factor of the above mentioned modes depends on the aspect ratio; the aspect ratio is an important parameter in designing a dielectric resonator antenna because it gives one more degree of freedom for the design.
6. Different methods can be used to excite the dielectric resonator antenna (slot, probe, coplanar, microstrip, waveguide, dielectric image guide, etc.) which make them easy to integrate with the existing technologies.
7. Dielectric resonator antennas are designed to operate over a wide frequency range of 1 to 40 GHz.
8. Dielectric resonator antennas have high dielectric strength which makes them capable to handle high power. This also helps them to work in a wide temperature range due to the temperature-stable ceramic materials.
9. The dielectric resonator antenna has much wider impedance bandwidth compared to the microstrip antenna. It is because the dielectric resonator antenna radiates through the whole antenna surface except for the ground whereas the microstrip antenna radiates only through the narrow slots.

The problem with dielectric resonator antennas is typically that ceramic materials which are machined to shape from a large block are used. To feed the antenna using probes, the antenna needs to be drilled since it is bounded to a ground plane or a substrate. The fabrication of dielectric resonator antennas is more complex and more costly compared to printed circuit antennas, especially for array applications. There are applications where performance is more important than cost. Hence the dielectric resonator antenna can provide the solution.

2.3 Limitations of DRAs

In general the bandwidth of the DRA is typically below10%. The bandwidth can be increased by applying different bandwidth enhancement techniques, but while fabricating it is very complex as compared to printed circuit antennas. As the DR element of high permittivity is very sensitive to frequency, when placing the DR on the required position, there is large chance of variations in position in terms of microns, which also affects the behavior of the antenna in a much large manner. So the automated placing machine is generally required for DR placing. Though there are many materials of different dielectric constants are available in literature, it is difficult to get the required material in perfect shape to integrate in an antenna.

2.4 Dielectric Resonator Materials

Depending on the applications of the dielectric resonator, different requirements are specified for the material to be used. The dielectric properties depend on the material, crystal structure, porosity and imperfections in the crystal lattice as well as on the preparation conditions. Dielectric resonators generally consist of a puck-formed cylinder of ceramic material of high permittivity and low dissipation factor. Traditional passive devices have been desired to have a high *Q*-factor (up to *20,000* between *2GHz* and *20GHz*) [11], high permittivity and near zero temperature coefficients for the resonant frequency which has been difficult to achieve simultaneously. The low-permittivity ceramics have so far been used for millimeter-wave applications and also as substrates for microwave integrated circuits (MICs). Ceramics with permittivity in the range between 25 and 50 have been used for satellite communication and in cell phone base stations. High permittivity materials are used in mobile telephones, were the compact size sets narrow limits. In all the mentioned cases the use has been for circuit components. There are about *2300* low-loss dielectric materials reported in the literature [18]. About *60%* of the dielectric resonator materials are based on alkaline earth metals such as *Ba*, *Mg*, *Sr* and *Ca* . About *46%* of the materials are titanates. Rare earth materials appear in *40%* of the cases.

2.4.1 Losses and Quality Factor

The total dielectric loss is the sum of intrinsic and extrinsic losses. Intrinsic dielectric losses are the losses in the perfect crystals which depend on the crystal structure. They can be described as interactions between phonons and an electric field. The electric field changes the equilibrium of the phonon systems and the subsequent relaxation is

associated with energy dissipation. As a result the relaxation dissipates heat energy and the material gets heated. The intrinsic losses depend on the crystal symmetry, electric field frequency and temperature. The intrinsic losses fix the lower limit of losses in crystals free from defects. Extrinsic losses are due to imperfections in the crystal lattice such as impurities, dopant atoms, vacancies etc. Crystals from different symmetry groups have different temperature and frequency dependence for the dielectric loss. A measure of the dielectric loss is given by the dielectric loss tangent, defined as:

$$\tan\delta = \varepsilon_r'' \big/ \varepsilon_r' \tag{2.1}$$

Where $\varepsilon_r = \varepsilon_r' - j\varepsilon_r''$ is the complex frequency dependent permittivity. For lossless materials, ε_r' is zero [18]. The inverse of the dielectric loss tangent is sometimes referred to as the quality factor by the manufacturers. The other measure of energy dissipation, namely the $Q-\text{factor}$, gives all the energy losses along with the material losses. The *Q*-factor is defined by

$$Q = 2\pi\left(\frac{E_{\max\, stored}}{E_{\text{avg}\, diss}}\right) \tag{2.2}$$

where $E_{\max\, stored}$,the maximum energy is stored in one cycle and $E_{\text{avg}\, diss}$ is the average energy dissipated during one cycle. The total loss in a dielectric resonator is the sum of dielectric, conduction, radiation and external losses which, in terms of $Q-\text{factor}$ can be written as:

$$\frac{1}{Q_L} = \frac{1}{Q_d} + \frac{1}{Q_c} + \frac{1}{Q_r} + \frac{1}{Q_{cpi}} \tag{2.3}$$

where Q_L is the loaded $Q-\text{factor}$, taking into account coupling effects that arise when an electric field is induced in the dielectric resonator. The field lines induce currents on objects in their way which is represented by the term $\frac{1}{Q_{cpi}}$.The dielectric loss, the conduction and the radiation $Q-\text{factor}$ are given by $Q_d = \frac{w_0 W}{P_d}$, $Q_c = \frac{w_0 W}{P_c}$, $Q_r = \frac{w_0 W}{P_r}$.

Here, W is the total electric energy stored in the resonator and P_d, P_c and P_r are the dissipated power in the dielectric, conduction and radiation, respectively. The metallic

coating around the dielectric resonator is removed so that the fields can leave the object. The radiation is to be maximized and the lack of metallic surfaces implies that no ohmic losses appear. This is one of the main advantages of the dielectric resonator antenna. Q_L is experimentally determined from the shape of the resonance peak in the reflection versus frequency diagram. The curve is drawn for a resonator coupled with an external circuit. The transmitted signal amplitude peaks at the resonant frequency. The 3-dB bandwidth is the frequency bandwidth at half power from the peak. The loaded $Q-\text{factor}$, Q_L is the resonant frequency divided by the 3-dB bandwidth. The quality factor of the microwave frequency materials is very sensitive to the structure of the material and the processing. The dielectric loss, which determines Q_d, can vary from one sample to another due to variations in the intrinsic crystal structure, density, concentration of impurities etc.

2.4.2 Zirconium – titanates

For the microwave frequency region, $Zr_xTi_ySn_2O_4$ have been reported as temperature-stable low loss dielectric materials [19]. The composition $Zr_{0-8}TiSn_{0.2}O_4$ gives the best microwave dielectric properties because of low porosity and its property as a highly homogeneous material.

2.4.3 Barium-titanates

The barium-titanates ($BaO-TiO_2$) have been used for a long time in the ceramic capacitor industry. The $Ti-\text{rich}$ compounds are few but exhibit good temperature compensation and high relative permittivity between 25 and 40. It was Masse et al [20] who first pointed out that $BaTi_4O_9$ is suitable for dielectric resonator applications at microwave frequencies. Doping with Mn, Sn and Pb, lowers the $Q-\text{factor}$ while doping with Zr, Sr and Ca raises the $Q-\text{factor}$ and depending on the doping the relative permittivity is between *33* and *37*.

2.4.4 Low Temperature Cofired Ceramics

Low temperature cofired ceramics (LTCC) are tapes of flexible ceramic glass. In this technology, several thin layers of low-permittivity ceramic composites and conductors are combined. A variety of components can be made from this material, including microstrips, striplines, antennas, filters, resonators, capacitors, inductors and phase shifters making possible a design on a substrate of these components. The latest

materials from this family show a low dielectric loss and a temperature compensated relative permittivity [19]. The low thermal expansion, high mechanical strength and high thermal conductivity of these materials make them interesting for low-loss, high-frequency circuits for high-speed data communication. The main drawback of these materials is that they are complicated and sensitive to manufacture. The permittivity is in the range 4 to 100. Materials of low relative permittivity with $\varepsilon_r = 4$ to 12 are used as substrate layers while materials with higher permittivity are used mostly as capacitor layers.

2.4.5 Pseudo-tungsten bronze-type

The materials in this category have high ε_r , low loss and are often used in the cell-phone industry. The ceramics $Ba_{6-3x}Ln_{8+2x}Ti_{18}O_{54}$ with Ln substituted by $Nd, Sm,$ or Eu have high quality factors up to *14,000*. The highest ε_r can be obtained by replacing Ln with La [21].

2.4.6 Titania

Titanium dioxide crystallizes in three forms. One of them is rutile which has properties suitable for microwave applications, and this form was also used by Okaya and Barash in their discovery [19] as mentioned in section 2.1. By hot pressing the rutile in a graphite die, a high quality factor (*Q>10,000*) can be obtained. The dielectric loss increases with the percentage of porosity of TiO_2 rutile. The $\tan\delta$ of TiO_2 also increases with temperature and rises from 0 to 5.10^{-4} between *0* and *100K*, where after the increase is slower and reaches 6.10^{-4} at room temperature. The dependence can be minimized by doping with AlO_3 with Titania.

2.4.7 Alumina

Alumina materials have a relative permittivity around *10*, relatively high thermal conductivity and low dielectric loss and are frequently used as packaging material for ceramics. The dielectric loss is highly variable and has oscillations within several orders of magnitude. Since the material is in powder form, the powder purity is very important. In polycrystalline alumina, the quality factor decreases rapidly by the presence of alkali ions and atoms from other metals, such as Fe . A small amount of TiO_2 can improve the quality factor considerably [20]. The purity does not have an impact on the dielectric loss tangent, which is more dependent on the sintering temperature and the humidity in the

powder. The dry powder alumina is having low dielectric loss tangent. This material has been considered for design of dual polarized DRA array in C-band applications in this research work.

2.4.8 Silicates

For substrates, materials with low dielectric loss and low permittivity are sought. The silicates, with their covalent bindings keep their atoms relatively tight bonded and cannot vibrate or move around. This leads to low dielectric loss. The low dielectric polarizer of silicon and the strong bonds also lead to low ε_r in silicates [21]. Silicates have been used for dielectric waveguides but have turned out to be good as substrates at millimeter wave frequencies. One useful silicate-based dielectric ceramic is Cordierite $\left(2MgO-2Al_2O_3-CaCO_3-5SiO_2\right)$. The relative permittivity of these materials are in between *6* and *11*.

2.4.9 Cerium oxide

Cerium oxide CeO_2 has a good lattice match with silicon, high chemical stability and high relative permittivity and is suited as an insulating material. Both Q and ε_r decrease when doping with $CaCO_3$ [21]. Depending on the concentration of doping $\left(\text{with either } CaCO_3 \text{ or } CaTiO_3\right)$ the relative permittivity is between *24* and *29*.

2.4.10 Bismuth Based Low-firing Ceramics

For cylindrical and rectangular dielectric resonator antennas, with dimensions between 5 and 10mm operating at frequencies between *2GHz* and *4GHz*, a bismuth based ceramic has been used with low reported return loss [20]: $Bi_{(3x)}Zn_{(2-3x-y)}Ay(Zn_xNb_{(2-x-z)}Bz)O_7$, was investigated by [18]. Manufacturers of dielectric resonators produce similar components for a certain application but there are small differences in circuit design, construction and packaging. The unique composition of materials implies a unique frequency drift as a function of temperature which in turn means that the temperature compensation needs to be unique as well. It is difficult to control the dimensions of the dielectric resonator and slight variations will result in different resonance frequencies.

2.5 Dielectric Resonator (DR) as an Antenna

Articles reporting about dielectric resonator antennas often use elements of high relative permittivity. This is due to the availability of such elements that are intended as circuit elements. Dielectric resonators used as both antennas and filters around *2.4GHz* have

been reported with a radius of about 13 mm and a relative permittivity of *36.6* [23]. These materials are hard ceramics difficult to machine. One provider is Trans Tech Incorporation [20]. Permittivity variations due to frequency and temperature changes in terms of tolerances can be custom defined if necessary. The advantage of ceramics is that they do not age or absorb moisture, although condensation on the resonator surface may alter the $Q-\text{factor}$. Ceramic materials are also sensitive to the use of adhesives when assembling more complex structures. Materials of lower dielectric constant, with values in between *3* and *25*, are provided by Cumming Microwave [21]. These materials consist of plastic stock filled with ceramic materials. The main drawback with the ceramic and other high-permittivity materials is the more narrowband resonator behavior compared to materials with lower ε_r.This is due to the fact that Q is proportional to ε_r which is related to the bandwidth by the relation

$$Q = w_0 / \Delta w \tag{2.4}$$

where w_0 is the resonant frequency and Δw is the bandwidth. For high permittivity, the relationship between Q and ε_r is analytically given by equation 2.15. Thus, for antenna elements, the materials of lower permittivity should be used whereas for filters higher permittivity and therefore higher $Q-\text{factors}$ should be used.

- **Plastic materials**:

  Materials of lower relative permittivity are Teflon based plastic materials. One provider of these materials is the Rogers Corporation [22], with sheets of materials with permittivity from around 2 to 10.2. These materials are easier to machine as they are softer. A typical Rogers laminate is made up from PTFE/ceramic sheets combined with PTFE/woven glass for increased rigidity [21]. Another construction of these materials is to use a ceramic filled, glass reinforced hydrocarbon based material. The dependence of the relative permittivity and dielectric losses restricts the frequency range. The RT/duroid series can be used for lower permittivities have a copper clad with planar resistor properties. The $\text{RT/duroid } 6010^{TM}$ laminate with permittivity 10.2 is suitable for operation below the Xband (8-12 GHz). The dielectric loss tangent for this material is low and little affected by moisture. The thickness control is within small margins. The lower permittivity RO3000- series are suitable for frequencies

up to 40 GHz. Examples of the lower permittivity materials are patch antennas, band-pass filters and voltage controlled oscillators [23].

- **Ceramic Materials**:

  Trans Tech Incorporation [20] has two types of materials. Custom permittivities between 4 and 270 can be obtained by compounds of dielectric powders. The compounds can be used to make polymers or sintered ceramic elements. The powder is supplied in milled form or in dried granules. Examples of these powders are Silicates, Barium Titanates, Calcium Titanate, alumina based ceramics and others. The other types are the standard dielectric materials. These are also ceramic materials (Magnesium Titanate, Forsterite, and Cordierite) which have permittivities of 15, 6.3 and 4.5, and a dielectric loss below 2×10^{-4} . The remaining standard dielectrics have permittivities of 37-100.

2.6 Modes in DRA

For an isolated dielectric resonator with no scattering objects in its vicinity, the complex valued natural frequency is given in (2.5)

$$S_{mnp} = \sigma + j\omega \tag{2.5}$$

Where 'σ' is the real part and 'ω' the imaginary part of the complex frequency. As for all passive devices, these frequencies lie in the left half of the complex plane. In particular, one certain mode would oscillate in an exponentially decreasing manner as a function of time if excited abruptly by an external source. A dielectric resonator of arbitrary shape can have confined modes, with a magnetic field distribution with no normal component to the boundary surface, and non-confined modes. The fields in and around the resonator peak to high values for high relative permittivity of the resonator at resonant frequencies and the sharpness of resonance increases with relative permittivity. Exact solutions for arbitrary shapes and permittivities exist only in special cases with particular symmetry. In the general case, all modes exist outside the boundary surface as well [2]. For the confined modes, the boundary surface acts as a magnetic wall as the magnetic field vanishes outside the resonator. The confined modes satisfy the following equations,

$$-\nabla\times(\nabla\times\vec{H}_{0m}) + k_m^2.\vec{H}_{0m} = 0;\ x \in V \tag{2.6}$$

and

$$\vec{H}_{0m} = 0; x \in S. \tag{2.7}$$

Here, 'V' is the volume of the resonator and 'S' is its boundary surface. The magnetic field vector comes from the expansion given in equation 2.9 and 'k_m' is the wave number of the mth mode.

$$\vec{H} = \vec{H}_0 + \frac{\vec{H}_2}{\varepsilon_r} + \frac{\vec{H}_4}{\varepsilon_r} + ... \tag{2.8}$$

These modes are identical to the electric eigenvectors of modes for empty cavities of volume 'V' bounded by metallic walls. Since the mode is confined, the normal component of the magnetic field vector is zero. This requires special symmetry for the shape (since there are no magnetic walls in the real world and implies that for the general dielectric resonator, there are no confined modes. The explicit expressions for the rectangular parallelepiped have no confined modes. The most general shape for confined modes is the cylindrical body of revolution, see Fig 2.3.

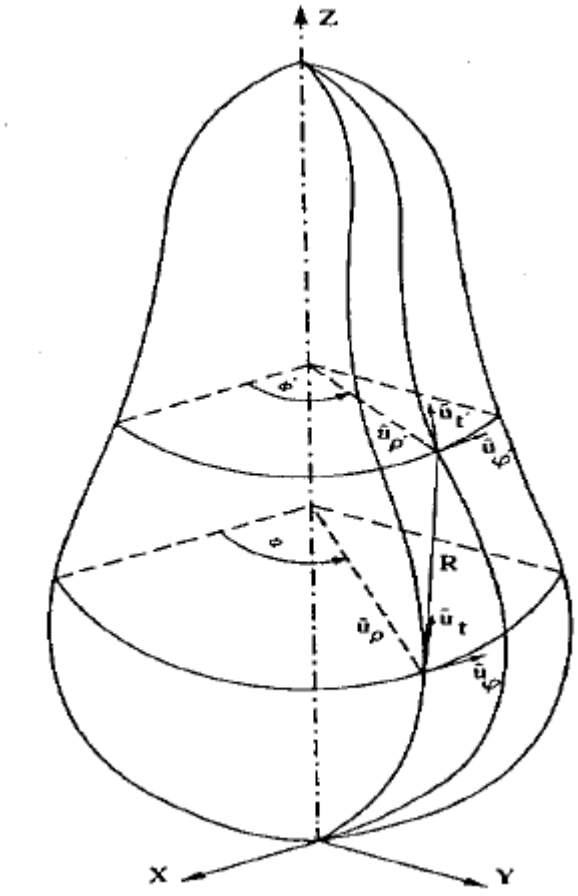

Fig. 2. 2 Example of a body of revolution with the *z*-axis as the axis of symmetry

These modes are not azimuthally dependent. The general form is:

$$\vec{H}_{0m} = \beta_m(r,z)\vec{u}_\phi,\ x \in V \tag{2.9}$$

Where 'β_m' satisfies, from equation 2.6 in cylindrical coordinates,

$$\frac{\partial^2\beta}{\partial r^2} + \frac{1}{r}\frac{\partial\beta}{\partial r} + \frac{\partial^2\beta}{\partial z^2} - \frac{\beta}{r^2} + k_m^2\beta = 0 \tag{2.10}$$

and

$$\beta_m = 0,\ x \in S. \tag{2.11}$$

The function 'β_m'also vanishes on the axis of revolution. For example, for a circular cavity of radius 'a'

$$\beta_{PS} = \sin\frac{P\pi z}{L} J_1\left(x_s\frac{r}{a}\right);\qquad J_1(x_s) = 0 \tag{2.12}$$

$$k_{PS}^2 = \left(\frac{P\pi}{L}\right)^2 + \left(\frac{x_s}{a}\right)^2 \tag{2.13}$$

Where 'P'and'S' are the longitudinal and radial eigenvalue parameters and 'J_1' is the Bessel function of first order. The sphere is an exception from the requirement of azimuthal independence. The sphere has special symmetry and supports a large number of confined modes. They have no radial component and their ϕ dependence is of the form $\cos(m\varphi)$ or $\sin(m\varphi)$. For traditional dielectric resonators used as filters and oscillators, a high relative permittivity is used in order to confine as many modes as possible [9], and thus most dielectric resonator microwave circuit components available on the market and are of high permittivity materials. For a dielectric resonator antenna, a low *Q*-factor, high radiation and non-confined modes are required. When ε_r is infinite, the electric field vanishes outside the resonator. No energy is radiated and the $Q-$factor becomes infinite. The $Q-$factor is the ratio between the reactive energy inserted in the resonator and the average dissipated energy per cycle. Only losses due to radiation have been considered below. For high values of ε_r, the dielectric resonator radiates like a magnetic dipole of moment [3]

$$\vec{P}_m = \tfrac{1}{2}\iiint_V \vec{r}\times(\nabla\times\vec{H}_{0m})dV \tag{2.14}$$

This dipole moment comes from the magnetic field outside the dielectric resonator as well. The high-permittivity $Q-$factor is ultimately given by [5]

$$Q=\frac{6\pi(\sqrt{\varepsilon_r})^3}{k_m^3}\frac{\iiint\limits_{V+V'}\left|\vec{H}_{0m}\right|^2 dV}{\left[\iiint\limits_{V}\vec{H}_{0m}dV-\iint\limits_{S}\psi_{0m}\vec{u}_n dS\right]^2} \tag{2.15}$$

Here $'V'$ is the volume outside the dielectric resonator, $\vec{u}_n$ is the unit normal vector to S and $'\psi_{0m}'$ is the scalar potential to $\vec{H}_{0m}$ outside the dielectric resonator, i.e.

$$\vec{H}_{0m}=\nabla\psi_{0m} \quad X\notin V \tag{2.16}$$

A numerical formula for the $TE_{01\delta}$ mode $Q-$factor of a cylindrical dielectric resonator is as follows.

$$Q=0.078192\varepsilon_r^{1.27}\left[1+17.31\left(\frac{h}{a}\right)-21.57\left(\frac{h}{a}\right)^2+10.86\left(\frac{h}{a}\right)^3-1.98\left(\frac{h}{a}\right)^4\right] \tag{2.17}$$

This indicates that the $Q-$factor grows as power function of $'\varepsilon_r'$. A plot of $Q-$factor versus aspect ratio is shown in Figure 2.4.

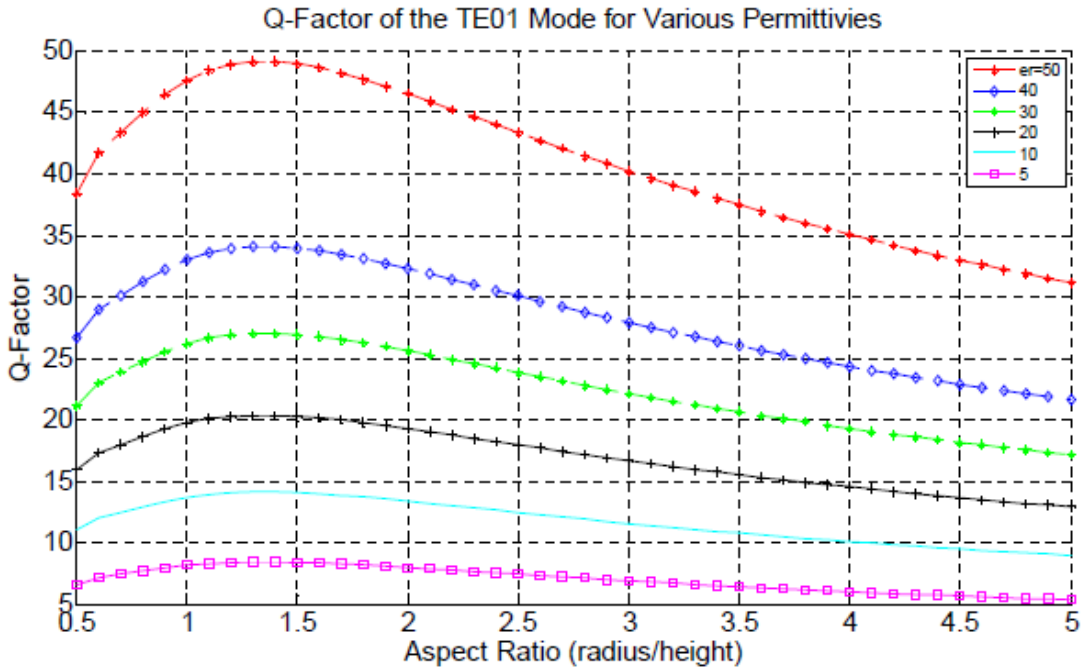

Fig. 2. 3 The $TE_{01\delta}$ mode Q-factor shows a clear dependence on the relative permittivity of the cylindrical dielectric Resonator[2]

The above statements indicate that a low relative permittivity is desired for a dielectric resonator used as an antenna. This must be weighed to the dimensions required for resonance in a piece of material at a certain frequency. For a frequency $'f'$, the dielectric wavelength is given as

$$\lambda_d = \frac{\lambda_0}{\sqrt{\varepsilon_r}} = \frac{c_0}{f\sqrt{\varepsilon_r}} \tag{2.18}$$

Where c_0 is the speed of light in vacuum and $'\lambda_0'$ and $'\lambda_d'$ are the wavelengths in free space and the dielectric respectively. For a cylindrical dielectric resonator, the minimum required dimensions are a diameter of $\lambda_d/2$ and a height of $\lambda_d/4$. Equation 2.18 concludes that the higher the relative permittivity, the more compact the dielectric resonator antenna element.

2.7 Excitation Techniques

There are some general rules which simplify the feeding mechanism, applicable to any DRA type and that can further be refined by using numerical methods[4]-[5]. While coupling to the DRA, typically one source (Electric or Magnetic) is considered that in turn defines the amount of energy being coupled. Using this principle, a resonance can be sought and tuned over a specific range while slightly displacing the feed position with respect to the DRA. As a normal practice it should be located within the stronger field influence whether Electric or Magnetic fields. Let $'J_1'$ is the source electric current and $'E_2'$ is the Electric field inside the DRA then the amount of coupling from electric source is given by

$$K \propto \int_V (E_2.J_1)dV \tag{2.19}$$

Similarly, if $'M_1'$ is the source magnetic current and $'H_2'$ is the magnetic field inside the DRA then the amount of coupling from magnetic source is given by

$$K \propto \int_V (H_2.M_1)dV \tag{2.20}$$

The coupling mechanism not only transfers energy to the DRA but also generates loading effect which directly controls DRA's $Q-$factor. Both external $Q-$factor and loaded $Q-$factor are expressed mathematically as given below.

$$Q_{ext} = \frac{Q}{K} \tag{2.21}$$

$$Q_L = \frac{Q}{1+K} \tag{2.22}$$

This phenomenon suggests that maximum power is transferred from the coupling port to the DRA when k =1 so in view of it a particular excitation method is selected.

2.7.1 Aperture Slot

It is a renowned coupling technique with the advantage of having the feed network located below the ground plane to avoid unwanted radiations that cause distortion and degrade the pattern shape [37-38]. For HEM_{11} or TM_{110} being the dominant resonant mode, the aperture at the DRA center behaves like magnetic current flowing parallel to its length. As a result it excites the magnetic fields in the DRA body causing broadside radiation pattern in the far field as shown in Figure 2.5. The slot is fed by microstrip line because it is easy to etch on the substrate and to seek impedance matching. This technique is particularly recommended for high frequency designs requiring highest level of precision and etching accuracy.

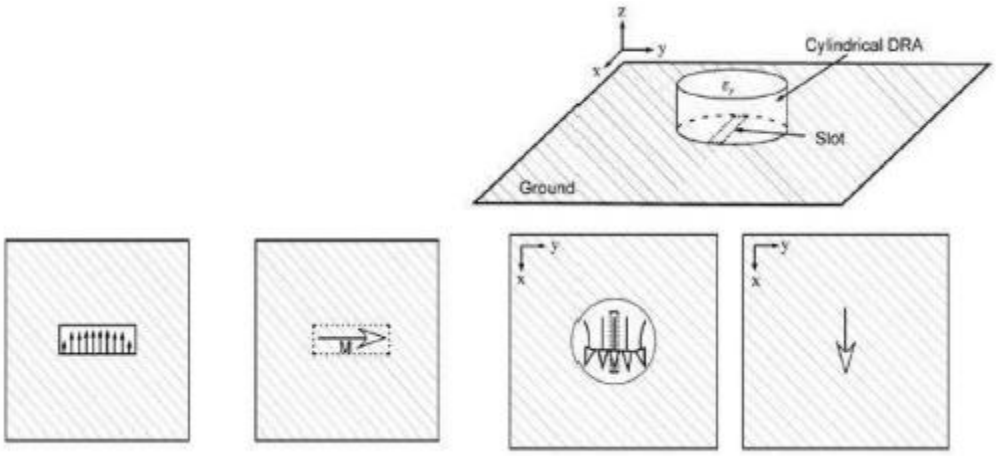

Fig. 2. 4 Electric and magnetic field distributions in slots

The slot's resonance is avoided to reduce backward radiation. So the slot's dimensions are kept small enough to avoid its resonance merge with that of the DRA and large enough to couple sufficient amount of energy. Although the exact size of the slot is determined by the numerical method. However, using the following formulae, length (l_s) and width (w_s) can be estimated.

$$l_s = \frac{0.4\lambda_0}{\sqrt{\varepsilon_e}} \tag{2.23}$$

$$\varepsilon_e = \frac{\varepsilon_r + \varepsilon_s}{2} \tag{2.24}$$

Where ε_e is the effective permittivity value. ε_r and ε_s are the dielectric constants of DRA and substrate respectively.

$$w_s = 0.2 l_s \tag{2.25}$$

A quarter wavelength stub length can significantly improve the coupling to the DRA as its reactance cancels out to that of the slot. It is given as

$$s = \frac{\lambda_g}{4} \tag{2.26}$$

Where λ_g is the guided wavelength in the used substrate.

2.7.2 Coaxial Probe

The probe can be considered as a vertical electric current that is positioned to achieve strong coupling to the DRA [39]. The level of coupling is optimized while adjusting the height and diameter of the probe. Depending upon the shape of DRA and probe location, different modes can be excited. TM modes are excited only when the DRA is fed axially. To be more precise that if TM_{01} mode is to be excited, the feed probe is expected to be located at the center yielding quarter wavelength monopole like far field radiation patterns. On the other side when HEM_{11} (TM_{110}) mode is required, the feed probe is supposed to be located close to the peripheral boundary so as to yield broadside radiation patterns. The location of probe at two different positions and associated electric and magnetic fields are presented in the Fig 2.6. This is a simple mechanism as in this case one can directly couple to $50\,\Omega$ without going for matching network [9-10].This technique is particularly recommended at lower frequencies to cope up with the fabrication issues, however it is equally efficient and result oriented at higher frequencies. For instance, compared to slot feed's approximate position in the peripheral area of the cylindrical DRA, it is simple to locate the probe at its center when to excite TM01 mode.

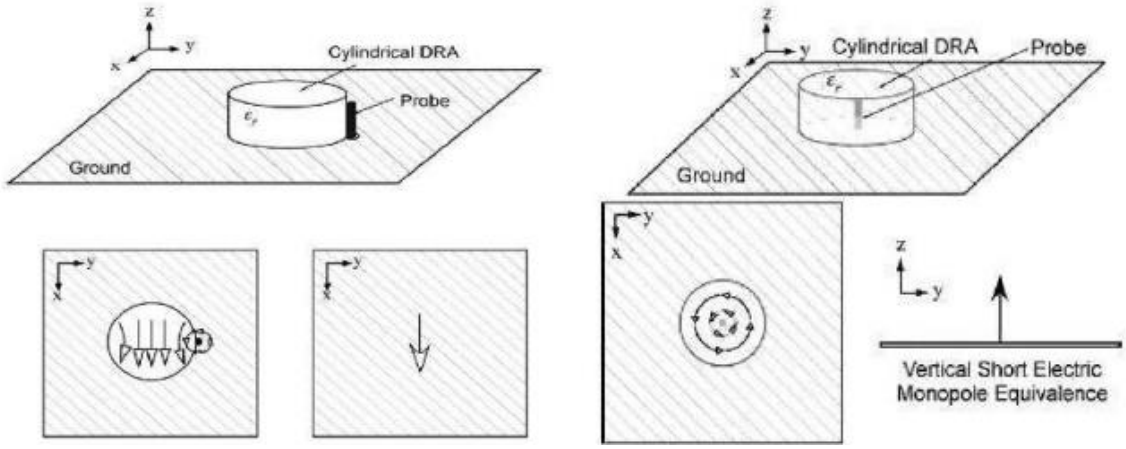

Fig. 2. 5 Electric and magnetic current distributions in co-axial probe feeding [2]

2.7.3 Microstrip Line

Direct and Proximity couplings are amongst the simplest methods [40-42]. It excites the magnetic fields in the DRA to produce the short horizontal magnetic dipole [9]. The amount of coupling can be improved by controlling a parameter *s* or by increasing the dielectric constant (permittivity) value of the material used. It is a common conclusion that for low value of dielectric constant, minimum energy is coupled. However, with increase in its value other limitations are encountered particularly at higher frequencies further reduction in size can cause fabrication process too sensitive and that may introduce faulty results. Similarly the consequence reduction in impedance bandwidth can limit its wideband applications. The behavior of the coupling fields can be observed from the Fig 2.7.

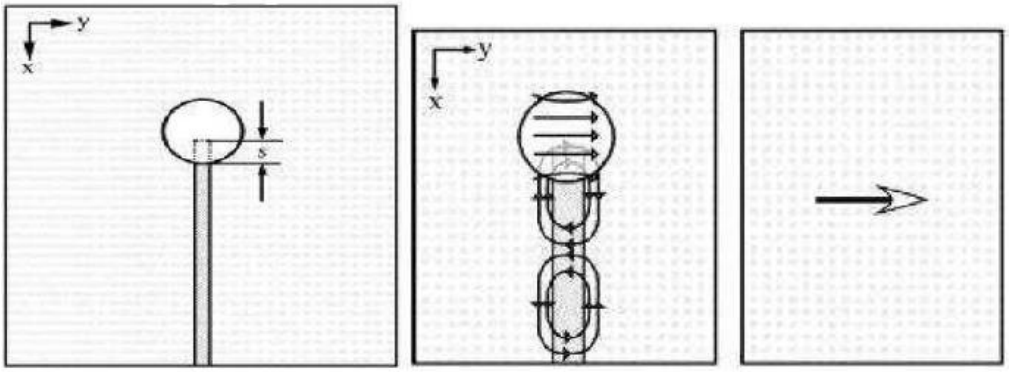

Fig. 2. 6 Electric and magnetic field distributions in proximity coupling

2.7.4 Coplanar Feeds

The coplanar loop efficiently couples energy to the DRA. The coupling level and desired mode excitation can be obtained by gradually sliding the DR element over the loop [3]. By shifting the loop from the edge to the center one can yield required resonance frequency and radiation patterns. One such arrangement with field distribution is shown in Fig 2.8.

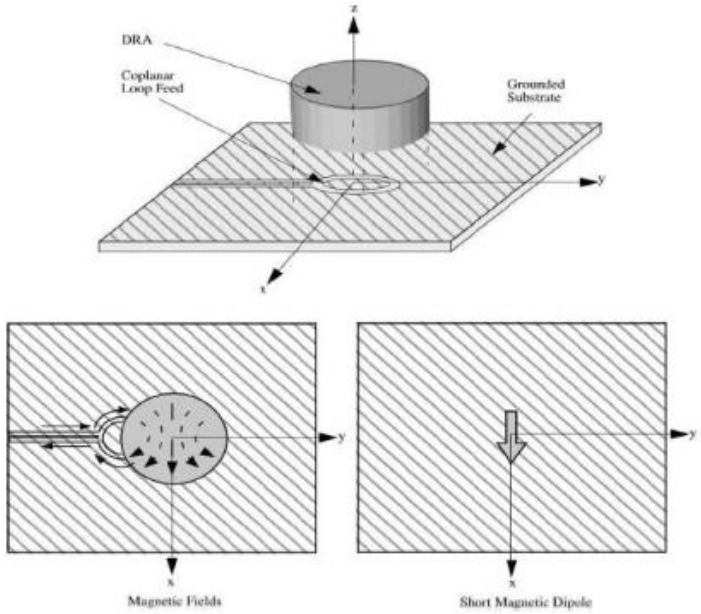

Fig. 2. 7 Magnetic fields distributions in coplanar feed coupling to DRA

2.7.5 Dielectric Image Guide

At millimetre-wave, if microstrip feed lines are used, the conductor losses become significant. To avoid this problem the use of dielectric image guide is the best solution. The dielectric image guide couples the energy to the DRA that is located in its proximity. Again, considering associated limitations, a higher permittivity value can be chosen to enhance the coupling level. This method also offers an added advantage that it can be utilized as series feed to linear array designs [8]. Fig 2.9 describes the magnetic fields distribution in the image guide and their coupling behavior to the resonator.

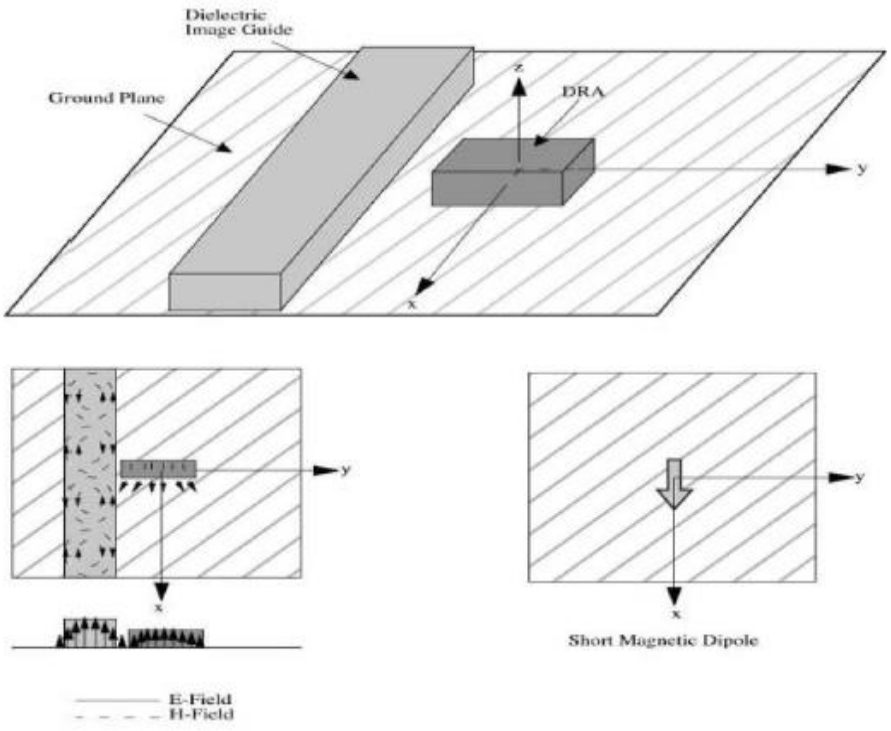

Fig. 2. 8 Magnetic fields distributions in dielectric image guide and its coupling to DRA

2.8 Bandwidth Enhancement Techniques

The use of the broadband devices in the modern communication systems is on the rise so a practical purposes antenna is supposed to have wider bandwidth [2-3]. The bandwidth limitation of antennas is usually linked to their input impedance because it is the quantity which changes with frequency so improvement in impedance response can help us to enhance its bandwidth. This approach can be implemented into four broad categories.

1. Controlling permittivity ε_r & aspect ratios (a/h)
2. $Q-$factors reduction
3. Usage of matching networks
4. Multiple resonators employment

2.8.1 Controlling Permittivity ε_r & Aspect ratios (a/h)

Among numerous choices, it is the most simple and result oriented approach. After selecting the resonant mode, it is the resonator's dielectric constant value and its aspect ratio (a/h) that define the obtainable bandwidth. In simple geometric shapes such as cylindrical DRAs the smallest possible ε_r value makes $Q-$factor low which as a consequence results in wider bandwidth [9].

$$BW = \frac{S-1}{Q\sqrt{S}} \times 100\% \quad (2.27)$$

Where S =desired VSWR at the input of DRA port.

However, there are some limitations which are always associated with each type of design. For example, in this case, though the $Q-$factor can be decreased accordingly by lowering the value of dielectric constant but if lowered drastically, it fails to capture enough amount of electromagnetic energy and to act as an efficient resonator. The other choice is to seek proper aspect ratio value (For cylindrical DRA $a/h = 0.329$) that generates two closely merged resonances such that a wider (-10dB) impedance bandwidth is obtained. It is preferred over other technique due to its easy fabrication process. One such device is shown in Fig 2.10.

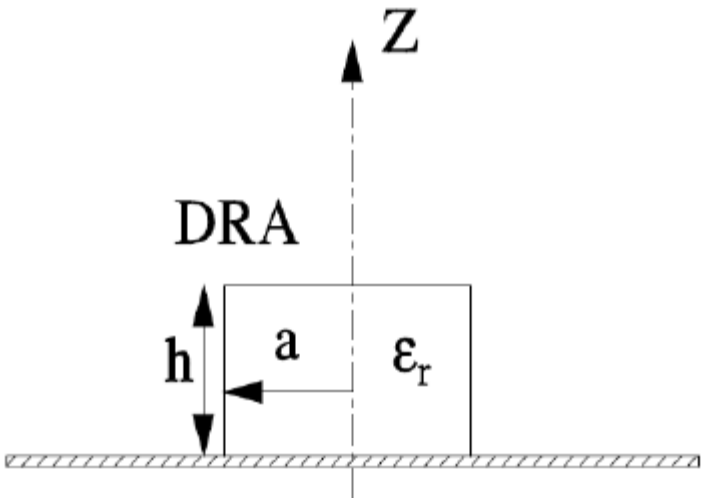

Fig. 2. 9 A single piece DRA structure with radius 'a' and height 'h'

2.8.2 Q-factors Reduction

By the introduction of air gap surrounding the monopole and enclosed by the DRA body helps in lowering the effective dielectric constant of the DRA [27] which, as a result lowers the $Q-$factor and thus increases the bandwidth while pushing the resonant frequency upwards. Comparatively wider bandwidths are achieved at the cost of higher complexity of the fabrication process. One such model is presented in the Fig2.11. Very slight displacement of DRA with respect to the centrally located monopole can shift the resonance frequency from desired position. A very careful and highly precise cutting and grinding of DRA piece is required otherwise undesired air gap size may drastically influence the results.

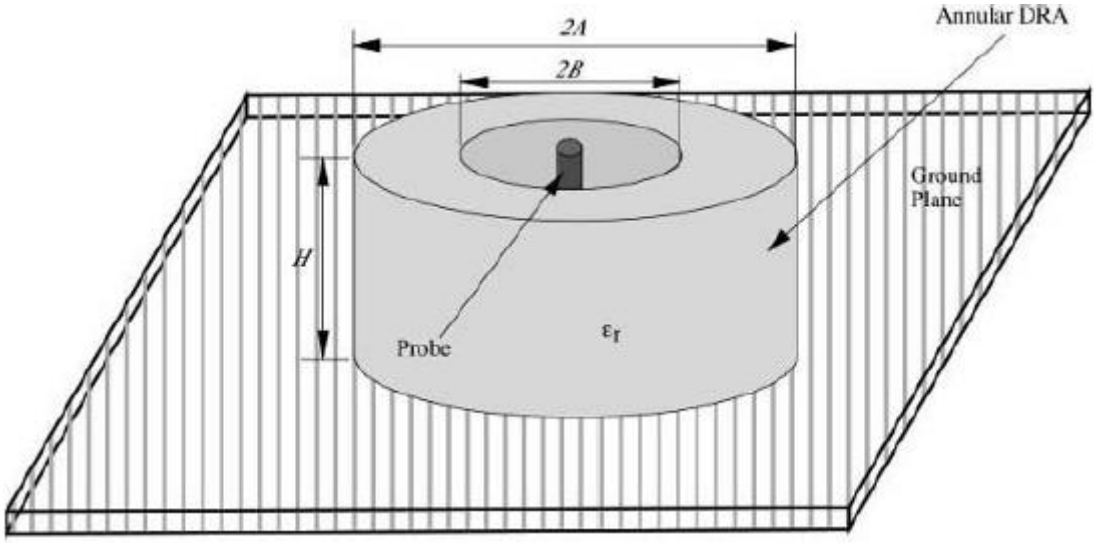

Fig. 2. 10 Air gap enclosed structure to enhance bandwidth

2.8.3 Impedance Matching

The bandwidth can also be enhanced by implementing impedance matching by using different types of material before matching to desired DRA. For instance flat matching inserts, loaded notches and multi-segment DRAs are common techniques. A high permittivity inserts between the feed and resonating body element is fitted to couple the energy efficiently. A rectangular shaped DRA with a flat metal strip for a probe-fed DRA is shown in Fig 2.12. Back radiation is a common problem with aperture slot feeds. If a matching strip is selected carefully, back radiation is controlled along with improved coupling.

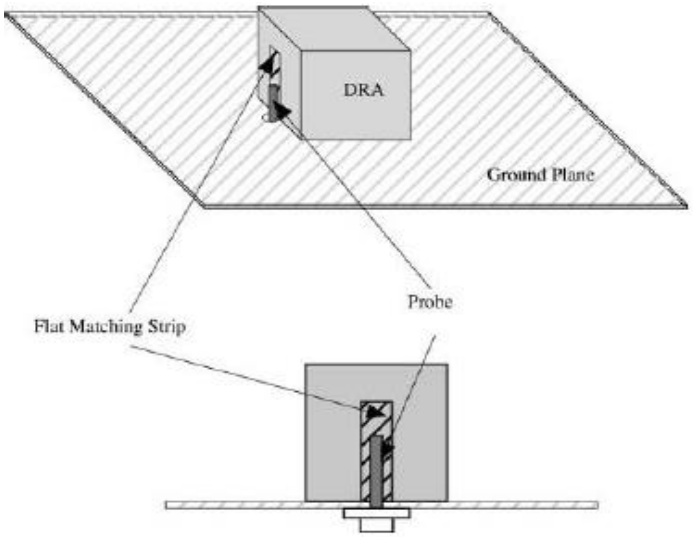

Fig. 2. 11 Impedance matching using a flat metal strip for a probe-fed DRA

2.8.4 Multiple Resonators Employment

Considering individual design sizes, multiple elements are made to resonate at slightly different frequencies which are shrewdly tuned either to merge to offer wider bandwidth or to separate to yield multi- bands [3]. Such types of stacked DRAs excited by a probe are depicted in Fig 2.13. The major disadvantage in this scheme is that it is difficult to position and paste the upper element accurately.

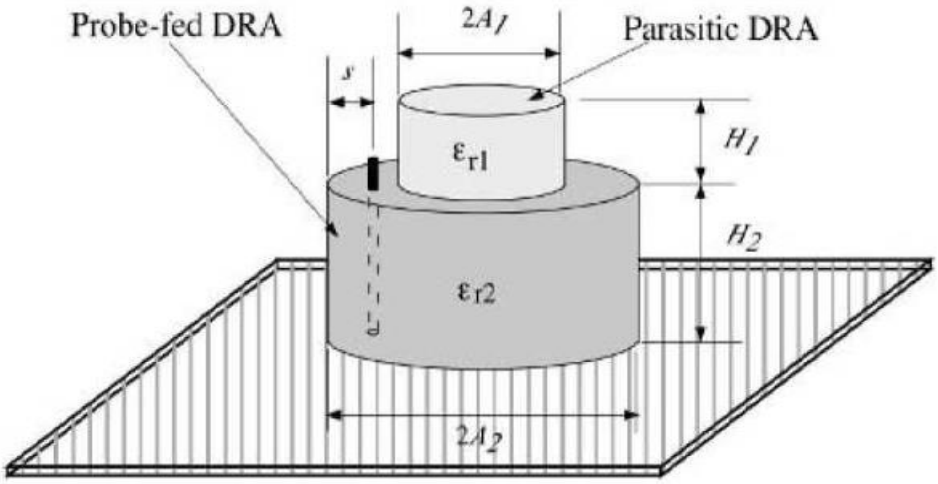

Fig. 2. 12 Stacked DRAs to merge two close resonant frequencies to enhance bandwidth

2.9 Polarization

The polarization is defined as the orientation of the electric field vector. The electric field vector is perpendicular to both the direction of the traveling wave and the magnetic field vector. In general, all electromagnetic waves are elliptically polarized. Figure 2.14 is showing the orientation of the electric field in two dimensions *x* and *y* .

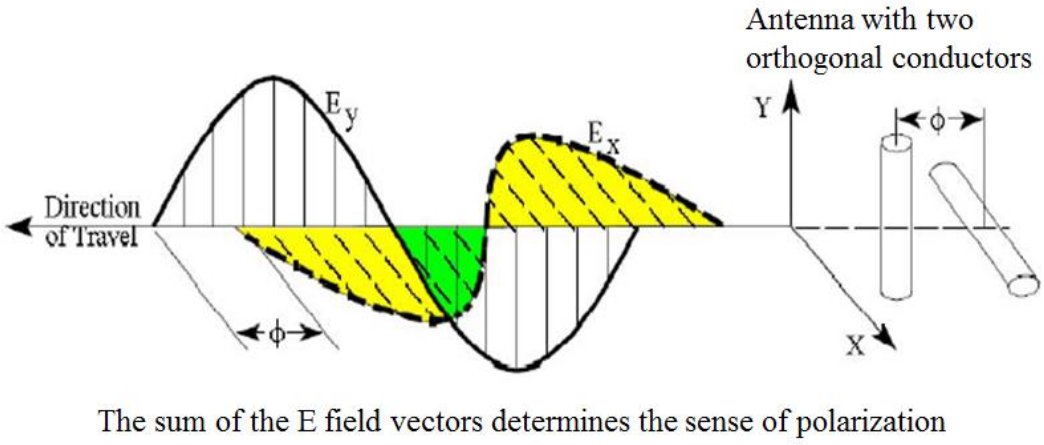

Fig. 2. 13 Orientation of the electric field in two dimensions *x* and *y*

The total E-field is the vector sum of the $\vec{E}_x$ and the $\vec{E}_y$ vectors. There are two special cases of elliptical polarization; linear polarization and circular polarization. A linearly polarized electromagnetic wave is comprised of a single electric component and the polarization is a fixed straight line. Linear polarization is further sub-divided into three types; vertical polarization, horizontal polarization and slant polarization. Vertical polarization is the one which travels orthogonal to the surface of the Earth and horizontal polarization travels parallel to the surface of the Earth.

A circularly polarized electromagnetic wave is the combination of two linearly polarized electromagnetic waves orthogonal to each other, having equal amplitude with 90 degrees out of phase. The axial ratio (AR) is the term used to describe the magnitude ratio of the two linearly polarized electric field components. In a circularly polarized wave the magnitude and axial ratio are equal, 1 or $0dB\left(10\log\left[AR\right]\right)$ and in linearly polarized waves the axial ratio is infinite.

2.10 Summary

In this chapter, an overview of Dielectric Resonator Antennas has been presented. The chapter started with introducing the Dielectric resonator from its historical prospective, followed by characteristics of the DR, materials used for DR, the applications of DR as antennas and different modes of excitations as well. The advantages and limitations of the DRA have been discussed with the concept of polarization and different coupling methods applied for DRA. The chapter also includes the discussion of different research work on bandwidth enhancements. Looking for today's demand in wireless communication for wide bandwidth application, the DRA can be a suitable candidate with high gain and low conductor losses.

Chapter 3

WIDEBAND SQUARE-RING DIELECTRIC RESONATOR ANTENNA

3.1 Introduction

Dielectric resonator antennas (DRAs) have largely been emphasized in last two decades because of several attractive features such as small size and light weight. Due to several advantages over the microstrip antenna such as wide impedance bandwidth, high radiation efficiency and small excitation of surface wave, DRAs have been introduced as vigorous candidates for wireless communications. The available basic shapes of dielectric resonators are cylindrical, rectangular and hemispherical, whereas different modified shapes are also possible, which include ring, disc, sectored cylindrical, half-split cylindrical, triangular, notched rectangular, conical and elliptical. Dielectric resonators were first popular as filter elements devices in microwave circuits. Recently the smaller size potential and higher frequency applications boosted the research into the dielectric resonator antenna.

Many applications such as direct digital broadcast, video conferencing, satellite communications, and wireless and radar applications require wide bandwidth. In a DRA, wideband is achieved for low values of a dielectric constant as the bandwidth of the DRA is inversely proportional to the dielectric constant [28-32]. Various enhancement techniques have been proposed to enhance the bandwidth of the DRA such as stair-shaped DRA [33] notched DRA [10], multilayer multipermittivity DRA [65], and tunnel DRA [36]. The bandwidth of a DRA can also be enhanced by adopting new feeding techniques [28], [66].

In this chapter, a U-shape microstrip line feed is used for exciting the proposed DRA. The Q-factor can be lowered as well as bandwidth can be improved by removing the central portion of the dielectric resonator. The shape of the DR element is taken as modified square, square-ring shaped, hence the name Square Ring Dielectric Resonator (SRDR) antenna. The SRDR antenna provides wide impedance bandwidth along with

satisfactory gain and radiation pattern characteristics for wideband application in WLAN bands.

3.2 U-Shaped Microstrip Fed SRDR

In the proposed work, an U-shape microstrip feeding technique is presented to excite a square ring dielectric resonator antenna. The U shaped feed line is chosen for better electromagnetic coupling between feed and the DR element. Wide band characteristics are obtained by the principle of decreasing the effective permittivity of the DR element. With proper design of the feeding network (here U shape microstrip feed line), the antenna structure has been arranged spatially in a particular fashion to get desired radiation pattern and gain.

3.2.1 Antenna Geometry and Design

In the proposed antenna, the SRDR is positioned symmetrically with respect to the U-shaped feed. It is shown in Fig 3.1(a) and the perspective view of the proposed ring dielectric resonator antenna is shown in Fig.3.1 (b). The defected ground plane is taken for support of wideband characteristics of the antenna shown in Fig 3.1 (c). The proposed antenna is pasted on FR-4 substrate of, $\varepsilon_{r1} = 4.4$, height $h_s = 1.58$ mm and loss tangent $(\tan\delta)$ of 0.001.

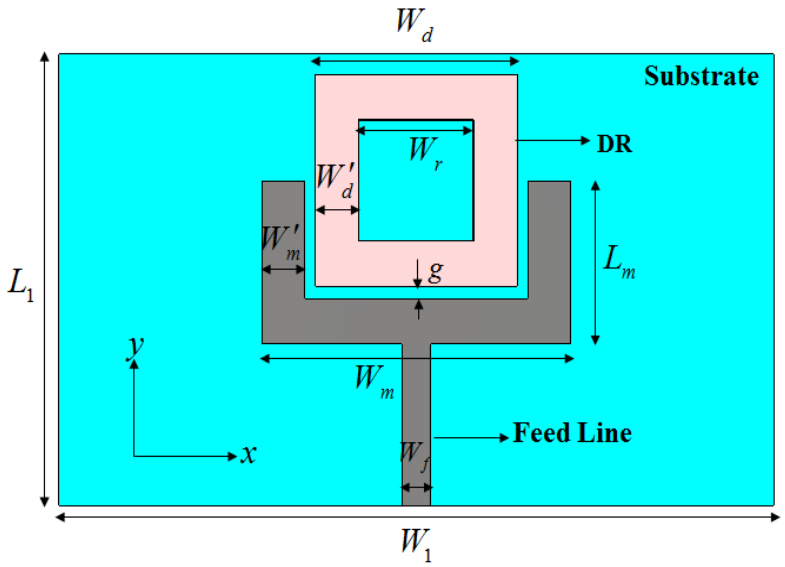

(a)

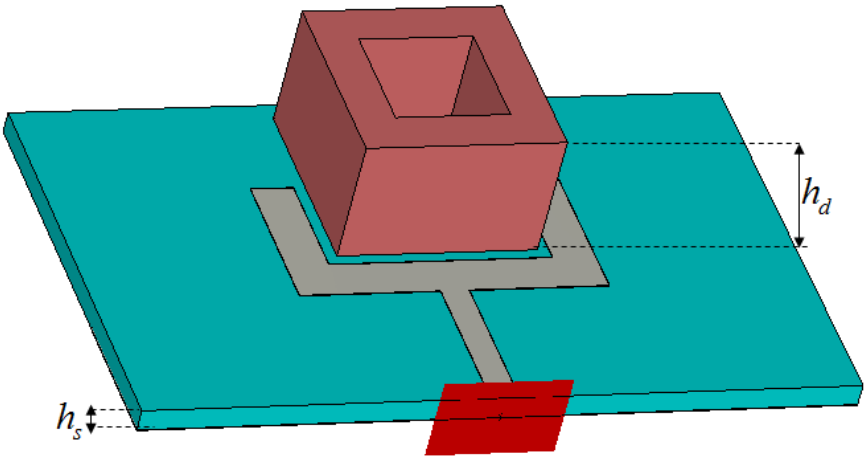

(b)

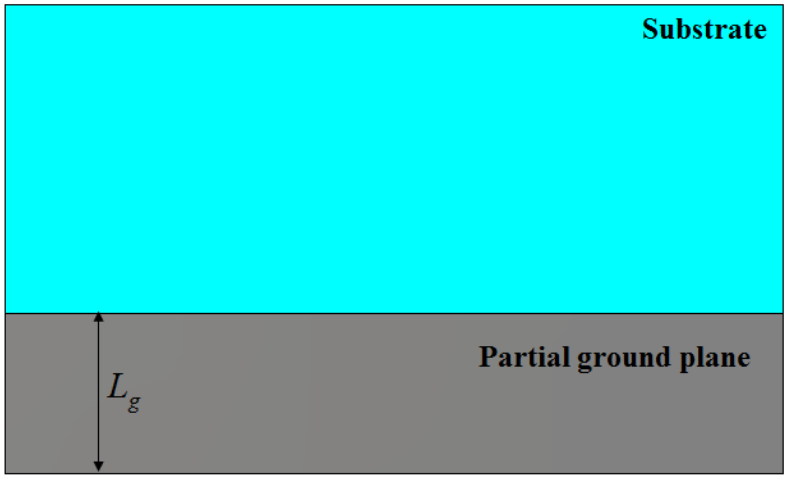

(c)

Fig. 3. 1 Proposed antenna, (a) Front view, (b) Perspective view, (c) Rear view

The SRDR of permittivity ($\in_r = 9.2$, Rogers TMM-10) is excited by 50 Ω branched microstrip line feeding offering an advantage of easy and cost-effective fabrication of the antenna. The feed line is terminated in an open circuit of U-shaped feed which creates a standing wave on the line where the voltage maxima or minima of each wave are located at multiples of $\lambda_g/2$ from the open-circuit location. The guided wavelength λ_g can be approximated using Equation(3.1), where ε_r is the relative permittivity of the dielectric resonator and λ_0 is the free space wavelength.

$$\lambda_g = \frac{\lambda_0}{\sqrt{\varepsilon_r}} \tag{3.1}$$

To find the wideband characteristics initially an arbitrary resonance frequency has been chosen falling under desired frequency of operation. For WLAN operation 4.4 GHz was chosen for the design process to be initialized. Square DR is designed at frequency of 4.4GHz by analysing the rectangular DR. The dimensions of the square DR at a particular resonant frequency can be found by analysis of rectangular DR with equal length and width [2].

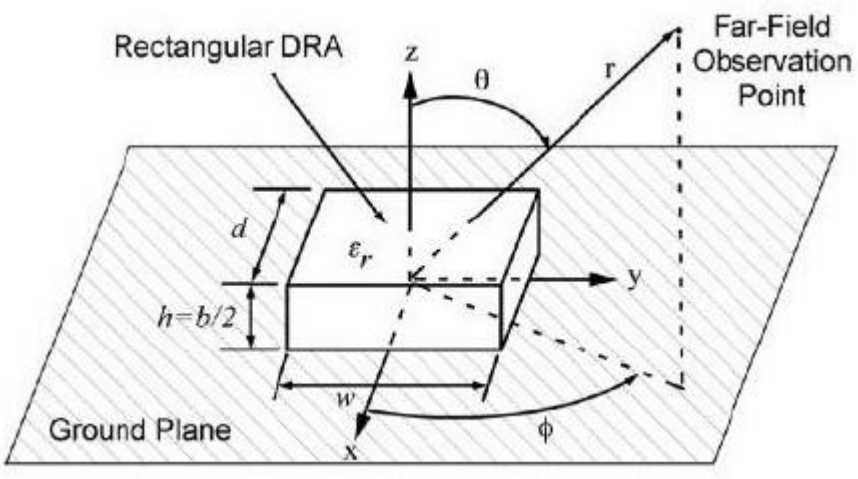

Fig. 3. 2 Geometry of the rectangular dielectric resonator

The rectangular dielectric resonator antenna as shown in Fig 3.2 is characterized by a height '*h'*, a width '*w'*, a depth '*d'*, and a dielectric constant 'ε_r'. The rectangular shape offers a second degree of freedom. A rectangular dielectric resonator gives more flexibility to the manufacturer making it more versatile in achieving the desired bandwidth characteristics for a given resonant frequency and dielectric constant. The ratios *w/h* and *w/d* can be chosen independently of each other. This helps to design either a resonator tall and slender or a thin and wide resonator by selecting the desired aspect ratio, depending on the particular application. An assumption of perfect magnetic walls for the four surfaces parallel to the longitudinal direction is made. The two end surfaces, normal to the direction of propagation are assumed to maintain a continuous transition of the tangential electric and magnetic fields. With the resonator placed on a ground plane, typically the *TE* modes are excited, but *TM* modes are possible as well. The *TE* modes radiate like short magnetic dipoles in the *x*, *y* and *z*-directions. The resonant frequency of each of these modes depends on the resonator dimensions. If $w > d > b$, unwanted modes will not appear in between these *TE* modes. By properly choosing a size, an undisturbed

frequency band of operation can be achieved. For the $TE^{x}_{\delta 11}$ mode, the resonant frequency 'f_0' is found by solving the following transdental equation

$$k_x \tan(k_x d/2) = \sqrt{(\varepsilon_r - 1)k_0^2 - k_x^2} \tag{3.2}$$

Where

$$k_0 = \frac{2\pi}{\lambda_0} = \frac{2\pi f_0}{c},\ k_y = \frac{\pi}{w},\ k_z = \frac{\pi}{b},\ \text{and}\ k_x^2 + k_y^2 + k_z^2 = \varepsilon_r k_0^2$$

The equation (3.2) has been solved for selected ratios of w/b as a function of d/b and the results can be represented by graph [2]. Using the particular values of the above two ratios, the normalized frequency 'F' can be defined as

$$F = \frac{2\pi w f_0 \sqrt{\varepsilon_r}}{c} \tag{3.3}$$

The equation (3.3) can also be rearranged in the more convenient form as

$$f_{GHz} = \frac{15F}{w_{cm}\pi\sqrt{\varepsilon_r}} \tag{3.4}$$

Where 'w' is expressed in cm, and the resonant frequency in GHz.

Using curve fitting the normalized frequency F can also be expressed by the following approximate equation

$$F = a_0 + a_1(w/b) + a_2(w/b)^2 \tag{3.5}$$

Where

$$a_0 = 2.57 - 0.8(d/b) + 0.42(d/b)^2 - 0.05(d/b)^3 \tag{3.6}$$

$$a_1 = 2.71(d/b)^{-0.282} \tag{3.7}$$

$$a_2 = 0.16 \tag{3.8}$$

The values of 'W_d' and 'h_d' are calculated using (3.4) and(3.5) which are found to be 13.57mm$\approx$14mm and, 8.64mm $\approx$ 9 mm respectively. These values are again compared with the results obtained from(3.2). Finally the next design process is considered fixing the calculated values of W_d and h_d. The radiator is excited via 50 microstrip line of 2mm width'W_f'. To enhance the impedance bandwidth air gap is introduced inside the square DR structure to make it square ring DR. Modifying the DR into square ring DR will decrease the effective permittivity hence the Q factor, and the bandwidth will be increased. The SRDR offers a compact configuration which does not require the use of

parasitic elements to broaden the bandwidth. The antenna performances are obtained by carrying out a detailed parametric analysis depicted in section 3.2.2. The dimensions of the antenna have been tabulated in Table 3.1.

Table. 3. 1 Dimensions of the SRDR antenna

W_d	W_r	W_d'	W_m'	L_m	g
14 mm	8 mm	3 mm	3 mm	10.8 mm	0.8 mm
W_m	W_f	W_1	L_1	h_d	L_g
21.6 mm	2 mm	50 mm	30 mm	9 mm	10.25 mm

3.2.2 Simulation Results and Parametric Analysis

The SRDR antenna with wideband response has been designed and analysed for WLAN applications. The results of the antenna discussed in terms of bandwidth response, input impedance, radiation pattern, and gain. The simulation studies for the proposed SRDR antenna have been carried out by using CST Microwave Studio suite™ 12, based on the three-dimensional finite integration time-domain (FITD) method. The wideband response requires decreasing of $Q-$factor. The central portion of the DR is notched out and the required dimensions of the inner square have been found by hit and trial method, suitable for the specific design. The parametric analysis of important design parameters have been carried out, where the other parameters not considered keeping constant. Figure 3.3 plots the antenna reflection coefficients by taking different dimensions of the inner cut portions to make the structure square ring. The inner side length W_r is varied against frequency. A shift in the higher cut-off frequency (with reference to -10 dB) towards the higher range can be noted with a distinct increase in W_r as expected. The W_r =5 mm provides the smallest -10 dB impedance bandwidth.

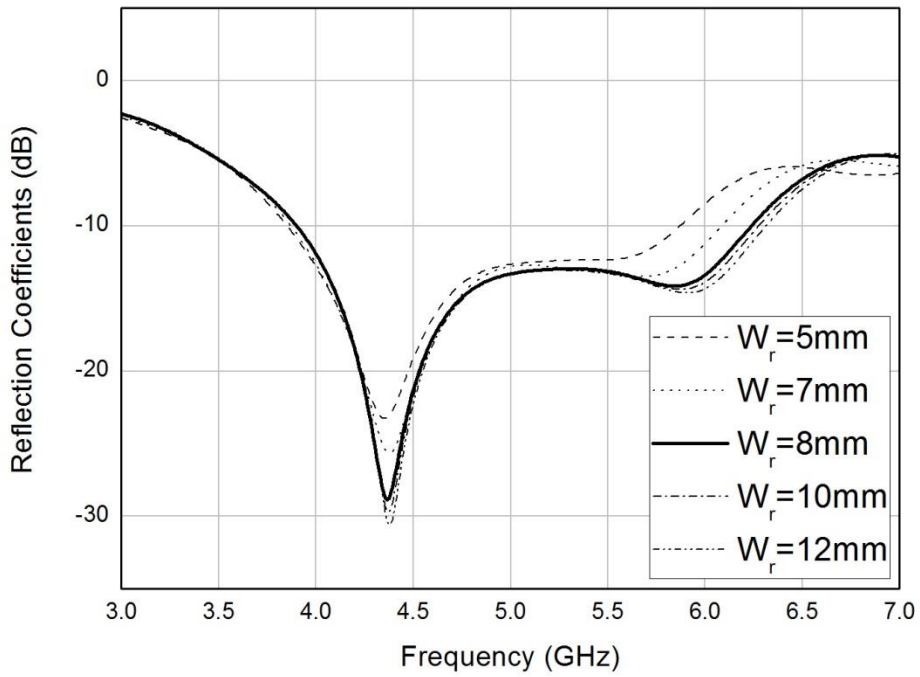

Fig. 3. 3 Comparison of Reflection coefficients for different values of W_r

It can be seen from the Fig 3.3 that the variation of W_r up to 8 mm increases the impedance bandwidth significantly but beyond 8 mm there is no significant change of bandwidth. The resonance frequency around 6GHz is due to the central notched out portion whereas the resonance of -30 dB deep at 4.3GHz is contributed by the square DR with the calculated dimensions found initially using(3.2). For the suitability of the design structure $W_r = 8$ mm has been chosen. The comparison of -10 dB impedance bandwidths with different values of W_r is presented in Table 3.2.

Table. 3. 2 Impedance bandwidths for different values of W_r

W_r (mm)	f_L (reference to -10dB) in GHz	f_H (reference to -10dB) in GHz	Impedance bandwidth in %
5	3.9	5.7	38.17
7	3.9	6.1	45.1
8	3.9	6.23	47.26
10	3.86	6.2	47.83
12	3.86	6.28	48.9

In order to identify the resonance modes of the antenna, its input impedance is plotted against frequency in Figure 3.4. The zero crossings on the reactance curve are identified as resonances which compares well with the dips in the reflection coefficient curve. Figure 3.4 shows that the DRA resonance takes place at around 4.3 GHz, where imaginary part of the impedance is zero while real part is around 50 ohm. The second resonance is taking place at around 6 GHz as depicted from impedance plot. This ensures about the matching of the U-shaped feed line to 50 ohm impedance. In Fig.3.5 comparison-plot of reflection coefficients with square-ring DR and square DR is provided. It is clear from the simulation results that square ring DR provides better reflection coefficients and covered bandwidth as compared with square DR. SRDR is considered taking W_r = 8 mm as analysed previously.

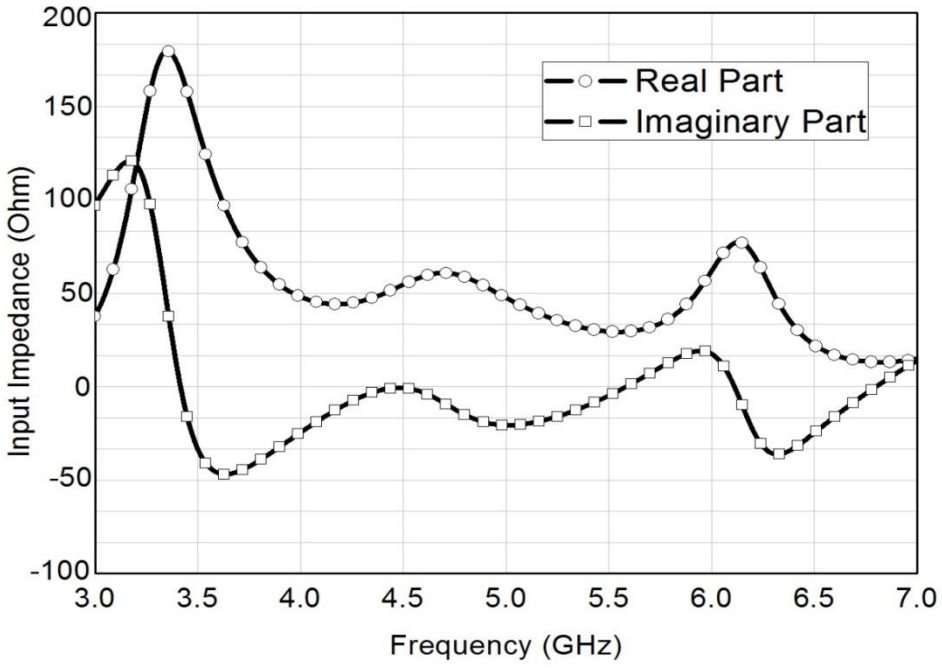

Fig. 3. 4 Simulated input impedance curve of the proposed antenna

The impedance bandwidth has been increased to 8% for SRDR antenna as compared to square DR. The matching with the U-shaped microstrip line feed is better for SRDR as compared to square DR. The reflection coefficient of -29 dB has been achieved as compared to square DR of 20 dB. Figure 3.6 shows the simulated reflection coefficient as function of gap W_d for the proposed antenna.

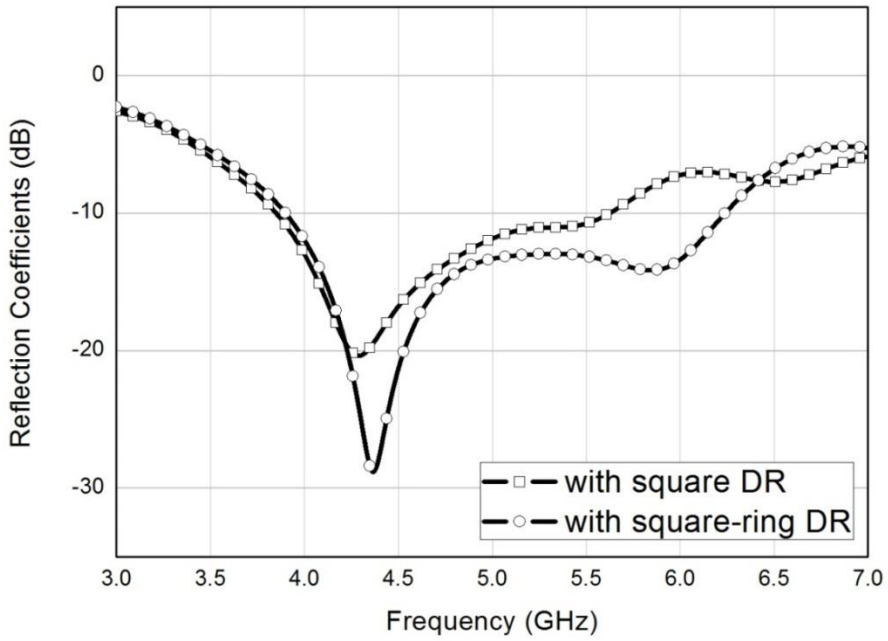

Fig. 3. 5 Comparison of reflection coefficients with square-ring DR and square DR

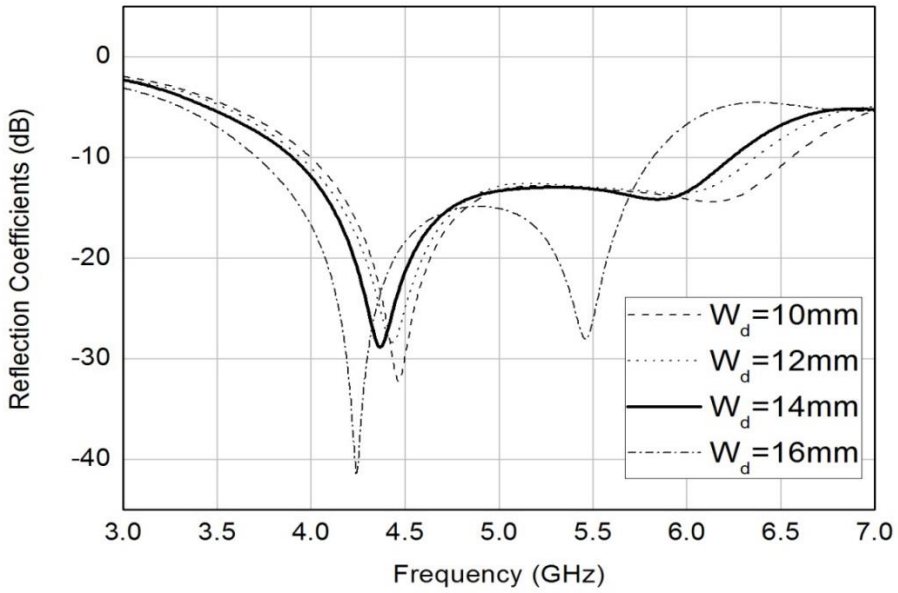

Fig. 3. 6 Simulated reflection coefficients of the SRDR antenna for different W_d values

The air gap (g) between the DR and U-shaped feed line is affected with the variation of W_d . The amount of coupling from the microstrip line to the SRDR can be controlled to a certain degree by adjusting the air gap. The 10 dB bandwidth of the proposed antenna

decreases as the gap is decreased or the W_d value increased. By increasing the gap beyond g =8 mm or W_d =14 mm the bandwidth remains almost constant, but the impedance matching around 6 GHz approaches to 5 GHz. In this case the entire bandwidth of 2.3 GHz has been achieved for w_d =14 mm. Hence the W_d =14 mm or g =8 mm has been considered for the design. Figure 3.7 shows the simulated reflection coefficient as a function of permittivity (ε_r) of the DR. The permittivity affects the degree of coupling of DR. The lower resonant frequency of the antenna is shifted to lower frequency as ε_r increased. For the upper-frequency region, with the decrease in ε_r value, the f_H value increases except for the ε_r =16.

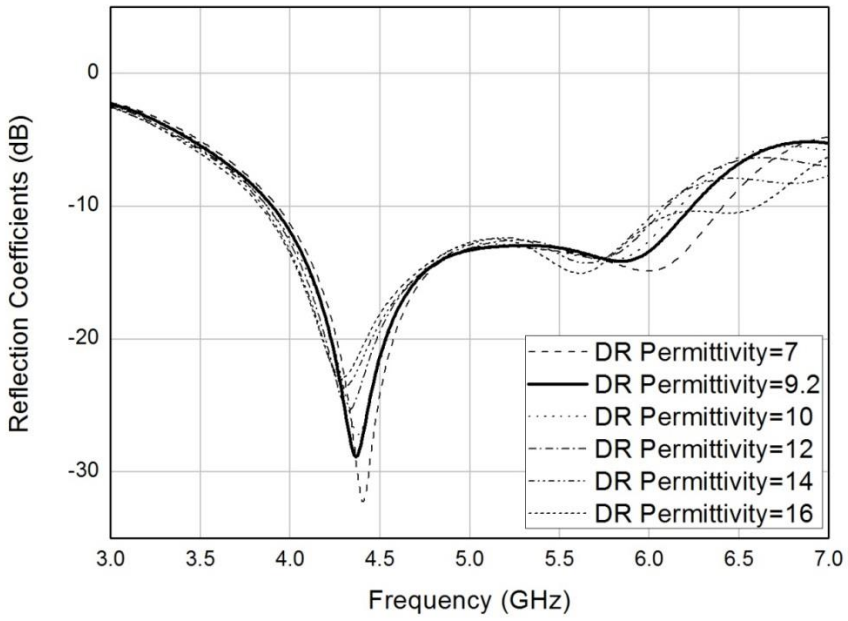

Fig. 3. 7 Simulated reflection coefficients of the SRDR antenna for different permittivity values

Another parametric study has been carried out by taking different heights of the ground plane L_g , shown in Fig 3.8. By setting different heights of the ground plane, the variations in the bandwidth curves are observed. It is concluded that for L_g = 10.25 mm, getting optimal covered bandwidth with -28dB of reflection coefficient value. For L_g value of 9.5, maximum reflection coefficient of –65 dB is achived but the bandwidth is the lowest. It can be concluded from the Fig 3.8 that there is always a trade off between

the reflection coefficient improvement and the bandwidth covered for different values of the partial groundplane heights.

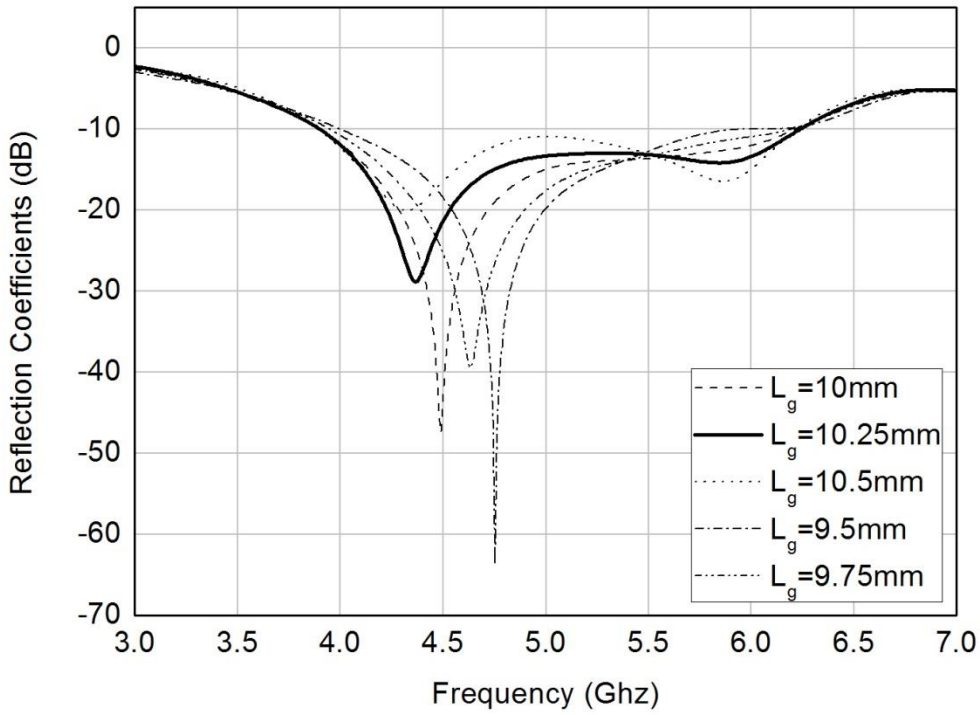

Fig. 3. 8 Simulated reflection coefficients of the SRDR antenna for different ground plane heights

Fig 3.9 and 3.10 show the simulated Co and cross polarized radiation patterns of E and H plane at resonant frequencies of 4.36 GHz and 5.9 GHz respectively. The H-plane radiation patterns are almost omnidirectional and the E-plane radiation patterns are in the broadside direction against frequency. Fig 3.9 shows that the cross polarization level is as low as around -18 dB for E-plane where as in case of H-Plane the cross polarization level is below -28 dB in the bore-sight direction. The radiation patterns show approximately symmetric characteristics for both the frequency of operation. It can be clear from Fig 3.10 that the cross polar rejection for E- plane is less than -25 dB whereas in case of H-plane it is around -20 dB in the direction of maximum radiation. The simulated radiation efficiency is found to be 91%.

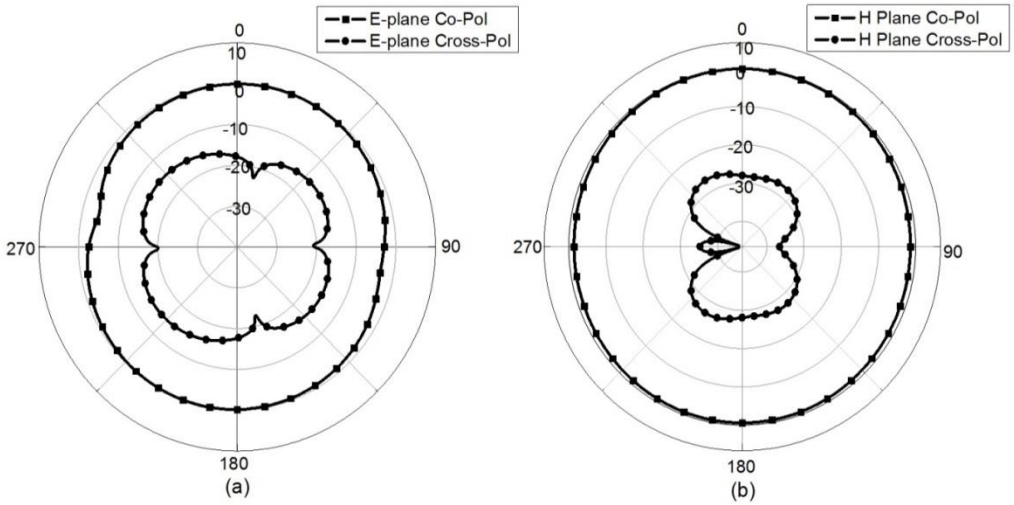

Fig. 3. 9 Simulated co-polar and cross-polar radiation patterns of the proposed SRDR antenna, (a) E-plane at 4.36 GHz, (b) H-plane at 4.36 GHz

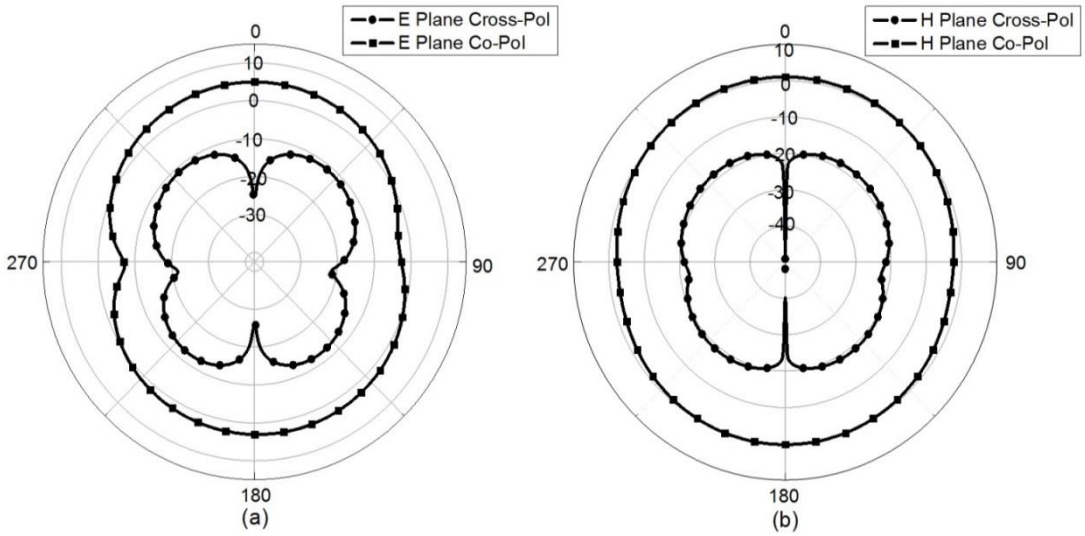

Fig. 3. 10 Simulated co-polar and cross-polar radiation patterns ofthe proposed SRDR antenna, (a) E-plane at 5.9 GHz, (b) H-plane at 5.9 GHz

Fig. 3.11 plots the simulated gain versus frequency of the proposed antenna, where the gain is 4.9 dB at 5.9 GHz and 3.1 dB at 4.36 GHz. The gain of the antenna is acceptable for the wide band of 4.36 GHz to 5.9 GHz.

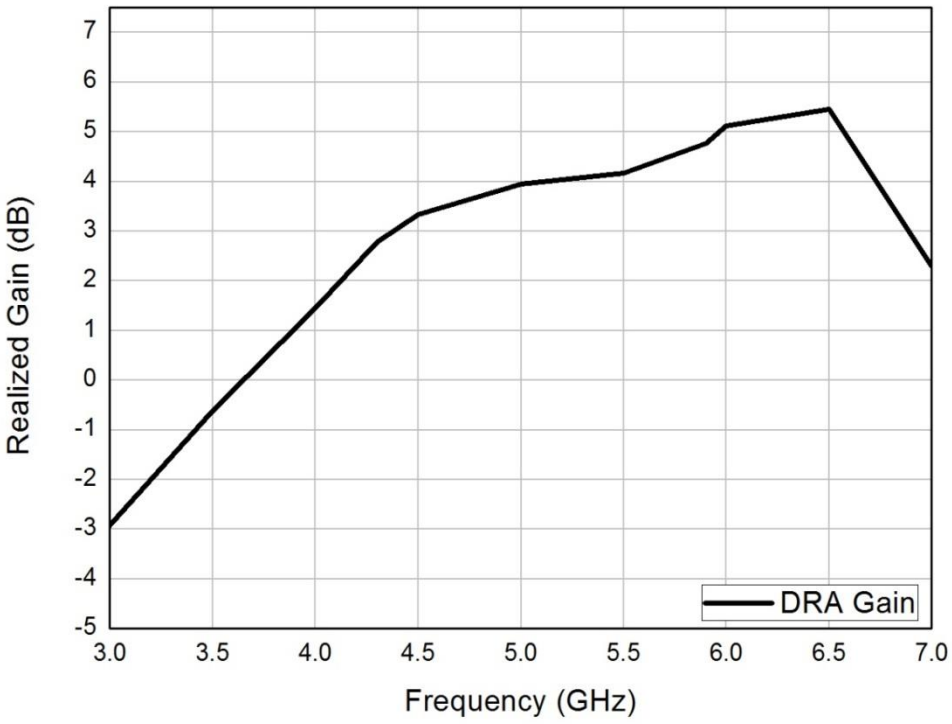

Fig. 3. 11 Simulated gain of the proposed SRDR antenna

3.3 Surface Currents and 3-D Radiation Patterns

The surface current distribution and the 3-D radiation patterns have been studied at the two resonant frequencies shown in fig. 3.12. The surface current distribution satisfies the radiation pattern. At frequency 4.9 GHz the surface current is more concentrated near the port and as the frequency increases the surface current is flowing more on the U-shaped feed structure. The radiation pattern for both the frequency of resonance is similar showing broad side radiation pattern for E-plane and omnidirectional for H-plane radiation pattern.

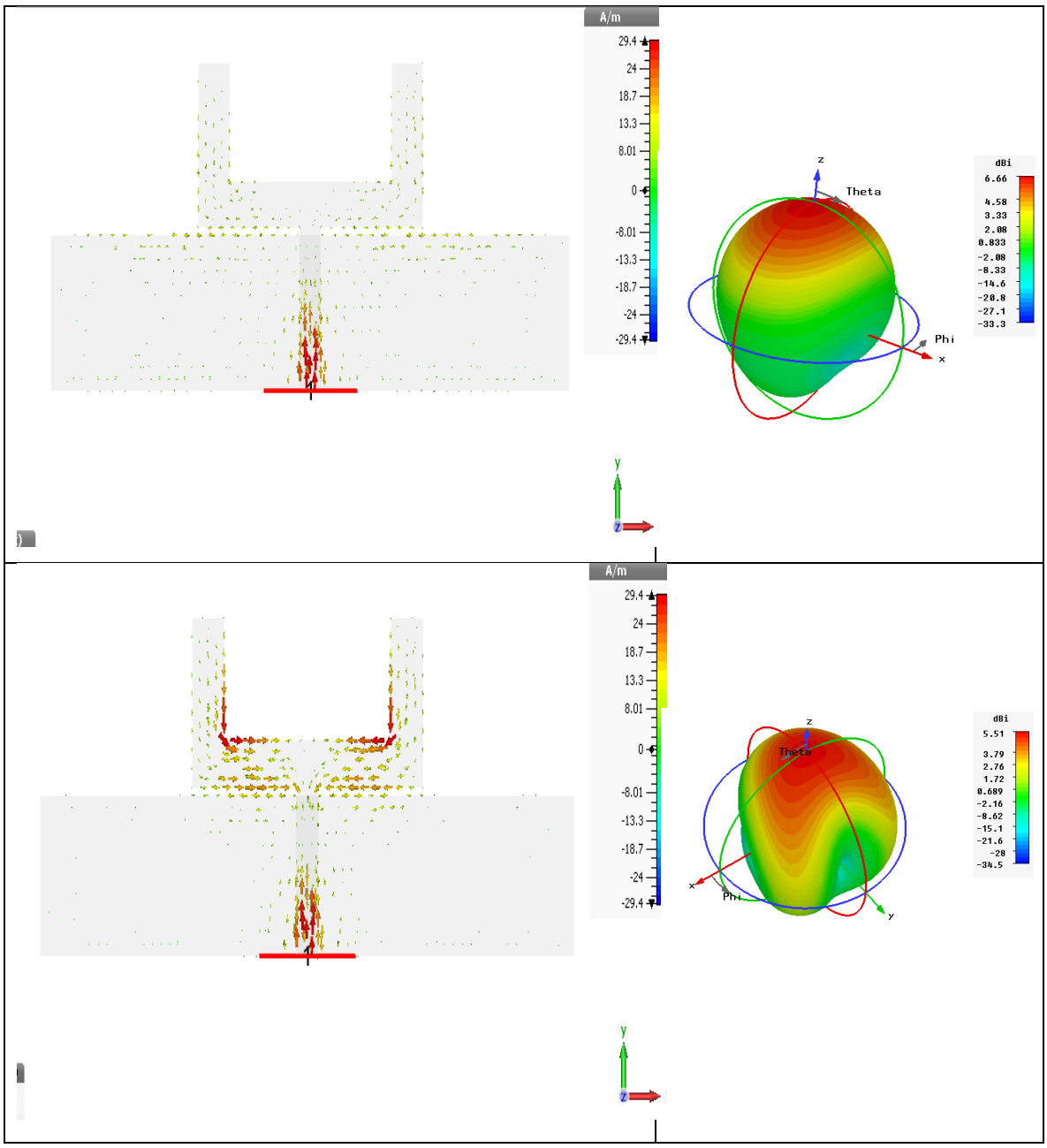

Fig. 3. 12 surface currents with the 3-D radiation patterns of the proposed antenna

3.4 Summary

A square ring dielectric resonator (SRDR) is presented with 'U'-shaped microstrip feed, which has been used to excite transverse mode in square ring dielectric resonator (SRDR). The simulated results demonstrate that the proposed DRA achieves an impedance bandwidth of 47.26 % for 3.9 GHz to 6.20 GHz, with simulated average gain of 4.9 dB at 5.9 GHz and 3.1 dB at 4.36 GHz respectively. The radiation efficiency is found to be 91%. Thus, it can be a good candidate for WLAN applications. The structure can also be easily integrated in planar circuitry. The small size of the structure renders it more useful for application at lower microwave frequency bands. The potential of the wideband antenna in short range communications are allowing equipment mobility and high data rates to facilitate information sharing. The high data rates can also be accomplished by polarization diversity performance as it can provide double transmission channels in a frequency reuse communication systems.

Chapter 4

DUAL-LINEARLY POLARIZED DIELECTRIC RESONATOR ANTENNA ARRAY FOR L AND S BAND APPLICATIONS

4.1 Introduction

The demand for increased information rate, while simultaneously reducing the multipath effects in modern wireless communication has raised the study of the polarization diversity antennas. It is relatively easy to realize a dual-polarized structure by making use of two ports in conjunction with a circular, square or annular microstrip antenna, but it is a challenge to design a structure that can support dual-band and dual-polarized operation. It is more challenging to achieve dual band with dual linear polarization [67-71]. In this case, Dielectric Resonator Antenna can be a suitable candidate. A fair amount of research has been performed to develop different feeding methods, various shapes of DRA with circular or linear polarizations [1], [3]. A dual polarized DRA with narrow bandwidth was reported in [7]. In this proposed work a cylindrical disk was excited by two orthogonal ports, which provides about 10% bandwidth. Dual polarized DRAs are very challenging at high frequencies for obtaining better isolation. In [46] a wideband dual polarized DRA was reported. The wideband has been achieved due to two step stair shaped DRA whereas dual polarization has been achieved due to cross-shaped slot of two orthogonal ports. Microstrip lines are terminated with U-shaped tuning stub to optimize the matching. Both ports are able to give more than 20% bandwidth. Recently dual-band and dual polarized antenna arrays have been widely studied for satellite and wireless communication applications, particularly for synthetic aperture radar (SAR) applications. A dual-band dual polarized antenna array design for WLAN applications is presented in [47]. A phased array by interleaving two types of dual-polarization elements to achieve dual-linear or dual-circular polarizations is presented in [48].

Two high input-isolation dual-polarized dielectric resonator (DR) antennas are presented in [7]. First, a slot-coupled feed technique with two narrow slots forming a “T” configuration is employed to design a dual-polarized DR antenna. Input isolation more than 35 dB has been obtained in the band for this design. Secondly, a hybrid feed

mechanism with a coplanar waveguide (CPW) feed and a slot feed is used to achieve a dual-polarized DR antenna. In [49], a dual-band dual-polarization stacked microstrip-dielectric antenna is analysed and designed. It transmits left-hand circularly polarized (LHCP) signals in L band and receives right-hand circularly polarized (RHCP) signals in S band. The antenna has been realized by two stacked square patches which are fed by four quadrature pins placed symmetrically on the two main axes.

In this chapter a hybrid feeding method has been used to design a 2×2 DRA array. A matching slot is suitably used between the two feeding points to get better isolation coefficients. A matching strip is properly placed in between the probe and the DR to get perfect electromagnetic coupling. The feeding network is designed using T-splitters and connected to four DRs to form a planar array.

4.2 Dual-Polarized DRA array in L and S band Operation

A 2×2 cylindrical dielectric resonator antenna (DRA) array, where each element is excited by a slot orthogonally placed to a strip fed probe is presented. The proposed design provides dual linear polarization with high isolation exceeding 36 dB in L-band and 40 dB in S-band operations respectively. The HEM_{111} and HEM_{113} modes have been considered to generate dual mode in cylindrical DRA to yield broadside radiation pattern. The DRA radius is slightly increased from its calculated value to reduce the dependencies of two DRA modes because of strip fed excitation. The co-polarization level in both planes is found to be nearly 35 dB higher than the cross-polarization in bore-sight direction. The proposed 2×2 cylindrical dielectric resonator antenna (DRA) array has been achieved -10 dB impedance bandwidth of 21% for 1.16 to 1.43 GHz (in L-Band) and 4.54% for 3.35 to 3.2 GHz(in S-Band) respectively. The radiation patterns with nearly broadside patterns are found to be stable with the realized gains of 9.6 dB and 10.7 dB for resonant frequencies of 1.28 GHz and 3.3 GHz respectively.

4.2.1 Antenna Design and Geometry

The proposed antenna geometry of the dual band and dual linear polarized DRA with slot and strip coupling technique is shown in Fig 4.1. The permittivity of the DR,(ε_r=6, Magnesium Aluminium Silicate) has been used. The DR is placed symmetrically above a substrate FR4 of 1.6 mm thickness with permittivity of ε_{rs}=4.3 and a size of 15×15 cm^2. A matching strip line is used to excite the DR, which is energized by a probe of height 5mm placed on the microstrip feed line of width w_f.

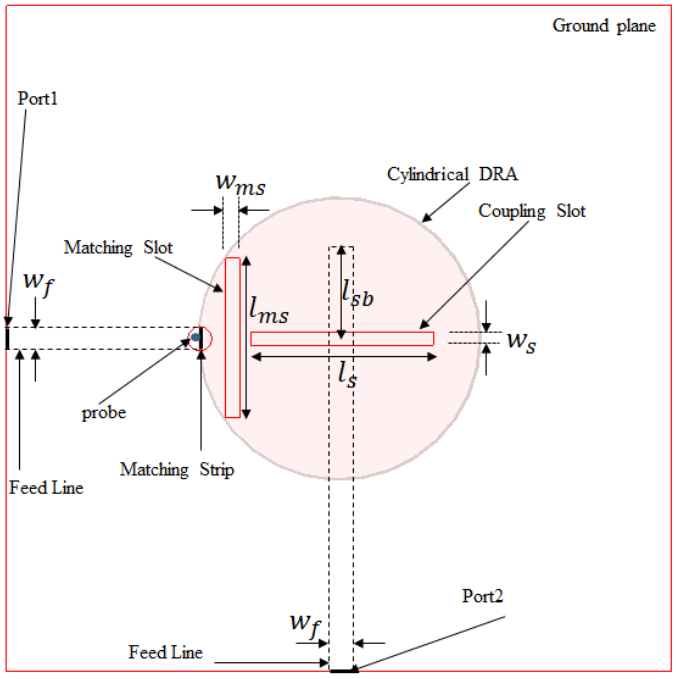

(a)

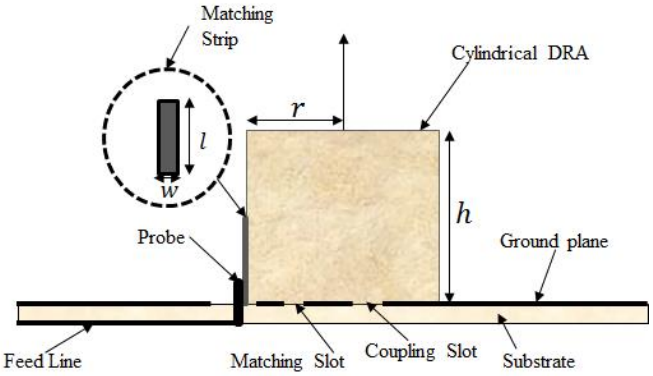

(b)

Fig. 4. 1 Dual-Linear polarized Dual Band Dielectric Resonator Antenna

(a) top view, (b) bottom view

Another slot is placed at the centre being excited by microstrip feed line directly. To get the better reflection coefficient value, the matching slot is introduced to the structure. The level of coupling can be adjusted by varying the relative coordinates of the matching slot and coupling slot. The distance of the matching slot is 24.6 mm from the DR centre. For cylindrical DRA of radius 'r' and height 'h' the field distribution can be described in terms of Bessel functions [6] as in (4.1)

$$\text{For TM mode: } E_z^{nmp} = J_n\left\langle (X_{np}^{TM} r)\middle| r\right\rangle \{\sin(\mathrm{n}\,\phi)\cos[(2\,\mathrm{m}+1)\pi\,\mathrm{z}/2h\} \tag{4.1}$$

$$n = 1,2,3....; \text{p} = 1,2,3...; \text{m} = 0,1,2...;$$

where J_n is the nth order Bessel function of the first kind. While X_{np}^{TM} is the root that satisfies the corresponding characteristic equation (4.2)

$$J_n(\text{X}_{np}^{TM}) = 0 \tag{4.2}$$

In the following formulations, for subscript $i = 1$ the fundamental mode is HEM_{111} and for $i = 2$ the higher order mode is HEM_{113}. $k_{\rho i}$ and k_{zi}, are the dielectric wave numbers along the radial (ρ) and axial (z) directions respectively. The resonance frequency f_i of the DR can be obtained from

$$k_{\rho i}^2 + k_{zi}^2 = \varepsilon_r k_{0i}^2, i = 1,2 \tag{4.3}$$

where $k_{0i} = 2\pi f_i / c$, is the wave number in the air, and c is the speed of light in the vacuum. The characteristic equation (4.4) can be used to find the wave number $k_{\rho i}^2$ taking $(i = 1,2)$

$$\left(\frac{j_m'(k_{\rho i}r)}{k_{\rho i} j_m(k_{\rho i}r)} + \frac{k_m'(k_{\rho i}'r)}{k_{\rho i}' k_m(k_{\rho i}'r)}\right).\left(\frac{\varepsilon_r j_m'(k_{\rho i}r)}{k_{\rho i} j_m(k_{\rho i}r)} + \frac{k_m'(k_{\rho i}'r)}{k_{\rho i}' k_m(k_{\rho i}'r)}\right) = \frac{m^2(k_{\rho i}^2 + k_{\rho i}'^2)(k_{\rho i}^2 + \varepsilon_r k_{\rho i}'^2)}{(k_{\rho i}k_{\rho i}')^4 r^2} \tag{4.4}$$

Where

$$k_{\rho i}' = \sqrt{(\varepsilon_r - 1)k_{oi}^2 - k_{\rho i}^2} \tag{4.5}$$

$k_{\rho i}'$ is the radial wave number outside the dielectric rod. $j_m(x)$ and $k_m(x)$are the Bessel function of first kind and the modified Bessel function of the second kind respectively. It has been taken $m = 1$ for this study. Next the axial wave number k_{zi} can be approximated by the TM_{01} mode wave number of infinite dielectric slab guide. The characteristic equation of the TM_{01} mode is given by

$$\frac{hk_{zi}}{p_i} = \tan^{-1}\left(\frac{\varepsilon_r\sqrt{\left((\varepsilon_r - 1)k_{0i}^2 - k_{zi}^2\right)}}{k_{zi}}\right) \quad i = 1,2 \tag{4.6}$$

Where $p_1 = 1$and $p_2 = 3$ for HEM_{111} and HEM_{113} modes respectively. The mathematical expressions (4.3) and (4.6) have been used to find out the radius and height of the DR element, for resonant frequency. The radius r has been increased to 31.42mm whereas the calculated value was 30mm to avoid the merging of the two modes of the DRA. The parametric analysis of the important design parameters have been carried out in the section 4.2.2. The resulting optimal design parameters of the proposed antenna are tabulated as in Table 4.1.

Table. 4. 1 Dimensions of the proposed antenna

DR Radius (r)	DR Height(h)	Width of the feed (w_f).	Stub length (l_{sb})	Coupling slot length (l_s)
31.42 mm	69 mm	4.9mm	13 mm	41.2 mm
Matching strip width (w)	Matching strip length (l)	Matching slot length (l_{ms})	Matching slot width (w_{ms})	Coupling slot width (w_s)
4.4 mm	25.4 mm	36 mm	3 mm	3.1mm

This approach not only allows placing the coupling slot accurately under the central region of the DR but also supports to manipulate the matching slot and excitation strip positions to improve the port isolation to 36 dB.

4.2.2 Simulation Results and Parametric Analysis

In reference to Fig. 4.1, there are number of parameters that influence the antenna characteristics. To achieve optimum antenna performance, a parametric study is carried out to investigate the characteristics of the DR antenna. The initial parameters for this design have been chosen as, $r = 31.42mm$, $h = 69mm$, $l_s = 41.2mm$, $W_s = 3.1mm$. The length and width of the 50 ohm microstrip line for port-1 are chosen to be 4.9 mm and 43.57 mm. The width of microstrip line for port-2 is same for 50 ohm impedance match with length as 88mm. Figure 4.2 plots the simulated reflection coefficients for Port 1 with different values of probe height ‘h’.

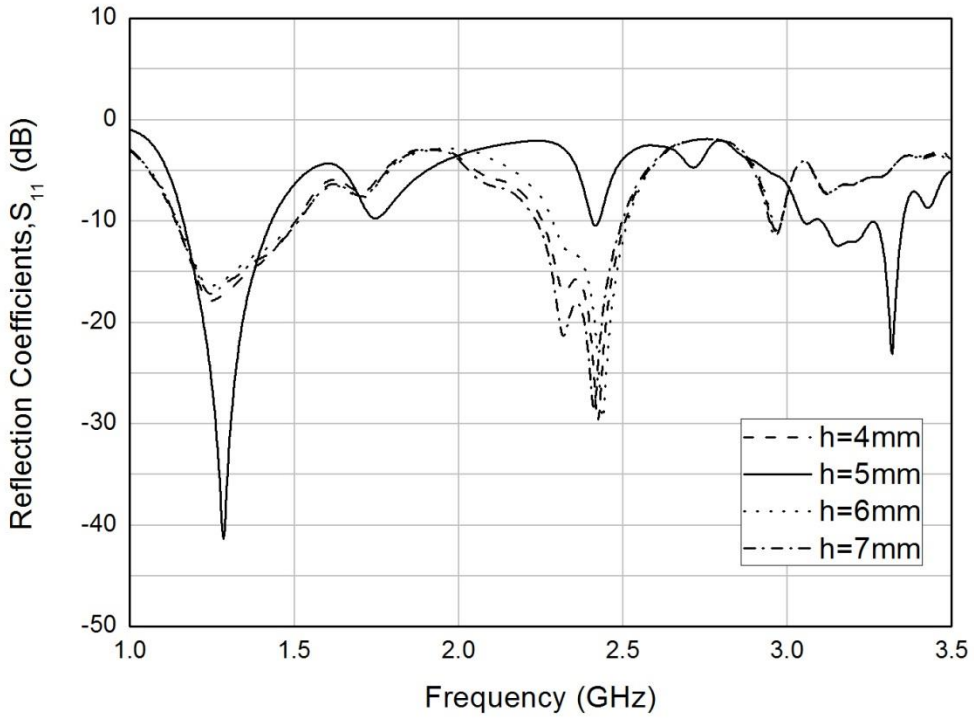

Fig. 4. 2 Simulated reflection coefficients at port-1 for different values of probe height

In probe feeding mechanism, the height of the probe controls the coupling between the feed and DR. The resonant frequency of the DRA varies as the value of *h* changes. The 'h' value of 5 mm corresponds to better reflection coefficient value of -42dB at 1.28 GHz and of -25dB at 3.3GHz. This resonance may be due to the effect of probe with the matching slot, which is not required for our frequency of operation. For further design, h=5 mm has been chosen. Maintaining this value constant, the effect of reflection co-efficient at port-2 has been studied, as shown in Fig 4.3. The reactance value can be nullified by taking different stub lengths. The stub length corresponding to the less reactance value is suitable for the design process. To get dual polarization characteristics, the proposed antenna should share same frequency of operation for individual port operation. That is the reflection co-efficient values for both the ports should be tuned to share same impedance bandwidth. From Fig 4.3 it is clear that with increase in stub length better reflection coefficient values are achieved. For l_{sb} = 12 mm there is slight downward shift of resonance frequency is observed.

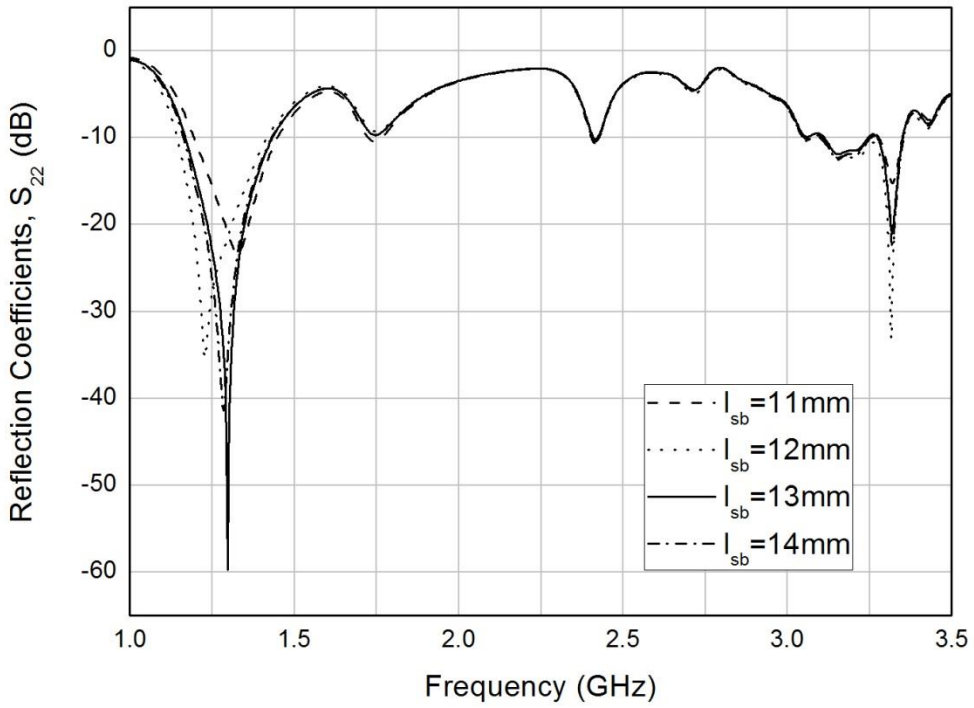

Fig. 4. 3 Simulated reflection coefficients at port-2 for different values of l_{sb}

l_{sb} =13 mm corresponds to the better matching with the reflection coefficient value of -60dB at port-2. The high isolation of two ports is achieved by using the hybrid feeding mechanism, one port connected to the probe and another with aperture fed. Dual polarization characteristics demand good agreement of isolation between the two excitation ports. As isolation is a decisive parameter for dual linear polarization further investigations have been carried out. The Fig 4.4 shows the effect of the matching slot length in between probe and coupling slot, with the isolation between the ports. The isolation between the ports is found to be more than 41dB at both the frequency of operation. Except the value of l_{ms} =35 mm, rest of the analysed values corresponds to the isolation less than 40 dB. For resonance frequency of 3.3 GHz isolation coefficients is better than 55 dB as favourable conditions for dual linear polarization.

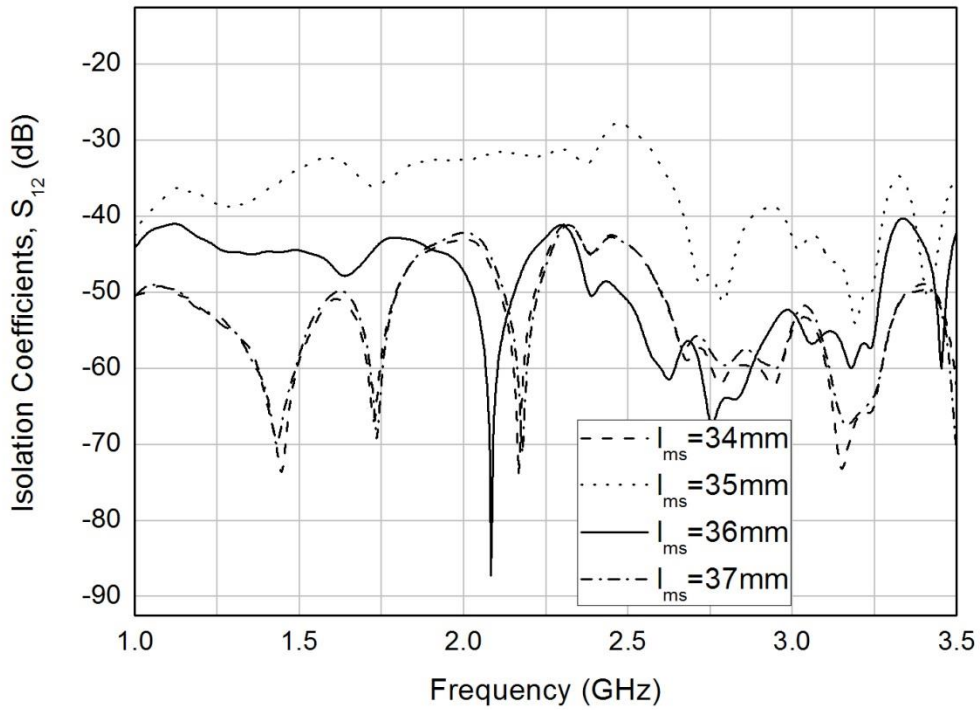

Fig. 4. 4 Isolation between two ports with different values of l_{ms}

4.2.2.1 Combined Performances of Port-1 and Port-2

Reflection curves are found to be shifted slightly when both ports working independently. Based upon the values as tabulated in 4.1 the two ports reflection co-efficient and isolation are shown in Fig 4.5 and Fig 4.6 respectively.

There is an excellent performance for shared impedance bandwidth for port-1 and port-2, from 1.16 GHz to 1.44GHz (in L-band) and from 3.16 to 3.4 GHz (in S-band). At the frequency of operation 1.28GHz the impedance bandwidth is 21.1% whereas at the frequency of operation at 3.3 GHz the impedance bandwidth is 6.86%. In Fig 4.6, the isolation between the ports is below 42 dB throughout the frequency of 1 GHz to 3.5 GHz, whereas at near to 1.28 GHz, it is below 50 dB in L band and below 65 dB around 3.3GHz in S band of operation.

The detailed EM behaviour of the antenna is revealed by examining the surface current distributions and the radiation patterns. The surface current distribution of the antenna substrate close to the resonance frequencies and their corresponding simulated 3D radiation patterns are plotted in Figure 4.7.

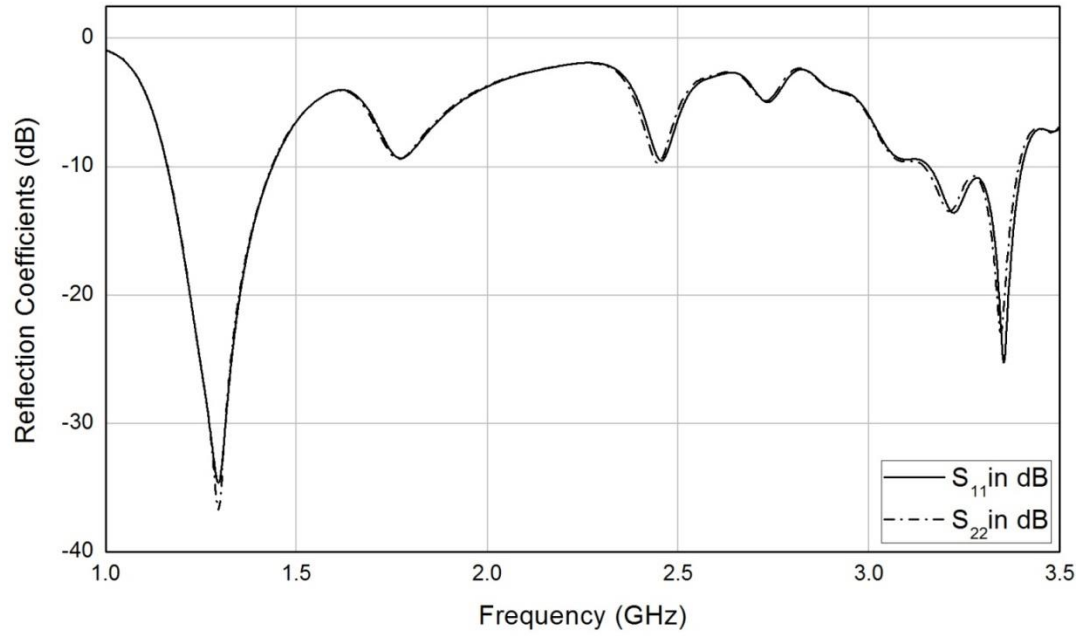

Fig. 4. 5 Simulated reflection coefficients at two ports

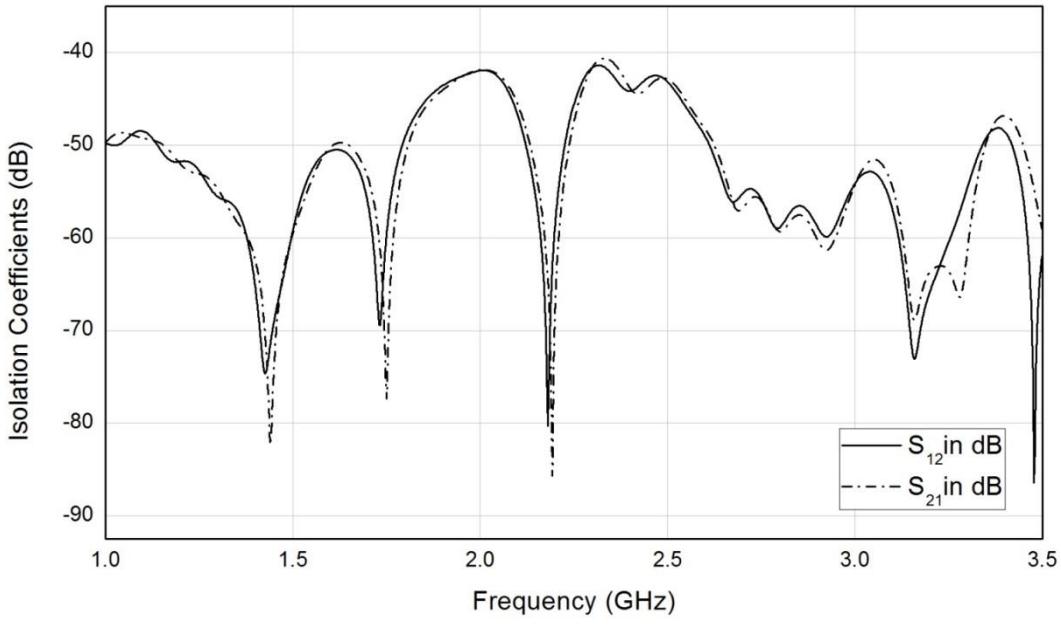

Fig. 4. 6 Simulated Isolation coefficients between two ports

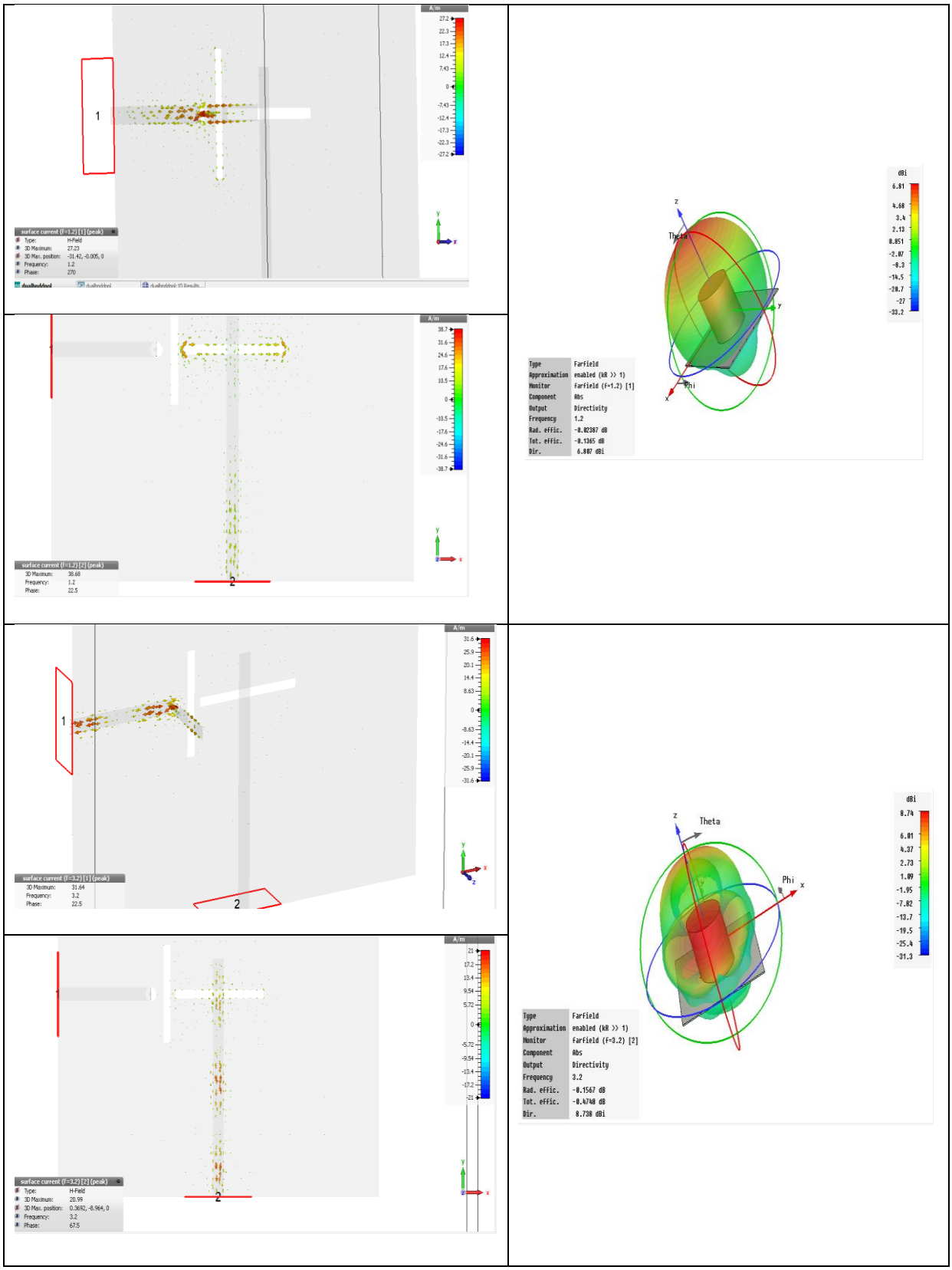

Fig. 4. 7 Simulated surface currents distribution of the prototype antenna along with its simulated radiation patterns at 1.2GHz and 3.3 GHz

The E and H plane far-field radiation patterns with co and cross polarizations, for port-1 and port-2 are shown in Fig.4.8 and Fig.4.9 respectively. The co-polarization level is found to be nearly 20dB higher than the cross-polarization level for both E and H plane radiation patterns in bore sight directions. Symmetric radiation patterns are found for both the ports.

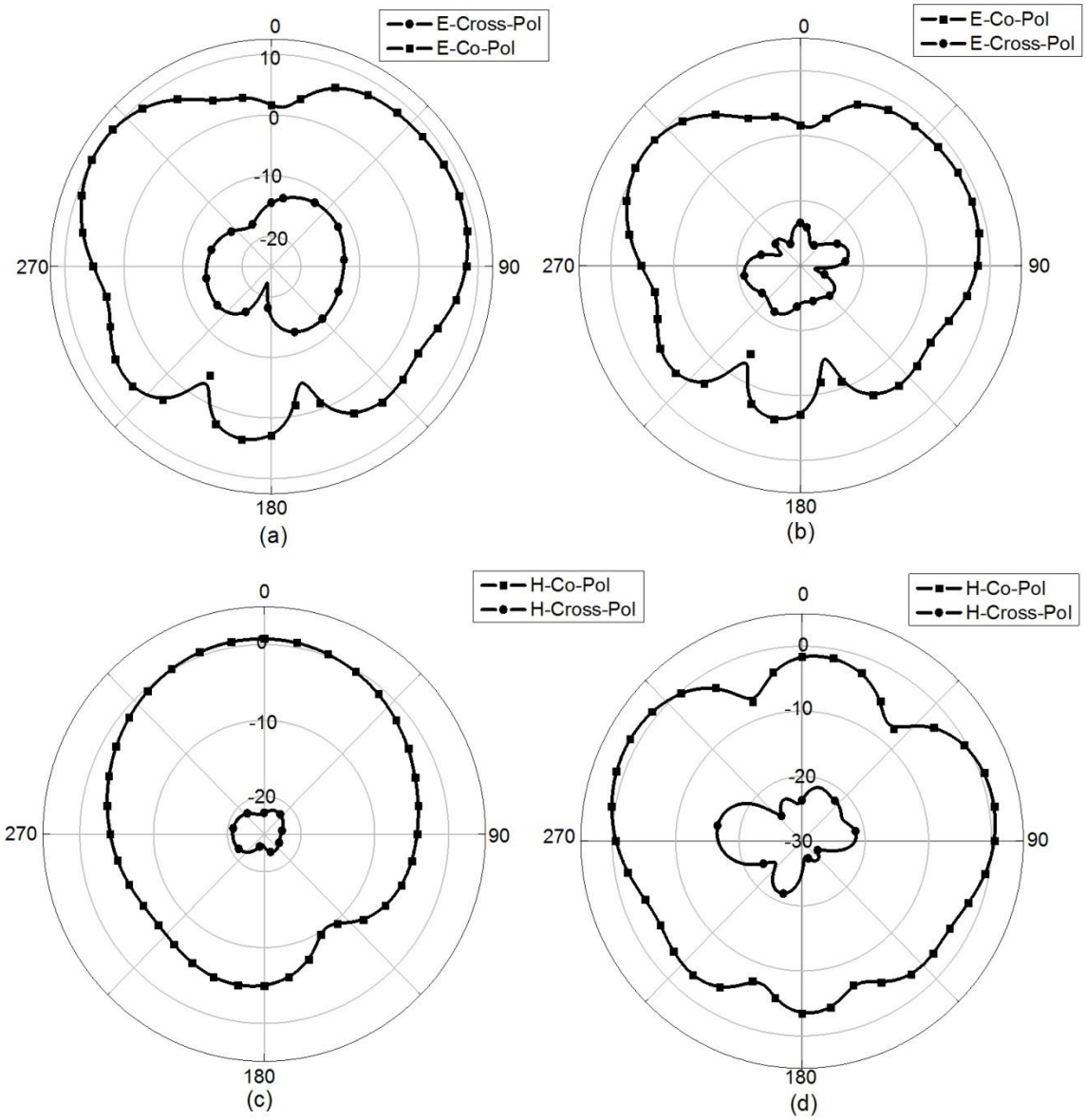

Fig. 4. 8 E-plane radiation patterns (a) at 1.28GHz (b) at 3.3 GHz. and H-plane radiation patterns (c) at 1.28GHz (d) at 3.3GHz of the proposed antenna for port-1

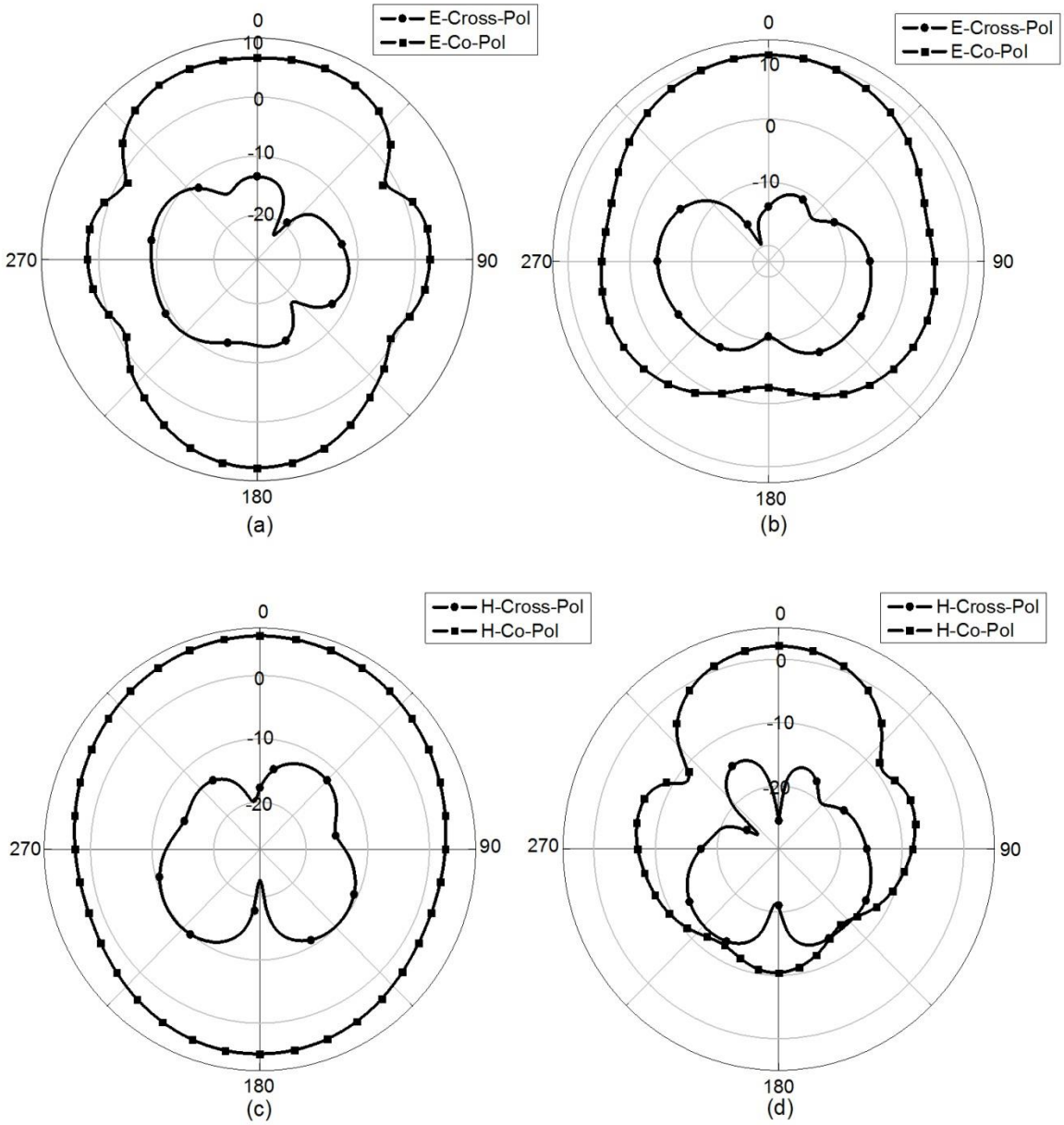

Fig. 4. 9 E-plane radiation patterns (a) at 1.28GHz (b) at 3.3 GHz. and H-plane radiation patterns (c) at 1.28GHz (d) at 3.3 GHz of the proposed antenna for port-2

4.2.3 Design of an Array

The array of 2×2 elements has been designed with substrate area of 31.5cm^2 as shown in Fig. 4.10. The inter element distance is maintained less than the guided wave length for resonance. The power distribution to each element of the array has been carried out by placing T-splitter microstrip feed line with quadrature wave transformer for impedance matching. The distribution of the feed network is maintained so as to decrease the coupling effect.

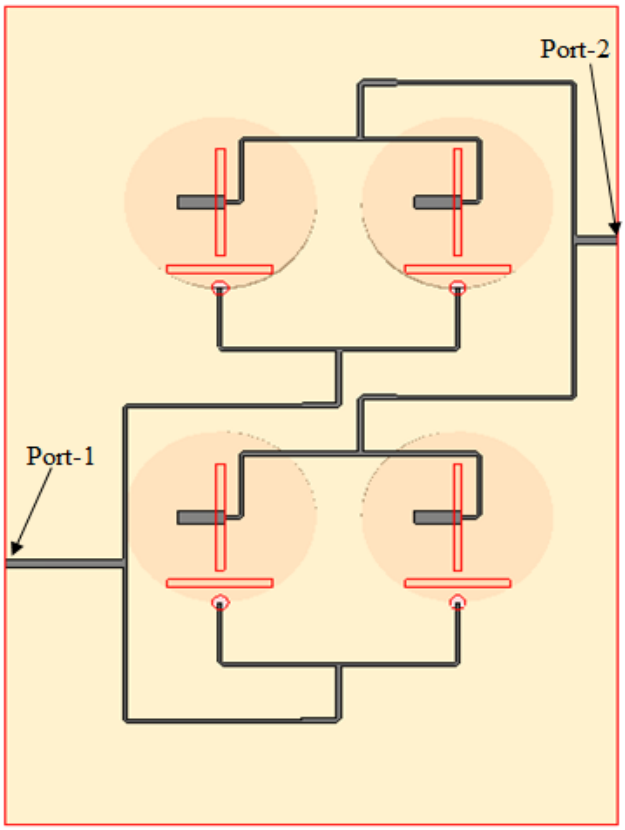

Fig. 4. 10 Schematic view of the proposed antenna array.

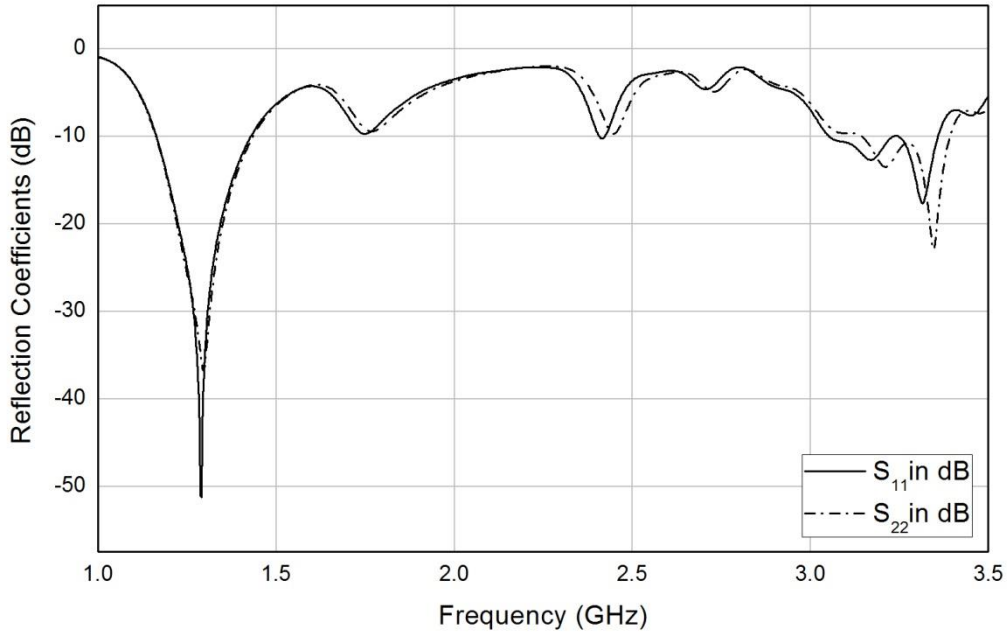

Fig. 4. 11 Simulated reflection coefficients of the proposed antenna array

The simulated reflection coefficients (S_{11} and S_{22}) and isolation (S_{12}) are shown in Fig. 4. 11 and 4.12 respectively. The common impedance bandwidth of 1.16 GHz to 1.43 GHz

(in L-band) is found to be 21% while for 3.2 GHz to 3.35GHz (in S-band) the bandwidth has been decreased to 4.54%. The Isolation of 36dB in L-band and of 40dB in S-band operations has been achieved.

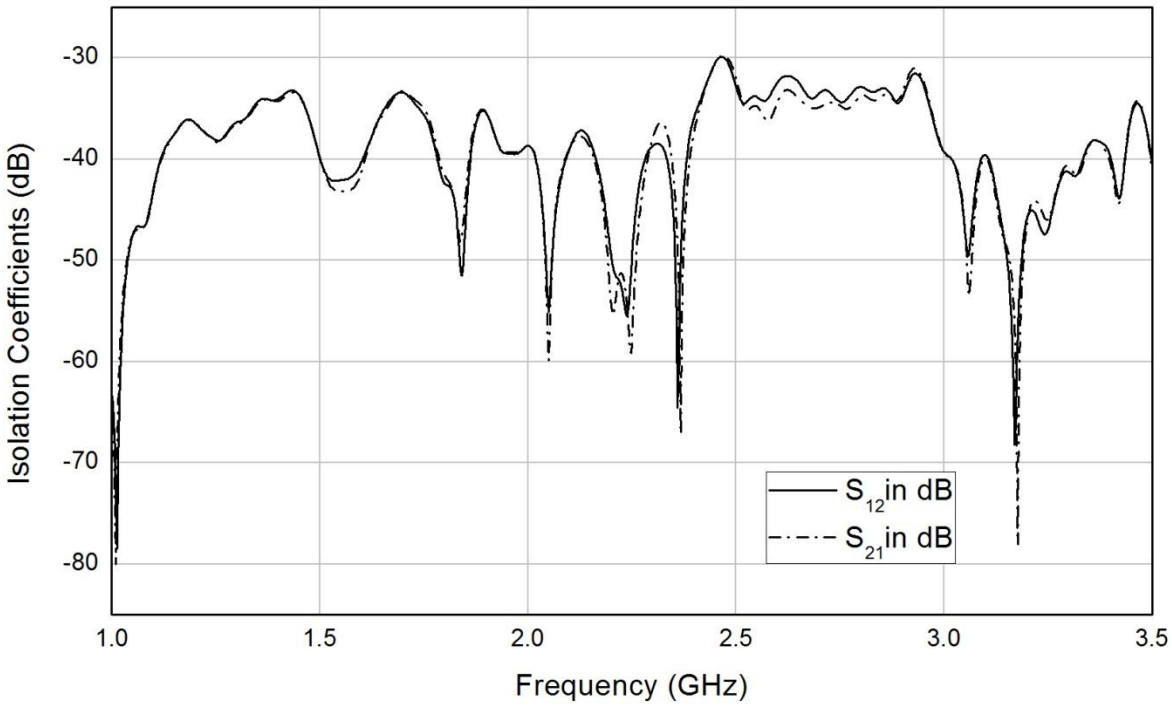

Fig. 4. 12 Simulated isolation coefficients of the proposed antenna array

Figure 4.13 shows the simulated 3D radiation patterns for the antenna array with the surface current distribution at each port. The behaviour of the aperture is like a magnetic current which runs parallel to the length of the slot and excites the magnetic field of the dielectric resonator antenna. Fig 4.13 describes that the surface current enters to the slot of resonance and as a whole acting as a magnetic current. If the aperture size is adjusted or the dielectric resonator antenna is moved with respect to the aperture, the coupling level can be adjusted. The feeding network is kept below the ground plane which gives the advantage of avoiding spurious radiation. Moreover, slot aperture is widely used for integrating the dielectric resonator with the printed feed structure. Through coaxial probe feed, the pin of the coaxial transmission line is extended through the ground plane. As

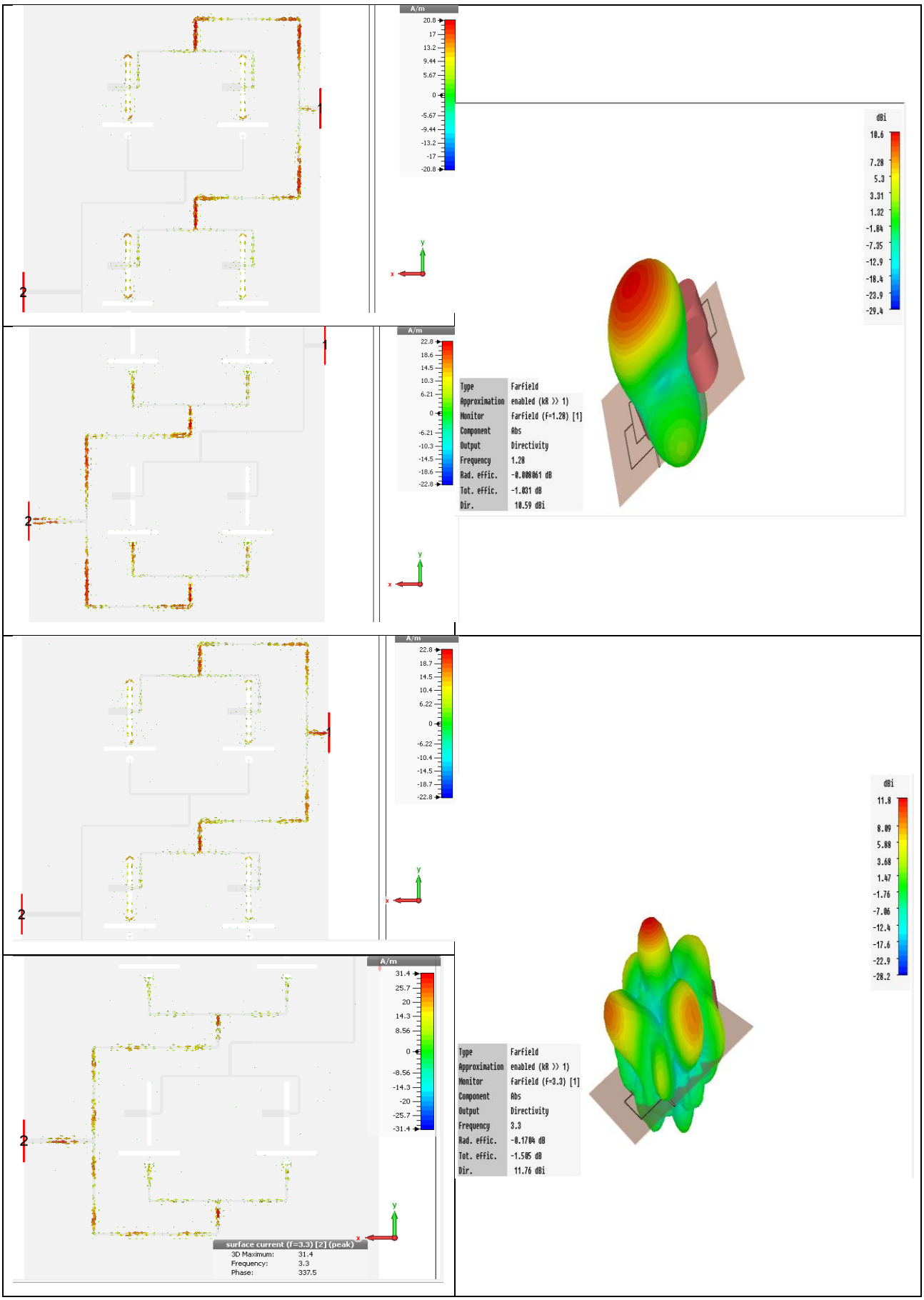

Fig. 4. 13 The simulated 3D radiation patterns for the antenna array with the surface current distribution at each port

shown in Fig 4.13 the surface current is flowing to the probe acts as an electric current running vertically through the dielectric resonator antenna. The strength of the coupling depends on the length of the probe and different modes can be activated by changing the location of the probe, depending on the desired mode. The matching strip is placed for better impedance match in between probe and the DR element.

The E and H plane far-field radiation patterns at 1.28 GHz and 3.3 GHz are shown in Fig. 4.14 and Fig.4.15 respectively at each port.

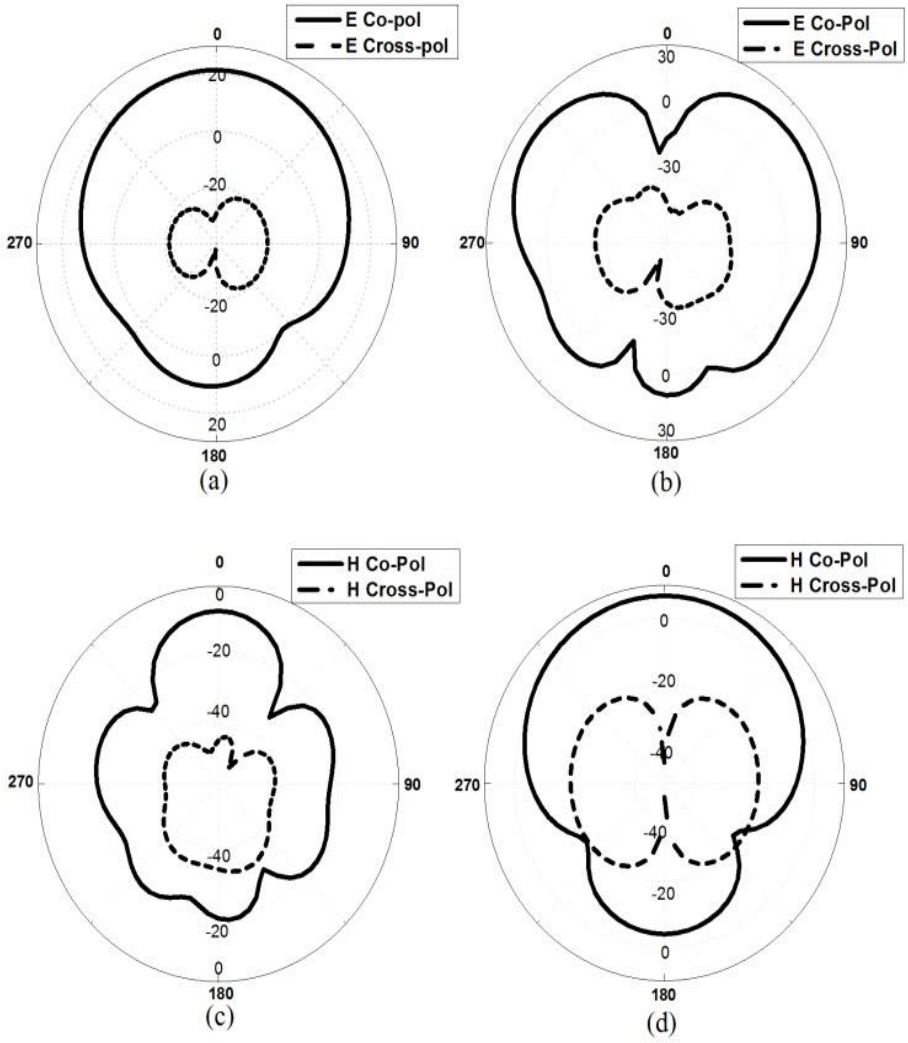

Fig. 4. 14 E-plane Radiation patterns (a) at 1.28 GHz (b) at 3.3 GHz. and H-plane Radiation patterns (c) at 1.28 GHz (d) at 3.3 GHz of the proposed Antenna Array, port-1

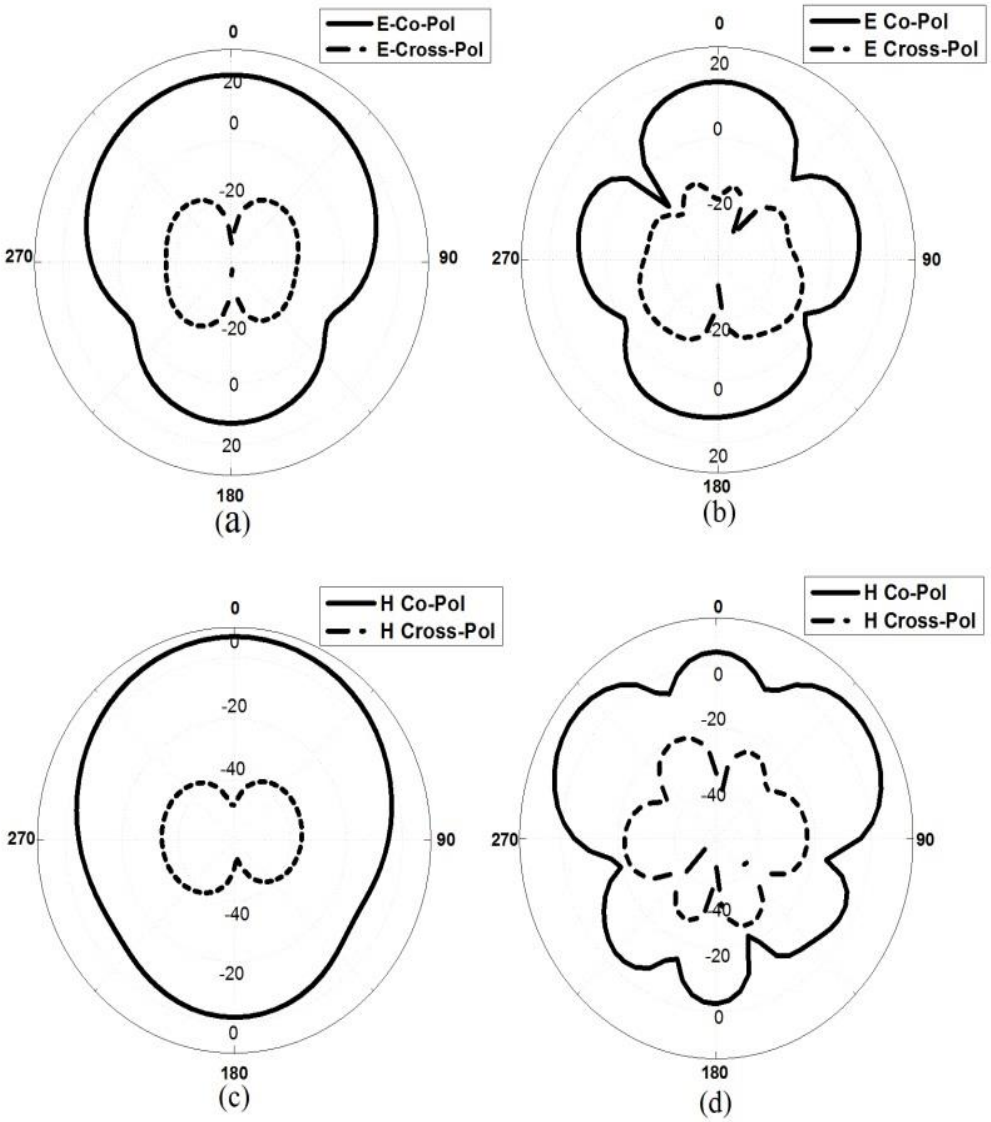

Fig. 4. 15 E-plane Radiation patterns (a) at 1.28 GHz (b) at 3.3 GHz. and H-plane Radiation patterns (c) at 1.28 GHz (d) at 3.3 GHz of the proposed Antenna Array, port-2

The co-polarization level is found to be 40dB higher than the cross-polarization level for both E and H plane radiation patterns in bore sight directions. Both plane patterns are exactly symmetric with 3 dB Half Power Beam Width (HPBW) of 90° however, E plane patterns are found to be slightly narrower towards horizon. The front to back ratio (F/B) in both the planes is estimated to be 10 dB. The radiation patterns are found to be stable with nearly same pattern shapes for 1.28GHz and 3.3GHz, however shape of the pattern degrades while shifting for higher frequencies.

The simulated realized gain versus frequency of the proposed antenna array as compared to single element antenna is shown in Fig. 4.16. The single element antenna has gain of

3.2dB at 1.28 GHz and 2.3dB at 3.3 GHz respectively. The proposed array achieves the gain of 9.6 dB at the resonance frequency of 1.28GHz in L-band and 10.7 dB at the resonance frequency of 3.3GHz respectively. The radiation efficiency of the DRA element is found to be 93%.

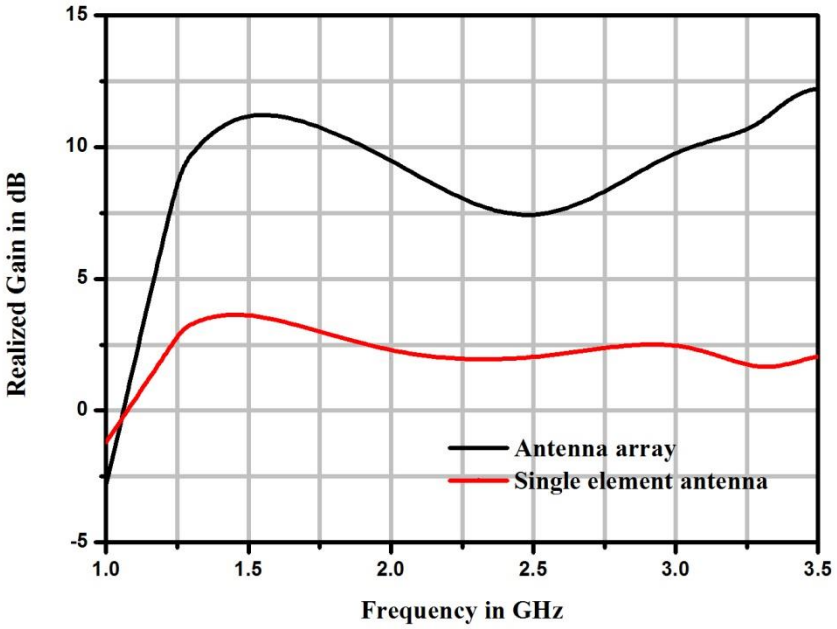

Fig. 4. 16 Simulated realized gains of the single element antenna and antenna array

4.3 Summary

A dual-band and dual linearly polarized DRA Array has been presented. The both ports are sharing the impedance bandwidth of 1.16 GHz to 1.43 GHz and 3.2 GHz to 3.35GHz perfectly. The input isolation exceeds 36dB and 40dB for lower L-band and higher S-band respectively, making the antenna a good candidate for wireless applications for avoiding multipath effects. The simulated radiation efficiency is found to be 95%. The proposed design has been achieved a good co polarization of 40dB. The impedance bandwidths of 21% (L-band) and 4.54% (S-band) have been achieved. As of dual band operation, the antenna can be simultaneously used as Global Positioning System (GPS) carriers and also satellite mobile phones for L-band and Weather radar for S-band operations.

Chapter 5

DUAL-LINEARLY POLARIZED DIELECTRIC RESONATOR ANTENNA ARRAY FOR C-BAND APPLICATIONS

5.1 Introduction

The polarization-diversity antennas have been an important subject for antenna designers. There have been significant works on different feeding methods, different shapes of DRA with linearly polarized or circularly polarized radiation patterns [2]. The study of DRA has been increasing in the last decade for their inherent merits of small size, low cost and no conductor loss as an efficient radiator [3]. In general the dual-polarized radiation has practical applications in wireless communication systems. With the capability of dual polarization, the antenna can optimize the system performance with increased information rate [6]. This technique combines two feed ports with mutually orthogonal polarization directions and works in the duplex model of transmitting and receiving signals.

In case of a dielectric resonator antenna, the dual linear polarization could be achieved by combining two dielectric resonators which have different geometrical orientation or size with respect to each other. The excitation of such an antenna could be more complicated. Another way of obtaining dual polarization could be to excite two modes at the same frequency in one resonator. These two modes could either be two degenerative modes that analytically have the same resonant frequency. The antenna element could be manipulated in some way to make two modes coincide in one frequency. The latter alternative has been successfully performed where two radiating modes and one filtering narrowband mode operate on the same frequency band. This multi-mode function requires individual excitation of each mode. Thus a combination of microstrip, slot, coaxial probe or other excitation techniques must be implemented simultaneously.

5.2 Dual-Polarized DRA array in C- band Operation

A cylindrical dielectric resonator antenna (DRA) excited by two orthogonally placed H-shaped aperture slot is presented with high isolation exceeding 32 dB in C-band. For dual linear polarization, the DRA in its TM_{110} (HEM_{11}) mode is excited to yield broadside

radiation pattern. To confine the slots to the central area of cylindrical DR for TM_{110} mode, the rectangular shaped slots are moulded to H-shaped slots. The co-polarization level in both planes is found to be nearly 30 dB higher than the cross-polarization in broad-side direction. The proposed feed for cylindrical (DRA) has been achieved -10 dB impedance bandwidth of 4.8% for 6.1 to 6.4 GHz. The broadside radiation patterns with nearly same pattern shapes are found to be stable with the gain of 5.2 dB for both ports. The cylindrical shape DR is used because the body of revolution is symmetrical along the longitudinal axis, which makes it neutral to excite from any azimuth angle. Another reason is that cylindrical shape is the simplest shape and its modes have a simple mathematical description with explicit analytical formulas in the case of a shielded cylindrical cavity.

5.2.1 Antenna Geometry and Design

The proposed antenna geometry of the dual linear polarized DRA with slot coupling technique is shown in Fig.5.1.

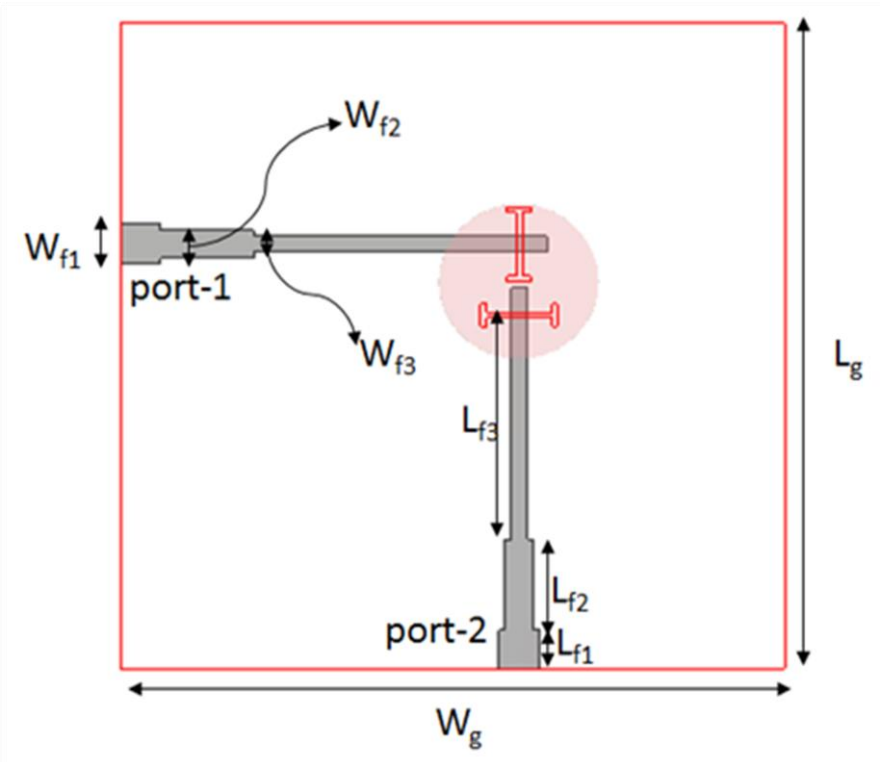

(a)

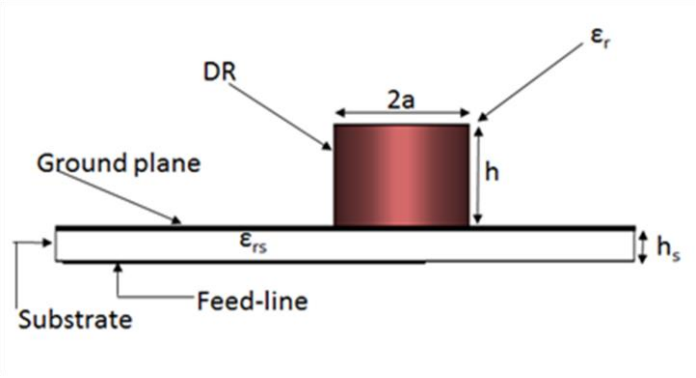

(b)

Fig. 5. 1 Geometry of the dual-polarized Dielectric Resonator Antenna

(a) Top view, (b) bottom view

In this proposed antenna, the cylindrical DR is placed unsymmetrically above a substrate FR4 of 1.6 mm thickness with permittivity of ε_{rs}=4.3. For better isolation the two feed-ports are kept in two different exciting modes. In this paper a slot coupled fed cylindrical DRA with dual H-shaped slots is demonstrated to obtain two orthogonally polarized fields. The aperture coupled technique has been considered for this design because it is suitable at high frequency operation as well as in MMIC application [4-5]. The DR element studied has a cylindrical shape with permittivity (ε_r=9.8, Alumina) with two slots kept under it. The level of coupling can be adjusted by the position of the slots with respect to DR. This technique combines two feed ports with mutually orthogonal polarization directions and works in the duplex model of transmitting and receiving signals. The antenna is designed and optimized using CST Microwave Studio suite™ 12, based on the three-dimensional finite integration time-domain (FITD) method. For cylindrical DRA of radius 'a' and height 'h' the field distribution can be described in terms of Bessel functions as(5.1). For TM mode:

$$E_z^{npm} = J_n\left\langle \left(X_{np}^{TM} r\right) \middle| a \right\rangle \{\sin(n\phi)\} \cos\left[(2m+1)\pi z/2h\right] \tag{5.1}$$

$$n = 1, 2, 2...;\ \mathrm{p} = 1, 2, 3...;\ \mathrm{m} = 0, 1, 2...;$$

Where J_n is the nth order Bessel function of the first kind. While X_{np}^{TM} is the root that satisfies the corresponding characteristic equation(5.2)

$$J_n(X_{np}^{TM}) = 0 \tag{5.2}$$

The simplified mathematical expression for the resonant mode frequencies is given by equation(5.3).

$$f_{npm} = \frac{c}{2\pi\sqrt{\varepsilon_r}}\sqrt{\left\{X_{np}^{TM^2}\right\} + \left[\frac{\pi a}{2d}(2m+1)\right]^2} \tag{5.3}$$

Employing the corresponding mode, for instance TM_{110} mode the expression (5.3) reduces to

$$f_{TM110} = \frac{c}{2\pi a\sqrt{\varepsilon_r}}\sqrt{\left\{X_{np}^{TM^2}\right\} + \left[\frac{\pi a}{2d}\right]^2} \tag{5.4}$$

$$\text{where } \left\{X_{np}^{TM^2}\right\} = (1.841)^2$$

The mathematical expression used to find out the radius and height of the DR element, for resonant mode frequency is given by(5.4). Two microstrip feed lines are etched on the bottom side of the substrate. Two H-shaped slots are designed on the topside ground plane to enable inductive coupling energy transfer as shown in Fig. 1. Ground plane and substrate dimensions are fixed to W_g= L_g=50 *mm*. The excitation of TM_{110} mode to achieve dual linear polarization strictly requires that these slots are confined to the central portion of the radiating element, and at the same time offer good level of isolation between the ports. As a result, this avoids radiation pattern degradation and resonance frequency shift. To resolve this issue, two rectangular shaped apertures are modified to orthogonally placed H-shaped slots with inter distance of $L_i = 5.5\text{mm}$. This approach makes the slot not only confined to the smaller central region of the DRA but also supports to manipulate the stub lengths and feed line positions in order to improve the port isolation to 32 dB.

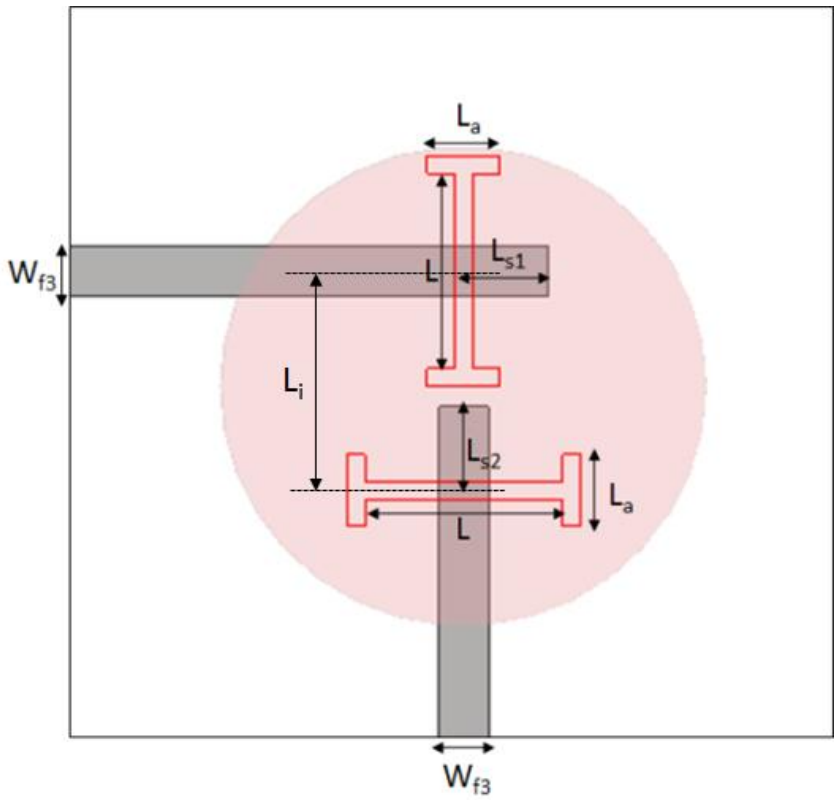

Fig. 5. 2 Enlarged view of an orthogonally H-shaped slot

The resulting optimal design parameters of the proposed antenna are tabulated in Table 5.1.

Table 5. 1 Design dimensions of the antenna element

a	h	W_{f1}	W_{f2}	W_{f3}	L_{f1}	L_{f2}
7.5mm	4mm	3.1mm	2.15mm	1.24mm	3mm	7mm
L_{f3}	L_{s1}	L_{s2}	L	L_a	W_s	h_s
17.4mm	1.8mm	2.1mm	4.9mm	1.8mm	0.45mm	1.6mm

5.2.2 Simulation Results and Parametric Analysis

The design is started taking the good preliminary dimensions of the DR using(5.4). There are no simple equations for designing the slot dimensions given the various antenna parameters. The slot length L is chosen large enough so that sufficient coupling exists between the DRA and the feed line but small enough so that it does not resonate with in the band of operation, which usually leads to a significant radiated back lobe. Using the initial value of the slot was found to be 5.2mm.

$$l_s = \frac{0.4\lambda_0}{\sqrt{\varepsilon_e}} \tag{5.5}$$

$$\text{where } \varepsilon_e = \frac{\varepsilon_r + \varepsilon_s}{2} \tag{5.6}$$

ε_r and ε_s are the dielectric constants of the DRA and the substrate, respectively. The parametric analysis for various values of stub lengths of port-1 and port-2 has been carried out as shown in Fig. 5.3 and Fig. 5.4 respectively.

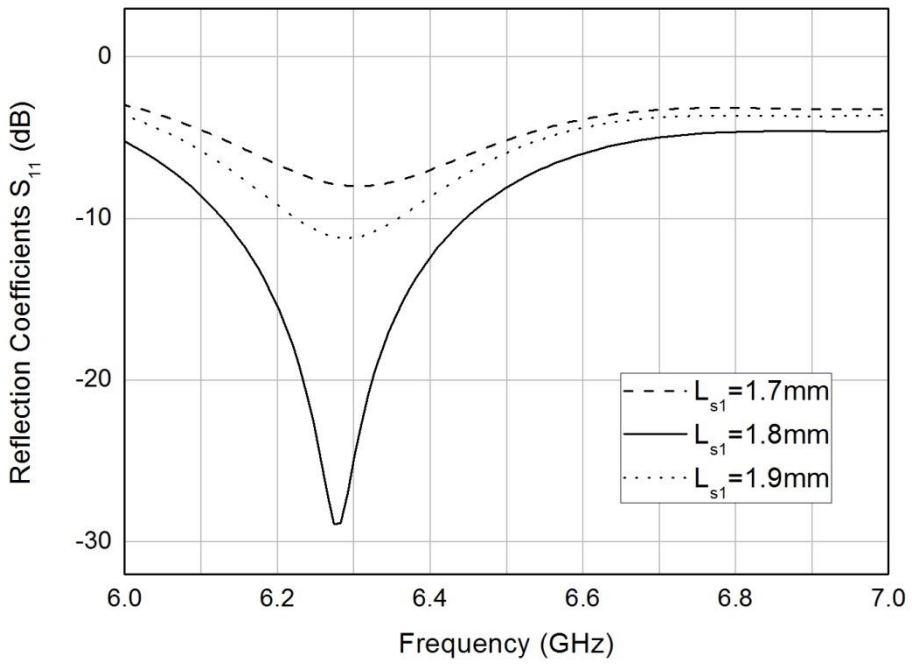

Fig. 5. 3 Reflection coefficient curves for different values of stub lengths L_{s1}

The stub lengths closely approximate quarter wave length ($\lambda_g/4$) which plays a significant role in improving the coupling mechanism when its reactance cancels to the reactance of the aperture. So choosing the slot lengths as 4.9mm and widths 0.45mm, stub lengths are varied for port-1 and port-2. It is observed from Fig 5.3 that for stub length of L_{s1}=1.8 mm the reflection coefficient, S11< -28dB is found much better as compared to L_{s1}=1.7mm and L_{s1}=1.9 mm respectively. Similarly from Fig. 5.4, S_{11}< -38dB has been found for stub length L_{s2}=2.1mm. From this analysis L_{s1}=1.8 mm and L_{s2}=2.1mm have been considered for the design. Fig 5.5 shows different values of isolation at frequency of operation 6.3 GHz for different spacing values in between the slots. Some space can be generated under the DR by shifting two similar H-shaped slots from the cylindrical DR centre. The new position is expected to confine to the desired resonant mode.

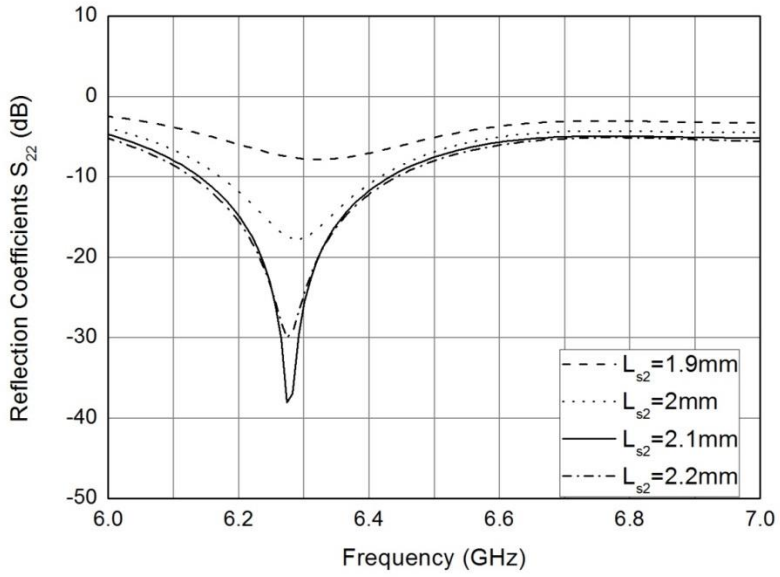

Fig. 5. 4 Set of reflection coefficient curves for different values of stub lengths L_{s2}

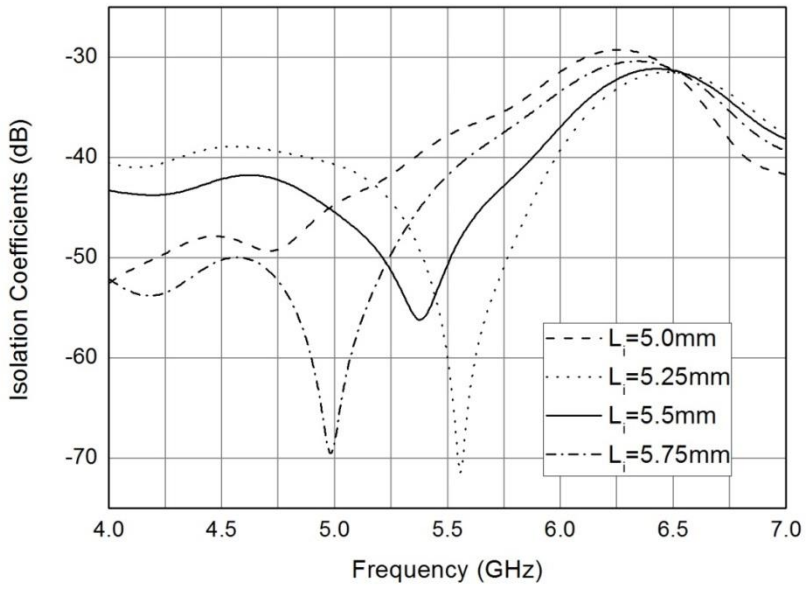

Fig. 5. 5 Set of isolation coefficient curves for different values of L_i

The spacing between the two H-shaped slots plays a major role in deciding the isolation between the two ports. To get desired dual polarization, isolation coefficient is an important parameter for the design. Very little variations in the space in between the two slots will affect the isolation. It is clear from Fig 5.5 that for L_i=5.5 mm the isolation better than 34 dB is achieved. Below 5.5GHz of operation other values of L_i gives better

isolation but as our required frequency of operation is 6.3GHz, L_i =5.5 mm is chosen. L_i =5.75mm is avoided for the design because to give at least some space for the vertical H-shaped slot to reside under the DR safely. The input impedance at port 1 and port 2 have been studied as shown in Fig 5.6and 5.7 taking the dimensions of table 4.1.

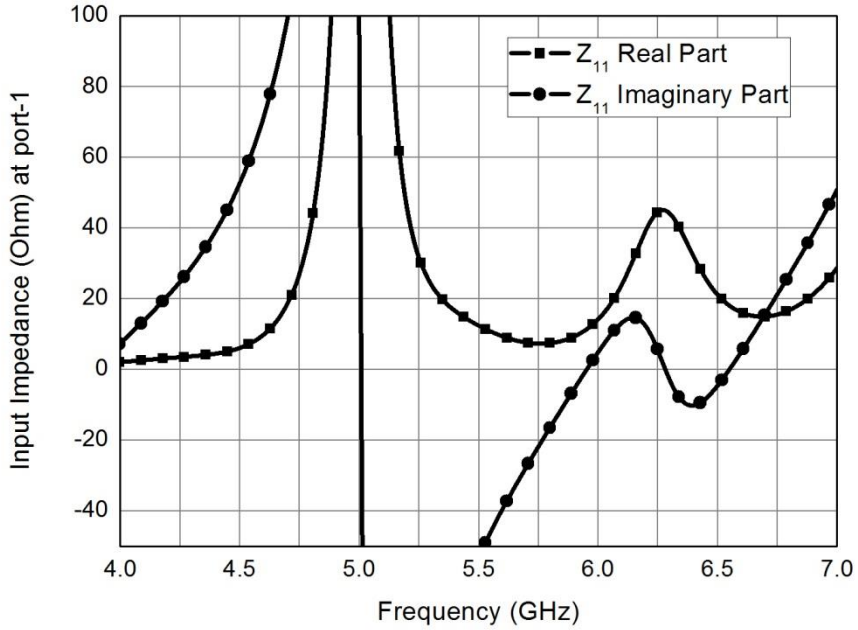

Fig. 5. 6 In put impedance curve with real and imaginary parts at port -1

The real and imaginary parts of impedance curves are calculated with the de-embedding process. The results available from Fig 5.6 suggest one possible resonance at port-1 which is taking place around 6.3 GHz, where the imaginary part is closely nullified because of the reactance cancellation of the stub length L_{s1} as studied from Fig 5.3. The real part is approximately close to 50 ohm. Similar observation can be found in Fig 5.7 where at around resonance frequency of 6.3 GHz, it can be seen that the imaginary part is near to zero and the real part of impedance is close to 50 Ohm.

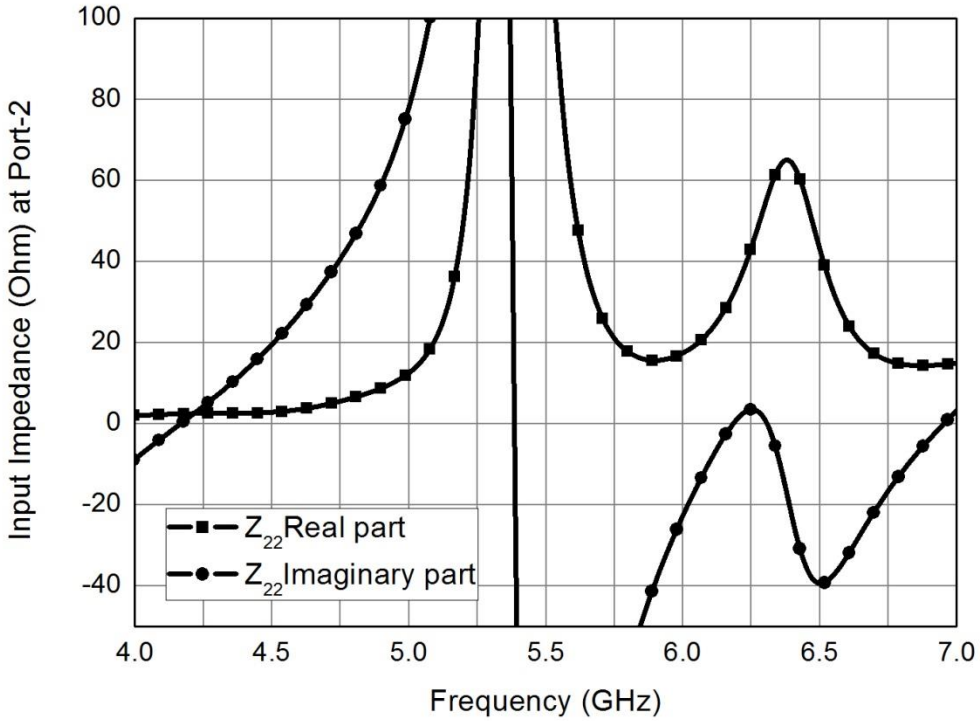

Fig. 5. 7 Input impedance curve with real and imaginary parts at port -2

The analysis of the input impedance curves with respect to frequency gives the idea that the antenna structure is resonating near to 6.3 GHz. The simulated reflection co-efficient (S_{11} and S_{22}) and isolation (S_{12}) are shown in Fig. 5.8 exciting both the ports simultaneously. There is an excellent performance for common impedance bandwidth for port-1 and port-2, starting from 6.1GHz to 6.4GHz. Fig. 5.8 shows, at the frequency of operation 6.3 GHz the impedance bandwidth is 4.8%. The reflection coefficient value for port-1 is -28 dB whereas at port -2 the value is improved to –38dB. The impedance curve of port-1 clearly depicts that the matching to the real part of impedance as 50 Ohm is weaker as compared to port-2. The isolation between the ports is found to be more than 32dB at the frequency of operation. This behavior is due to the H-shaped slots with an addition to the isolation which provides the required radiation modes for dual polarization.

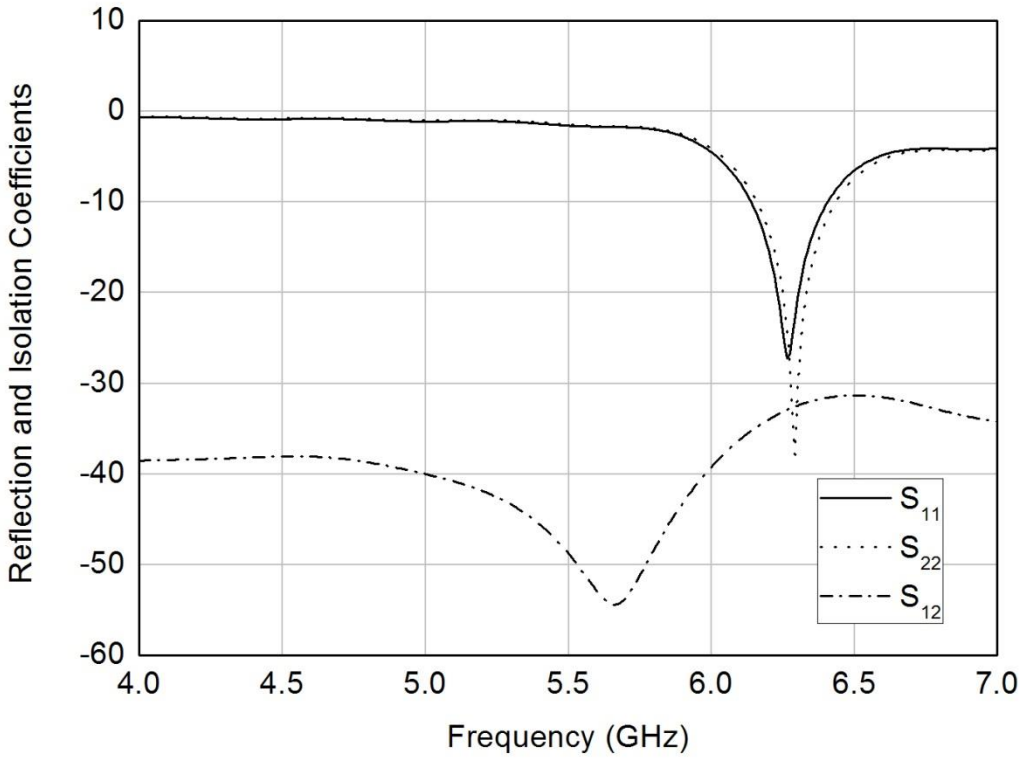

Fig. 5. 8 Simulated reflection and isolation coefficients of the proposed design

5.2.3 Experimental Verifications of the Antenna Element

The designed antenna is fabricated with DR with 9.8 dielectric constant on a dielectric substrate FR4 ($\varepsilon_s = 4.4$, tanδ=0.0024, h=1.6mm) and experimentally studied. The reflection coefficients and isolation coefficients measurement of the fabricated antenna is performed by using an Agilent 8720B network analyser and the radiation performance has been measured using anechoic chamber. The photograph of fabricated dual polarized antenna is shown in Figure 5.9. The measured and simulated reflection and isolation coefficients are shown in Fig 5.10 and Fig 5.11 respectively. It is not possible exactly to find the thickness and permittivity value of the adhesive material used, with which the DRA body is glued to the ground plane. Generally if the permittivity value of the adhesive material is lower than the DRA, as assumed in this case the frequency of operation shifts to the upper side. The applied thickness of adhesive material is also equally important. The frequency of operation at port-1 shifted to 6.2GHz-6.4GHz, whereas for port-2 the the range is shifted to 6.14GHz to 6.6GHz, hence sharing 4.14% of common impedance bandwidth.

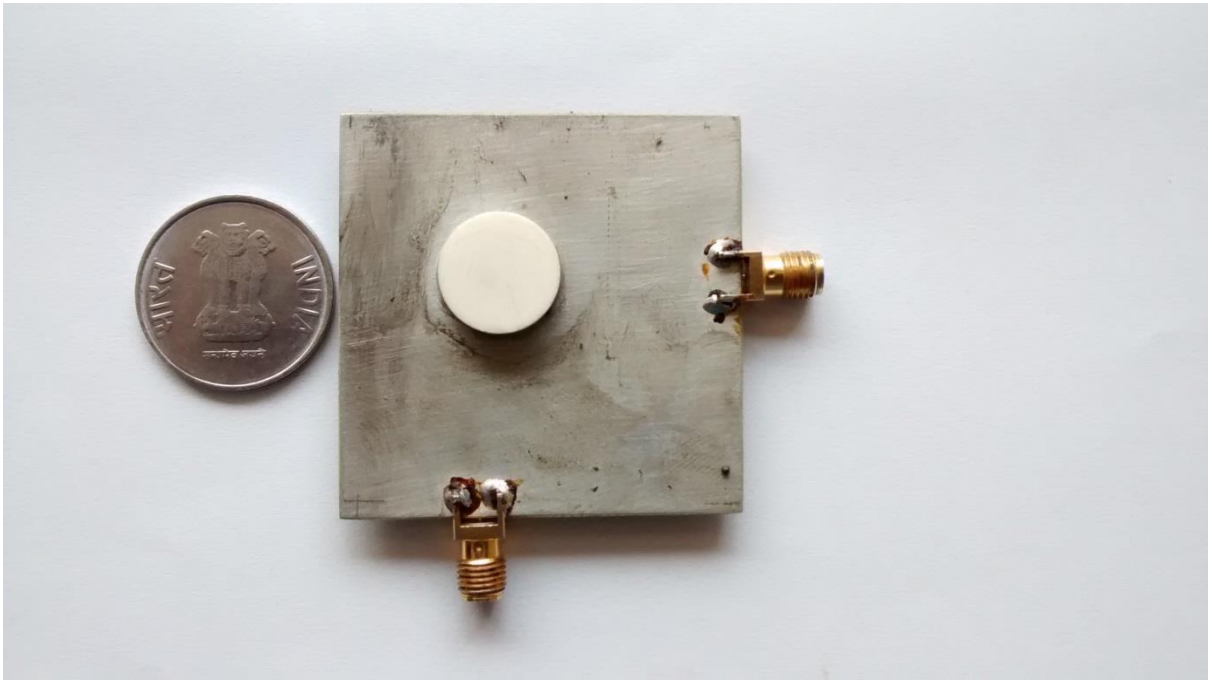

(a).

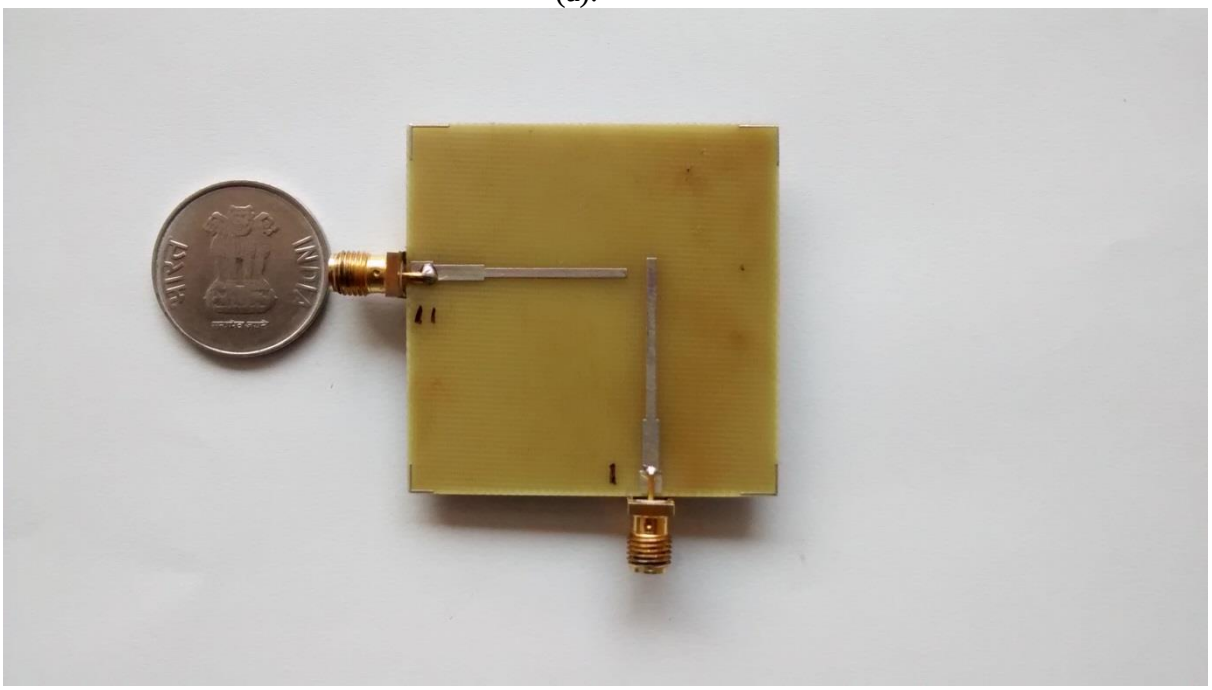

(b)

Fig. 5. 9 The fabricated dual linear polarized antenna prototype

(a) Front view, (b) Rear-view

The measured S_{22} plot closely matches with simulated results. The measured isolation between the two ports are depicted from Fig 5.11 is better than 39 dB. The isolation has been improved after measurement as compared to the simulation study.

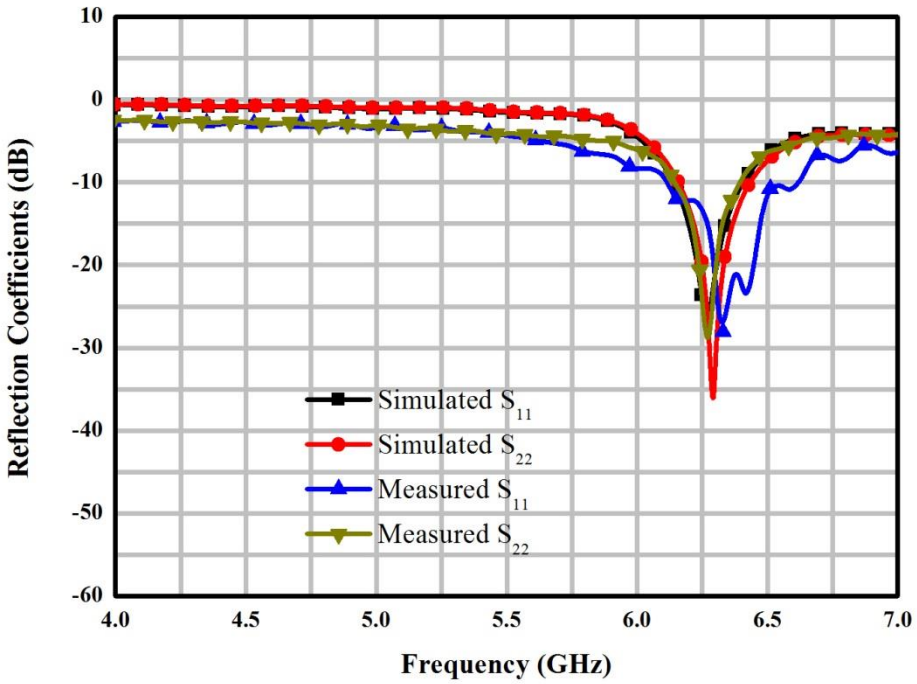

Fig. 5. 10 Measured and simulated reflection co efficients at port -1 and port-2

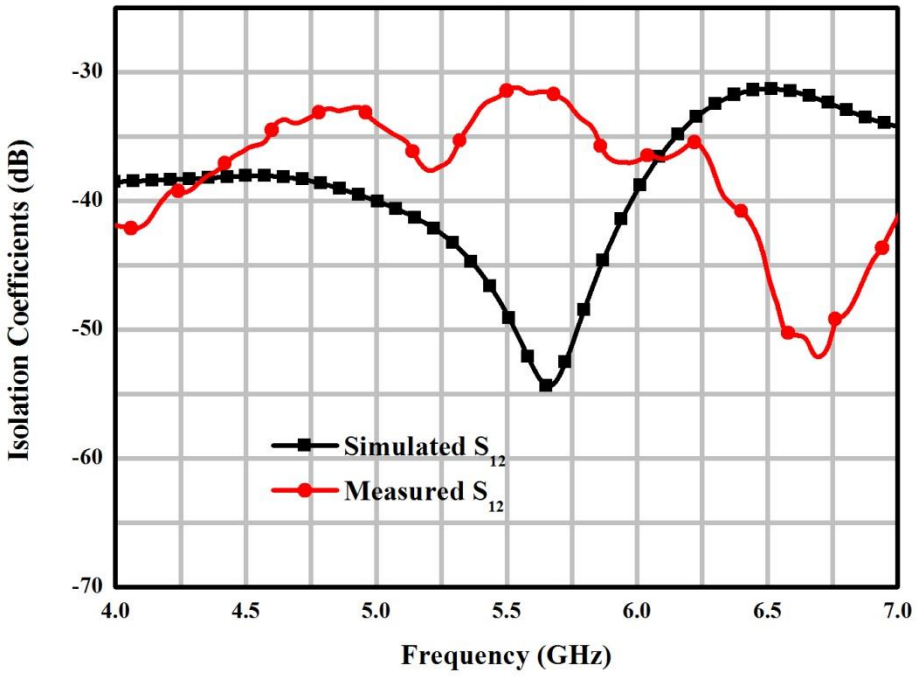

Fig. 5. 11 Measured and simulated isolation co efficient between port -1 and port-2

Fig. 5. 12 Far field measurement of the antenna element in anechoic chamber

Antenna measurement in an anechoic chamber has been shown in Fig 5.12. The measured and simulated far field radiation patterns at 6.3 GHz have been shown in Fig 5.13 for port-1.

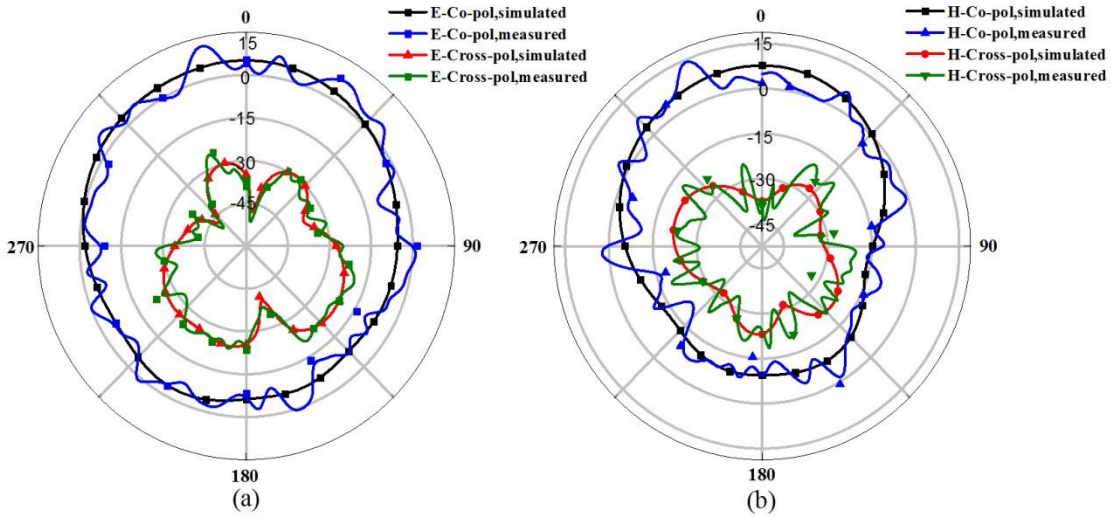

Fig. 5. 13 Measured and simulated Co-pol and cross pol radiation patterns at 6.3 GHz for port-1, (a) E-plane pattern (b) H-plane pattern

For both planes, the co-polarization level is nearly 30dB higher than the cross-polarization level in the broadside direction. Both the planes are more or less found to

be symmetric. For individual excitation of port-1, the 3-dB beam widths are found to be 96º and 66º in E- and H- planes respectively.

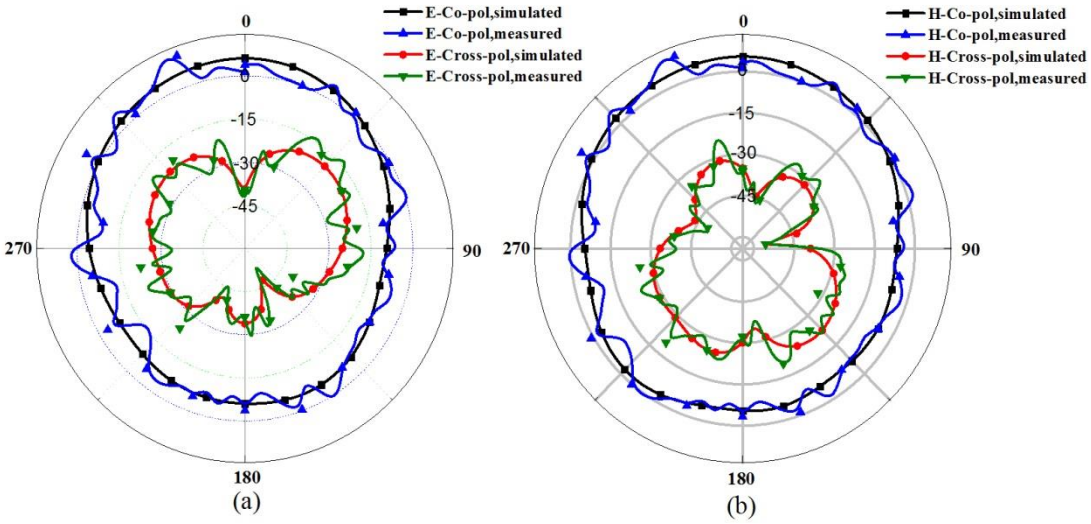

Fig. 5. 14 Measured and simulated Co-pol and cross pol radiation patterns at 6.3 GHz for port-2, (a) E-plane pattern (b) H-plane pattern

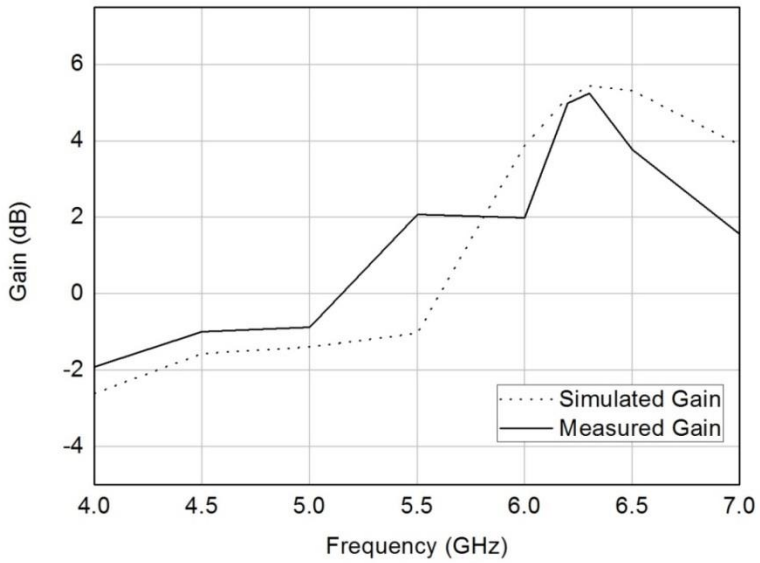

Fig. 5. 15 Measured and simulated gain curves of the proposed antenna element

The measured E-plane and H-plane radiation patterns at 6.3 GHz with the co-polarization and cross-polarization levels are shown in Fig.5.14 for port-2. The 3-dB beam widths of nearly 76º, for E-plane and H-plane patterns have been achieved with the individual excitation of port-2. The wider beam width for E-plane pattern at port-1 is due to the

effect of the slight shift of positioning the slots under the DR center. The front to back ratio (F/B) in both the planes is found to be 9dB. The comparison between the simulated gain and the measured gain versus frequency of the proposed antenna has been shown in Fig 5.15. The peak gain at both the ports reaches 5.1 dB.

5.2.4 Design of 2-element Dual Linearly Polarized Array

The antenna element studied in detail in previous sections has been considered for the array. The Wilkinson power divider having bandwidth of 22% has been used to construct the DRA arrays, for giving better isolation. The antenna model in CST Microwave Studio suite™ 12 has been shown in Fig. 5.16.

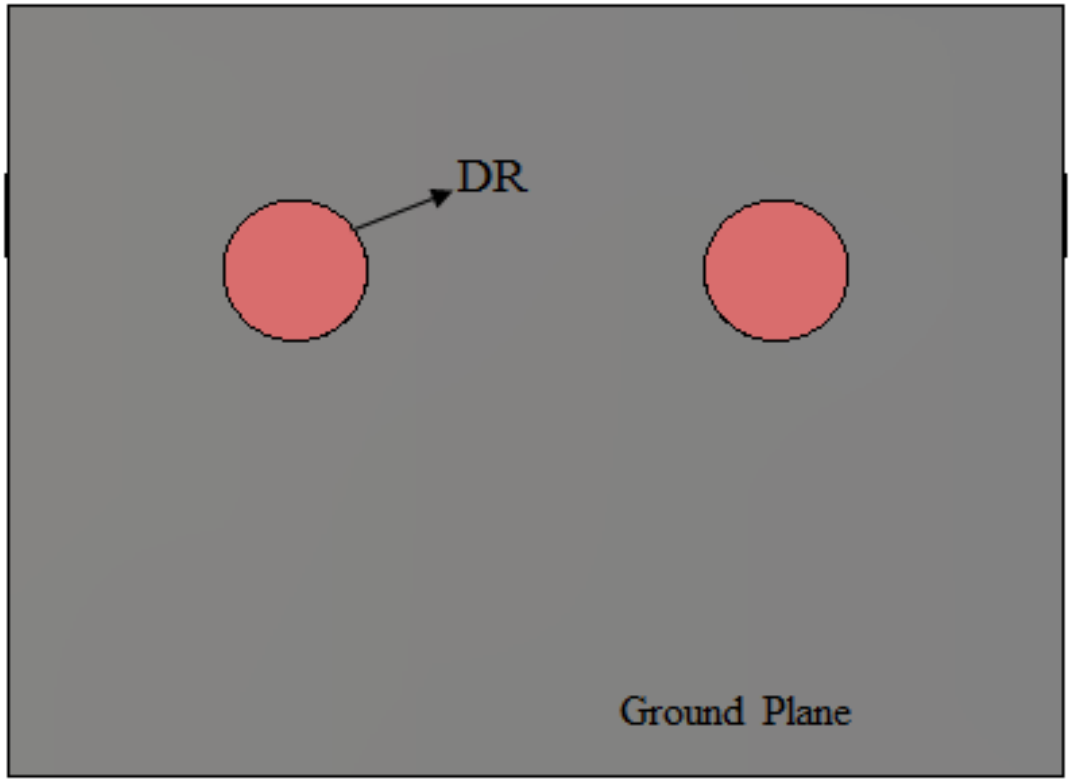

(a)

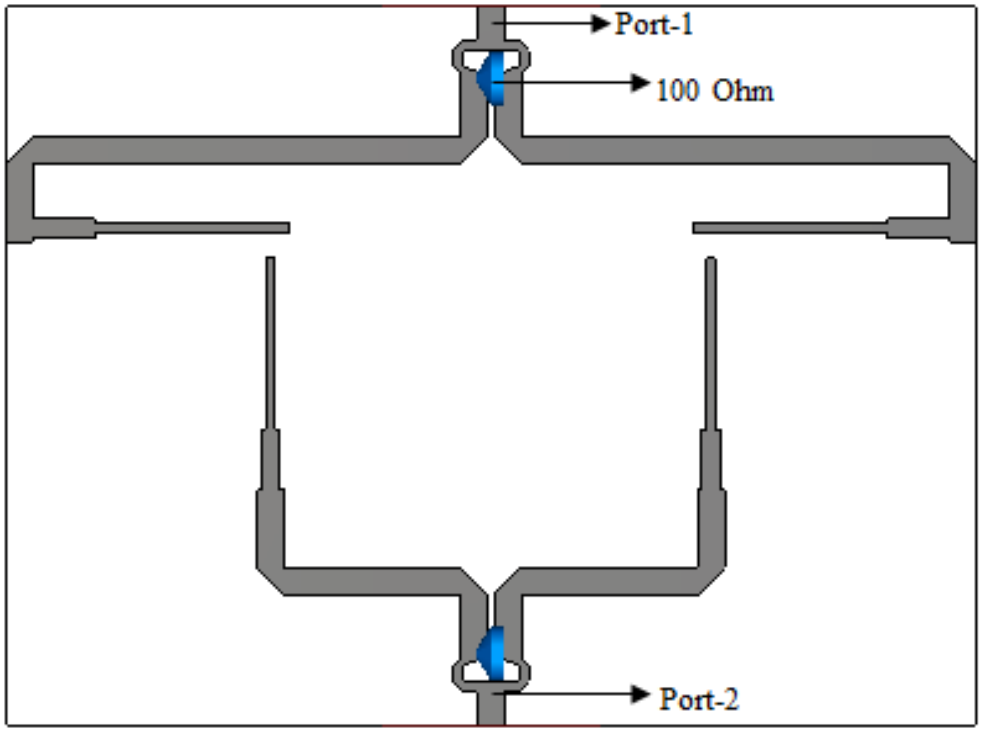

(b)

Fig. 5. 16 The proposed antenna array, (a) Front view (b) Rear view

The conventional single sectioned Wilkinson power divider is used for this purpose as it has usable bandwidth of $1.44:1$ for ($VSWR < 1.22$), high isolation value and ease of designing. The Wilkinson power divider consists of an input line, two quarter wave lines, two output lines and an isolation resistance. Here two Wilkinson power dividers are designed for the centre frequency of $6.5\ GHz$ where input and output lines have impedance values of 50Ω, quarter wave lines of 70.71Ω and isolation resistance of 100 as shown in Fig. 17.

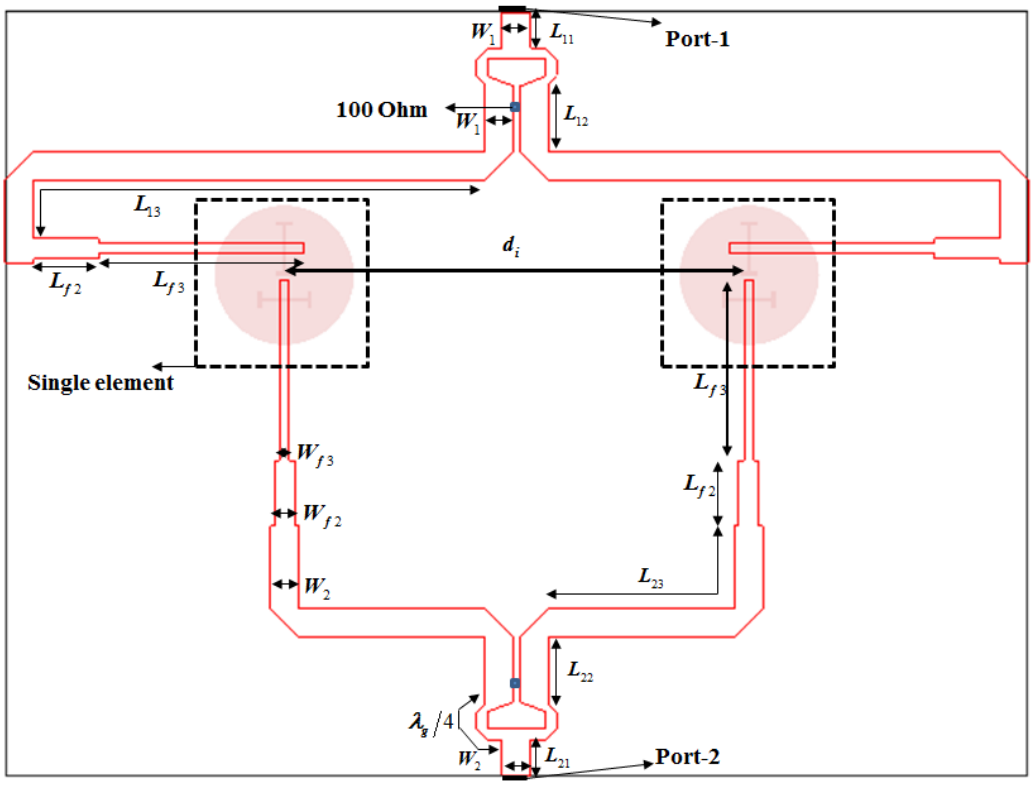

Fig. 5. 17 The feed network for the proposed antenna array

One power divider is integrated to the upper part of the antenna array whereas the other is integrated to the lower side to excite two orthogonal modes. Additional matching stubs of lengths L_{f2} and L_{f3} are connected to the output arms of the Wilkinson power divider to achieve proper impedance matching between the feed and radiators. Detailed dimensions of the feed network are presented in table 5.2.

Table 5. 2 Design dimensions of the feed network

W_1	$L_{11} = L_{21}$	$L_{12} = L_{22}$	L_{13}	L_{23}
3.1 *mm*	3.85 *mm*	7.28 *mm*	54.4 *mm*	28.8 *mm*
L_{f2}	L_{f3}	W_{f2}	W_{f3}	W_2
7 *mm*	17.4 *mm*	2.15 *mm*	1.24 *mm*	3.1 *mm*

5.2.5 Results and discussion

The antenna array has been modelled and simulated CST Microwave Studio suite™ 12. The reflection coefficient and isolation characteristics of the antenna have been studied and shown in Fig 5.18. The inter-element distance between the two radiating structures is maintained less than the guided wave length for better resonance and required radiation pattern.

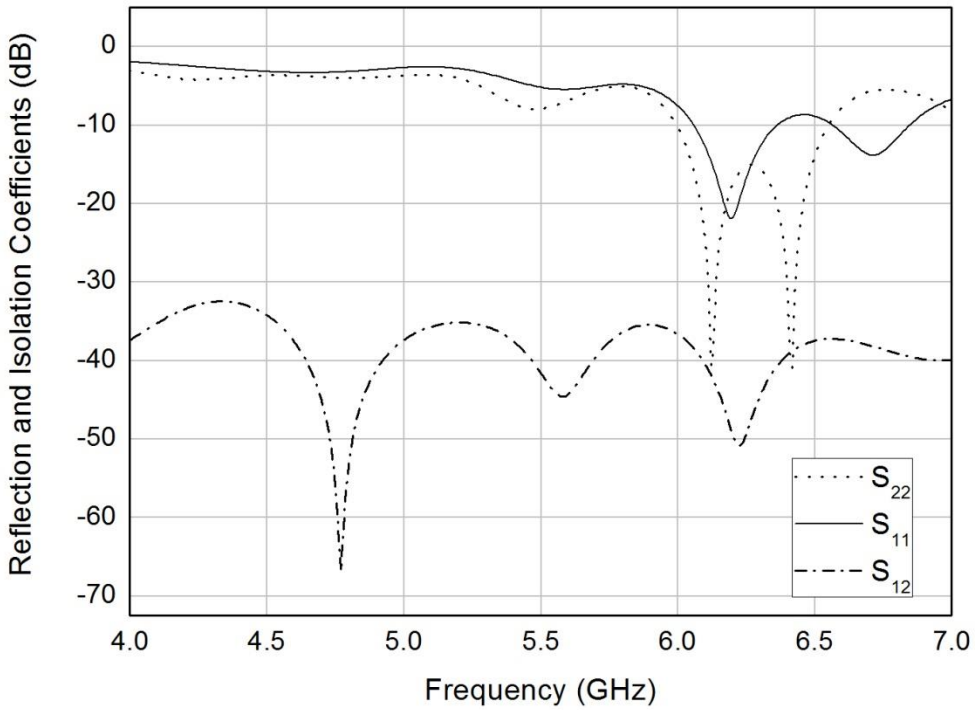

Fig. 5. 18 The simulated reflection and isolation coefficients of the 2-element array

The shared common impedance bandwidth by both the ports is from 6GHz to 6.35GHz. The port-1 shows narrow bandwidth as compared to port-2. The reflection coefficient value for port-1 at operating frequency of 6.2GHz is found to be less than –20dB whereas for port-2 it is less than –40dB. The isolation between the ports is achieved better than 37dB. The fabricated antenna has been shown in Fig 5.19. The reflection and isolation coefficients measurement of the fabricated antenna is performed by using an Agilent 8720B network analyser and radiation patterns by anechoic chamber. The measured and simulated reflection and isolation coefficients have been presented in Fig 5.20 and Fig 5.21 respectively. The DRA bonded to the ground plane and the associated feed network is expected to go under certain changes in its performance.

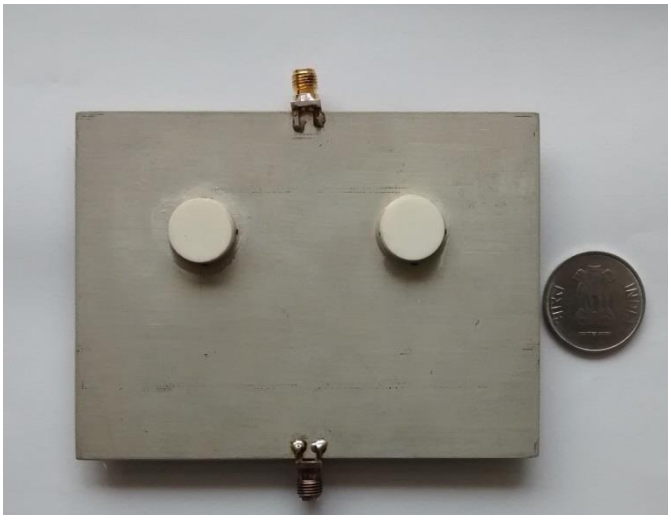

(a)

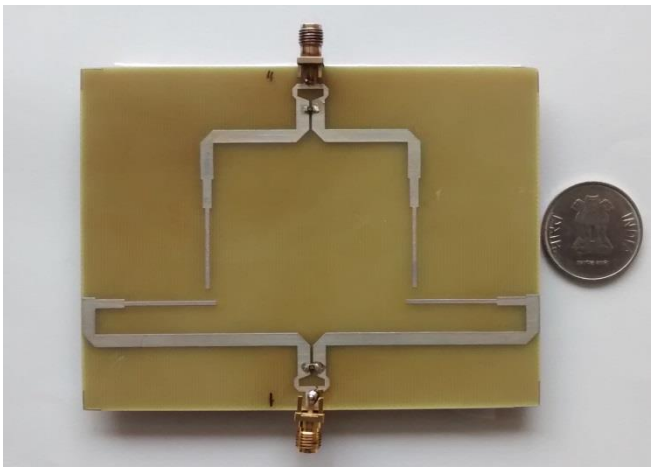

(b)

Fig. 5. 19 The fabricated dual linear polarized antenna array

(a) Front view, (b) Rear-view

The effect of the adhesive material and its thickness can shift the performance characteristics to the upward frequency range as analysed in the previous section for single element prototype. The similar phenomenon is expected for the measured reflection coefficient values of the 2-element array shown in Fig 5.20. The shift in this case is quite more as compared to the single element case. The reflection co-efficient at port-1 is shifted to the range of 6.4GHz to 6.6GHz while at port -2 it varies from 6.4GHz to 6.7GHz. The frequency of operation is from 6.4GHZ to 6.6GHz for both the ports satisfying dual linear polarization characteristics. The shared impedance bandwidth is

decreased to 3% with increased gain. Figure 5.22 presents the photograph of fabricated DRA inside an anechoic chamber.

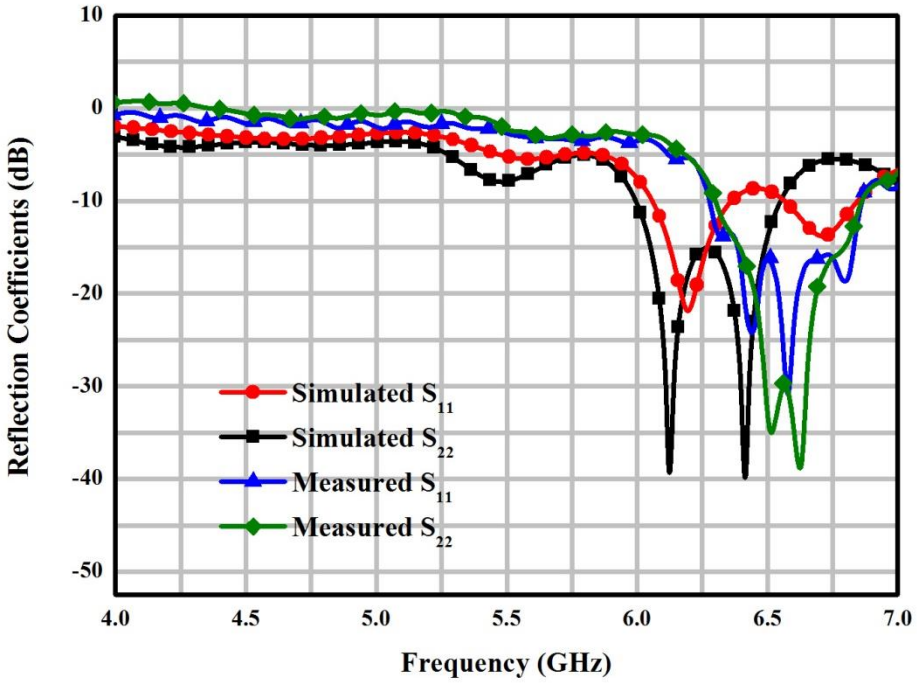

Fig. 5. 20 Measured and simulated reflection coefficients of the array at port -1 and port-2

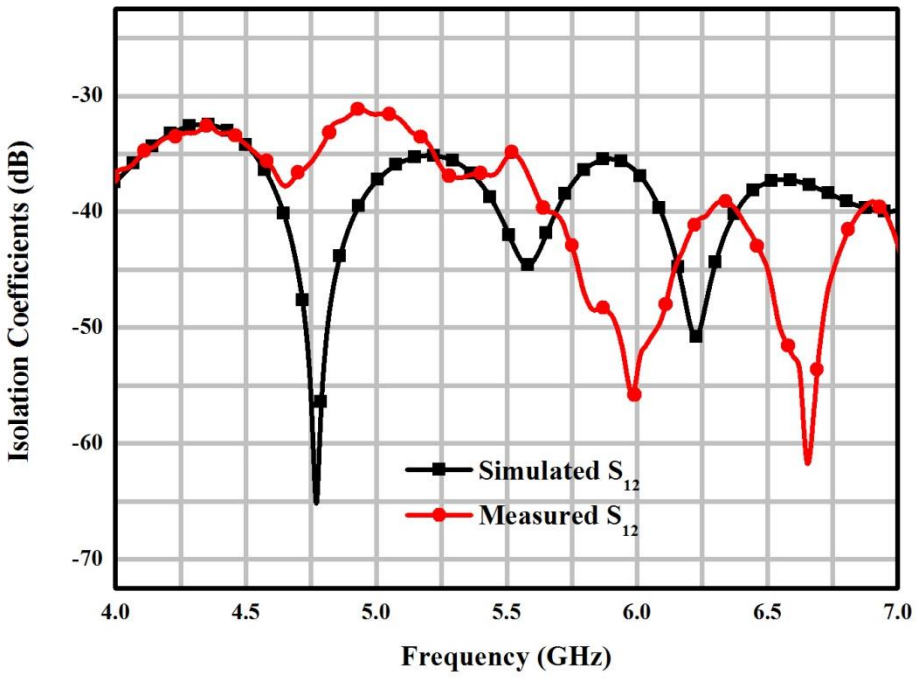

Fig. 5. 21 Measured and simulated isolation coefficients of the array between port -1 and port-2

Figure 5.23 and Figure 5.24 plot the measured and simulated radiation patterns for E and H-planes at 6.3GHz for both the ports.

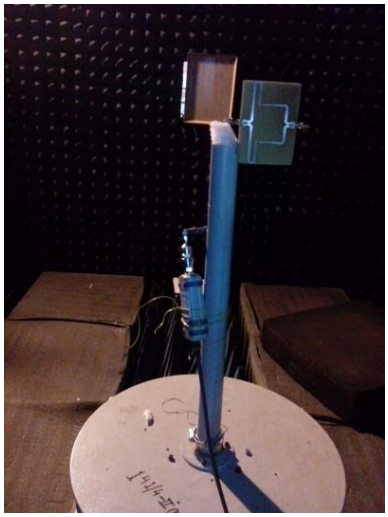

Fig. 5. 22 Far field measurement of the antenna array in anechoic chamber

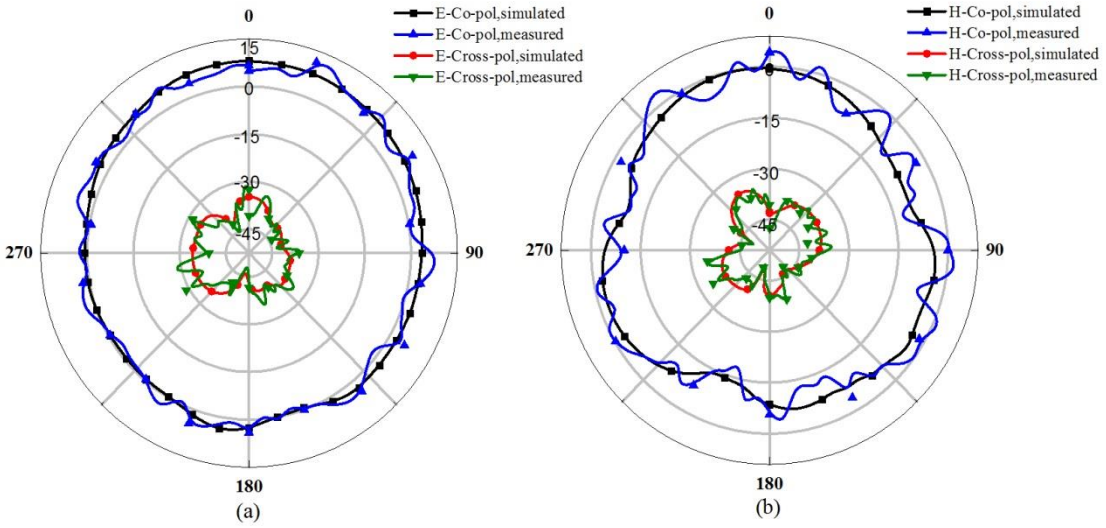

Fig. 5. 23 Measured and simulated Co-pol and cross pol radiation patterns at 6.3 GHz for port-1, (a) E-plane pattern (b) H-plane pattern

For the port-1 the broad side radiation patterns are depicted in Fig 5.24. The co-polarization level is 32 dB higher than the cross polarization level in the broad side direction. The E and H plane radiation patterns are approximately symmetric. The front to back ration (F/B) is observed to be 15 dB. The measured radiation pattern for port-2 is shown in Fig 5.24. The cross polarization level is less than 32 dB as similar to radiation

pattern at port-2. Both the patterns are symmetric with slight tolerable asymmetric pattern for the E-plane. The −3dB HPBW is around 130° at both the ports.

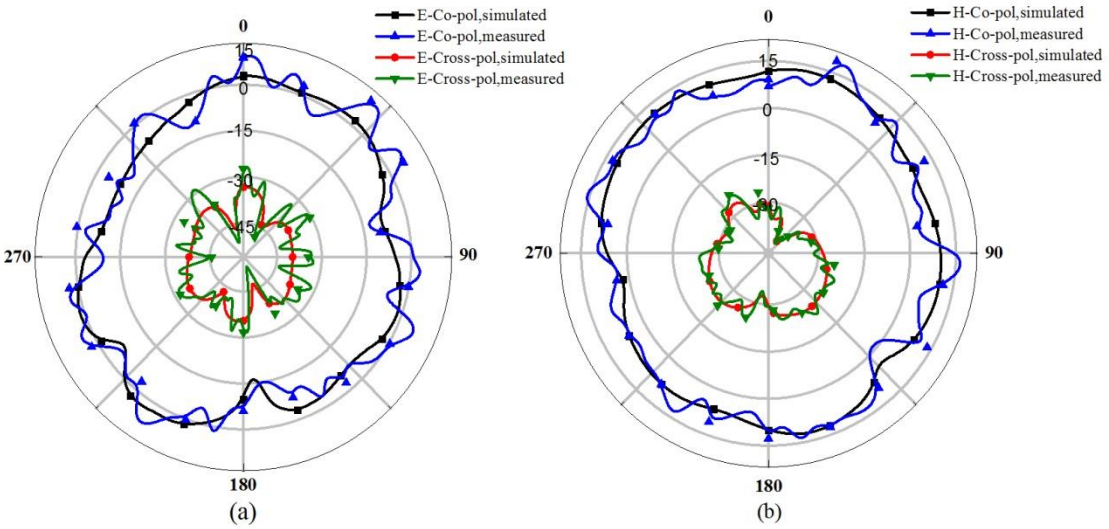

Fig. 5. 24 Measured and simulated Co-pol and cross pol radiation patterns at 6.3 GHz for port-2, (a) E-plane pattern (b) H-plane pattern

The surface current distributions of the antenna prototype with the 3-D radiation pattern have been shown in Fig. 5.25.

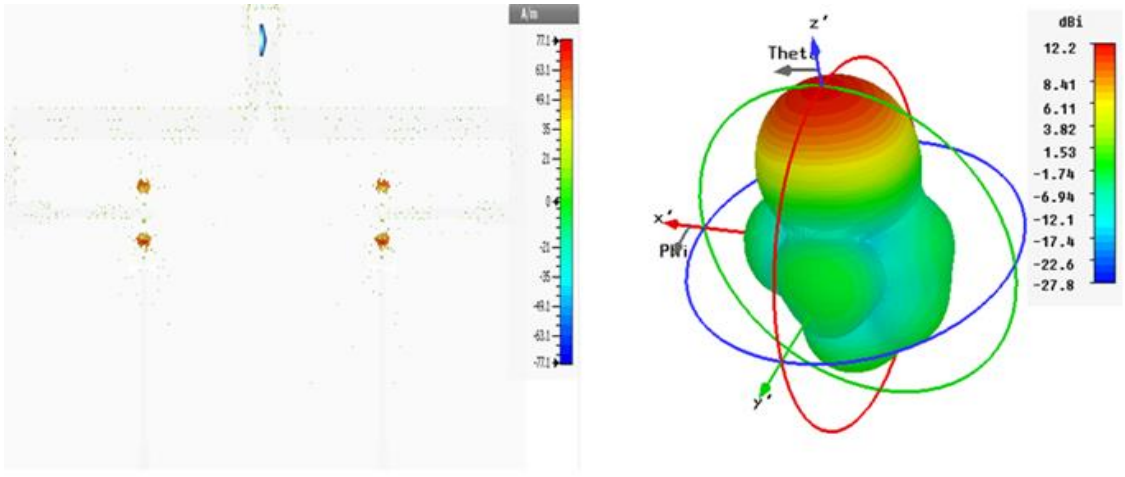

Port-1

(a)

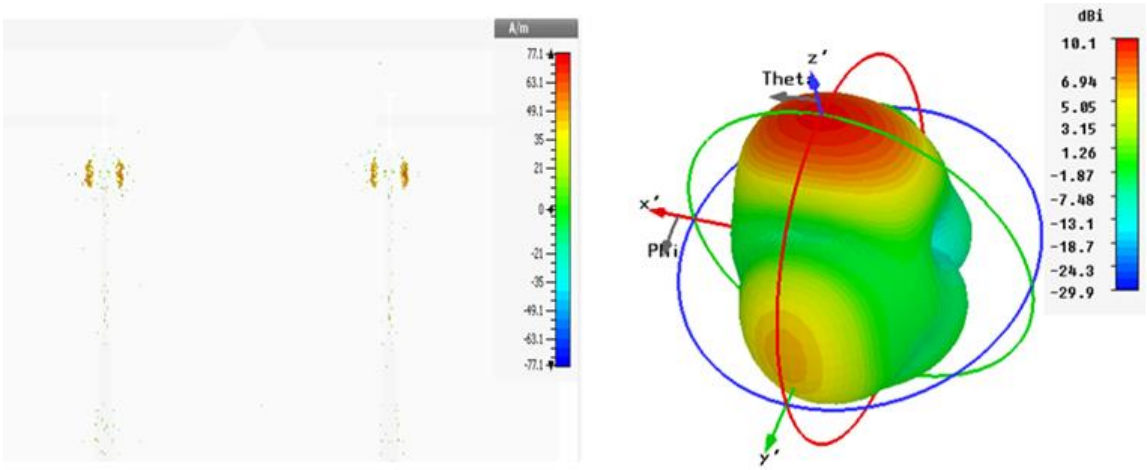

Port-2

(b)

Fig. 5. 25 Surface current and the 3-D radiation patterns at 6.3 GHz

For (a) port-1, (b) port-2

It is clear from the Fig. 5.25 that the surface current entering to the H-shaped slots and exciting the hybrid mode inside the cylindrical DRA. The surface current on the slot acts like a magnetic conductor and induce magnetic coupling with the DR. The radiation patterns at both the ports are symmetric in nature. Fig 5.26 shows the comparison between the simulated and the measured gain of the 2-element antenna array. It is clear from the figure that the gain is 12.5 dB, which is quite large as compared to the single prototype antenna represented in Fig 5.15. The simulated radiation efficiency is found to be 94%. The measured gain matches with the simulated gain curve with small amount of dissimilarity. The mismatch in between the simulated and the measured gain plot may be due to the fabrication tolerances due to connector and placement of DR on the slot.

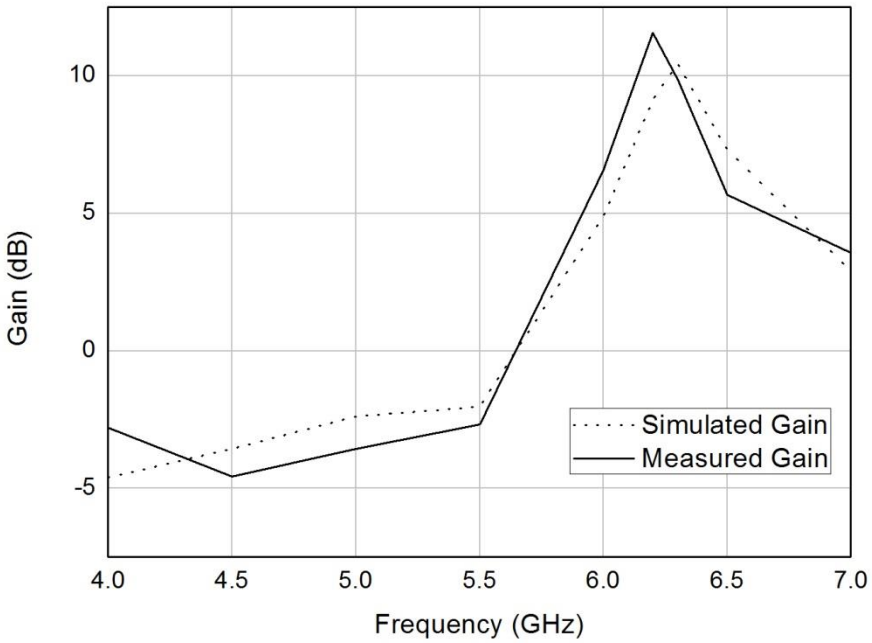

Fig. 5. 26 Measured and simulated gain curves of the proposed antenna array

The comparative study of different dual linear polarized DRA with different types of feeding applied is tabulated in Table 5.3.

Table 5. 3 Comparative study of dual polarized DRA with various feeding

Feeding method	Microstrip and microstrip [6]	Slot and slot [7]	Ring aperture [72]	Proposed antenna
Resonant frequency (GHz)	2.2	2.1	8.8	6.3
Bandwidth (%)	2.6	12	4.5	3
Isolation (dB) (worst with in band)	17.7	35	17	37
Radiation pattern	asymmetry	asymmetry	symmetry	symmetry
Cross-polarization level(dB)	-13	-20	-16	-35

5.3 Summary

A dual-polarized DR antenna array design has been presented. At first the single element prototype has been analysed in detail. With the use of Wilkinson power divider, the antenna array has been designed and analysed. For the two input ports, input isolation exceeds -30dB among them makes this antenna a good candidate for wireless applications in avoiding multipath effects. The simulated radiation efficiency of the proposed design has been found to be 94%. It is found that the proposed design has much lower cross-polarization level (-30dB) as compared to co-polarization level. The measured results demonstrate that the proposed DRA array achieves an impedance bandwidth of 3% for 6.4 GHz to 6.6 GHz, with simulated gain of 12.5 dB at the frequency of 6.4 GHz. The structure can be easily integrated with planar circuitry. It seeks promising applications in the satellite and synthetic aperture radar communication systems operating in C-band.

Chapter 6

CONCLUSIONS AND FUTURE WORKS

This chapter summarizes and highlights the overall conclusions drawn from the thesis. Further research problems are outlined related to the research work.

6.1 Conclusions

In this thesis investigations have been done in designing wideband DRA and dual linearly polarized DRA array with low conductor loss and high data rate. The effect of variations of the hybrid feeding techniques on the performances like bandwidth, Co and Cross polarizations of the radiation patterns, gain have been studied. The performance by variation of the dielectric material has been studied for the first discussed wideband SRDR (Square Ring Dielectric Resonator Antenna). The single prototype antennas have been analysed in detail before considering for array.

The **FIRST** chapter of the thesis explains the motivation for carrying out this research work. The problem statements of the research work and the organization of the thesis are also outlined in this chapter.

The **SECOND** chapter discusses different bandwidth enhancement techniques applied to DRA with overall review of the DRA as a suitable candidate for wireless applications. Different types of DR materials have been discussed. The chapter also throws light on excitation techniques of the DRA with modes and polarization characteristics of the DRA.

In the **THIRD** chapter a U-shaped fed SRDR has been designed and analysed. The hybrid modes are generated by the feeding structure. The enhancement of bandwidth is achieved by lowering the Q-factor. The proposed DRA achieves an impedance bandwidth of 47.26 % for 3.9 GHz to 6.20 GHz, with simulated average gain of 5.3 dB at 5.9 GHz and 3.1 dB at 4.36 GHz respectively. The H-plane radiation patterns are almost omnidirectional and the E-plane radiation patterns are in the broadside direction against frequency was observed. The cross polarization level is as low as around 18 dB for E-plane where as in case of H-Plane the cross polarization level is below 28 dB in the

bore-sight direction. This characteristic makes this proposed antenna for WLAN applications with high data rate because of large bandwidth.

Polarization diversity antennas have been designed and analysed in order to increase the data rate. In the **FOURTH** chapter, a 2×2 cylindrical dielectric resonator antenna (DRA) array, where each element is excited by a slot orthogonally placed to a strip fed probe is presented. The proposed design achieves a good co polarization of 40dB. The impedance bandwidths of 21% (L-band) and 4.54% (S-band) have been noticed. As of dual band operation, the antenna can be simultaneously used as Global Positioning System (GPS) carriers and also satellite mobile phones for L-band and Weather radar for S-band operations.

A dual linearly polarized slot coupled 2-element array has been proposed and designed in chapter **FIVE**. The design is sharing the common impedance bandwidth of 6.4 GHz to 6.6 GHz perfectly by port-1 and port-2 respectively. For the two input ports, input isolation exceeds -37dB and makes this antenna a good candidate for satellite and synthetic aperture radar communication systems operating in C-band.

6.2 Scope for Future Work

It is clear from this research work that DRAs offer promising applications at L, S, and C bands due to their high radiation efficiency and negligible dielectric losses. They have accomplished successfully nearly all the requirements targeted in our research work. The size of the DRA as part of the diversity antenna has a great potential to be reduced. With the commercial availability of high permittivity dielectric material, size of the antenna can be reduced. There are various techniques for optimizing the performance indices of antenna arrays. Similarly there is need to explore new range of miniaturized antennas which require simple integration techniques with DRAs and both been cohabited to each other. This strategy is expected to introduce more compactness to the overall structure and assure significant improvement in the overall performance of the diversity antenna.

References

[1] T. S. Rappaport, *Wireless Communications*. Principles and Practice. Prentice Hall, 1996.

[2] A. Petosa, *Dielectric Resonator Antenna Handbook*. Artech House Publishers, Norwood, USA, 2007.

[3] K. M. Luk and K. W. Leung, *Dielectric Resonator Antennas*. Herttordshire, U.K. Research Studies Press Ltd, 2002.

[4] S. Y. Liao, *Microwave devices and circuits*. Prentice-Hall, 3rd ed., 1996.

[5] D. Pozar, *Microwave Engineering*. New York. Wiley, 3rd ed., 2005.

[6] C.Y. Huang, T. W. Chiou, and K. L. Wong, "Dual-Polarized Dielectric Resonator Antennas," *Microwave and Optical Technology Letters*, Vol. 31, no. 5, pp. 222-223, Nov. 2001.

[7] Y. X. Guo and K. M. Luk, "Dual-polarized dielectric resonator antennas", *IEEE Trans. Antennas and propagat.*, vol. 51, no. 5, pp. 1120-1123, May. 2003.

[8] M. T. Birand, and R. V. Gelsthorpe, "Experimental Millimetric Array Using Dielectric Radiators Fed by means of Dielectric Waveguide," *IEE Electronics Letters*, Vol. 17, no. 18, pp.633-635 , Sept. 1981.

[9] R. D. Richtmeyer, "Dielectric Resonators", *Journal of Applied Physics*, Vol. 10, pp. 391-398, Jun. 1939.

[10] A. A. Kishk and Y. M. M. Antar, "Dielectric Resonator Antennas", from J. L. Volakis: *Antenna Engineering Handbook*, Chapter 17, 4th ed., McGraw-Hill, USA, 2007.

[11] D. J. Masse, R. A. Purcel, D. W. Ready, E. A. Maguire, and C. D. Hartwig, "A New Low Loss High K Temperature Compensated Dielectric for Microwave Applications*," Proceedings IEEE*, Vol. 59, no. 11, pp. 1628-1629, Jun. 1971.

[12] J. V. Bladel, "On the Resonances of a Dielectric Resonator of Very High Permittivity", *IEEE Transactions on Microwave Theory and Techniques*, Vol. MTT-23, pp. 199-208, Feb. 1975.

[13] E. M. O'Connor and S. A. Long, "The History of the Development of the Dielectric Resonator Antenna," *ICEAA International Conference on Electromagnetics in Advanced Applications*, Turin, Italy, pp. 872-875, Sept. 17th-21st, 2007.

[14] S. A. Long, M. W. McAllister and L.C. Shen, "The Resonant Cylindrical Dielectric Cavity Antenna", *IEEE Transactions on Antennas and Propagation*, Vol. AP-31, pp. 406-412, May. 1983.

[15] G. L. Conway, S. A. Long and M. W. McAllister, "Rectangular Dielectric Resonator Antenna", *IET Electronics Letters*, Vol. 19, pp. 218-219, Mar. 1983.

[16] S. A. Long and M.W. McAllister, "Resonant Hemispherical Dielectric Antenna", *IET Electronics Letters*, Vol. 20, pp. 657-659, Aug. 1984.

[17] M. Haneishi, H. Takazawa, and T. Aoki, "Planar Array Composed of Dielectric Resonator Antennas", *Transactions of the Institute of Electronics and Communication Engineers of Japan*, Vol. J67B, pp. 1486-1487, Dec. 1984.

[18] M. T. Sebastian, "Dielectric Materials for Wireless Communication", *Elsevier*, United Kingdom, 2008.

[19] Z. Peng, H. Wang and X. Yao, "Dielectric Resonator Antennas using High Permittivity Ceramics", Ceramics International, Vol. 30, no. 7, pp. 1211-1214, 2004.

[20] Trans Tech Incorporation. *Dielectric Materials Overview*.
http://www.trans-techinc.com/products_detail.asp?ID=2.

[21] Cumming Microwave. *Dielectric Materials Overview*.
http://www.cumingmw.com/Product%20Applications/dielectric_materials.html.

[22] Rogers Corporation. *Product Overview*.
http://www.rogerscorp.com/pages/overview/products.aspx.

[23] L. K. Hady, D. Kajfez and A. A. Kishk, "Triple Mode Use of a Single Dielectric Resonator", *IEEE Transactions on Antennas and Propagation*, Vol. 57, pp. 1325-1335, May. 2009.

[24] M. McAllister, G. L. Conway, and S. Long, "Rectangular dielectric-resonator antenna," *IEE Electronics Letters*, vol. 19, pp. 218–219, 1983.

[25] R. Mongia and A. Ittipiboon, "Theoretical and experimental investigations on rectangular dielectric resonator antennas," *IEEE Transactions on Antennas and Propagation*, vol. 45, no. 9, pp. 1348–1356, 1997.

[26] G. P. Junker., "Effect of an Air Gap on a Cylindrical Dielectric Resonator Antenna opearting in the TM_{01} mode," *IEE Electronics Letters*, Vol. 30, no. 2, pp. 97-98, Jan. 1994.

[27] R. Kumari, and S. K Behera, "Ring Dielectric Resonator Antenna for Broadband Applications", *IEEE International Conference on Computational Intelligence and Communication Systems, (CICN)*, Bhopal, India, Nov. 2010.

[28] D. M. Pozar and B. Kaufmann, "Increasing the bandwidth of a microstrip antenna by proximity coupling," *Electron. Lett.*, vol. 23, pp. 368–369, 1987.

[29] K. Wong and C. H. Wu, "Wide-band omnidirectional square cylindrical metal-plate monopole antenna," *IEEE Transactions on Antennas and Propagation*, vol. 53, pp. 2758–2761, Aug. 2005.

[30] K. L. Lau and K. M. Luk, "A wide-band circularly polarized l-probe coupled patch antenna for dual-band operation," *IEEE Transactions on Antennas and Propagation*, vol. 53, pp. 2636– 2644, Aug. 2005.

[31] W. S. Lee, D. Z. Kim, K. J. Kim, and J. W. Yu, "Wideband planar monopole antennas with dual band-notched characteristics," *IEEE Transactions on Microwave Theory and Techniques*, vol. 54, pp. 2800–2806, Jun. 2006.

[32] K. Ryu and A. Kishk, "Ultra wideband dielectric resonator antenna with broadside patterns mounted on a vertical ground plane edge," *IEEE Transactions on Antennas and Propagation*, vol. 58, no. 4, pp. 1047–1053, 2010.

[33] R. Chair, A. A. Kishk, and K. F. Lee, "Wideband stair-shaped dielectric resonator antennas," *IET Microw. Antennas Propag.*, vol. 1, pp. 299–305, Apr. 2007.

[34] R. Chair, A. A. Kishk, and K. Lee, "Wideband simple cylindrical dielectric resonator antenna," *IEEE Microwave and Wireless Components Lett.*, vol. 15, pp. 241–243, Apr. 2005.

[35] C. S. D. Young and S. A. Long, "Wideband cylindrical and rectangular dielectric resonator antennas," *IEEE Antennas and Wirel. Propag. Lett.*, vol. 53, pp. 126–129, 2006.

[36] T. H. Chang, Y. C. Huang, W. F. Su, and J. F. Kiang, "Wideband dielectric resonator antenna with a tunnel," *IEEE Antennas Wireless Propagation Letter*, vol. 7, pp. 275–278, Sept. 2008.

[37] G. P. Junker, A. A. Kishk, A. W. Glisson, and D. Kajfez, "Effect of an air gap around the coaxial probe exciting a cylindrical dielectric resonator antenna," *IEEE Electronics Letters*, vol. 30, pp. 177–178, Feb. 1994.

[38] J. T. H. S. Martin and Y. M. M. Antar, "Dielectric resonator antenna using aperture coupling," *Electronics Letters*, vol. 26, pp. 2015–2016, Nov. 1990.

[39] G. P. Junker, A. A. Kishk, and A. W. Glisson, "Input impedance of dielectric resonator antennas excited by a coaxial probe," *IEEE Transactions on Antennas & Propagation*, vol. 42, pp. 960–966, Jul. 1994.

[40] R. A. Kranenburg and S. A. Long, "Microstrip transmission line excitation of dielectric resonator antennas," *Electronics Letters*, vol. 24, pp. 1156–1157, Sept. 1988.

[41] R. K. Mongia, A. Ittipiboon, and M. Cuhaci, "Experimental investigations on microstrip fed series dielectric resonator antenna array," *Symposium on Antenna Technology and Applied Electromagnetics ANTEM 94*, pp. 81–84, Aug. 1994.

[42] K. Leung, "Conformal strip excitation of dielectric resonator antenna," *IEEE Transactions on Antennas and Propagation*, vol. 48, no. 6, pp. 961–967, 2000.

[43] X. S. Fang, K. W. Leung, "Linear-/Circular-Polarization Designs of Dual-/Wide-Band Cylindrical Dielectric Resonator Antennas, " *IEEE Transactions on Antennas and Propagation*. vol.60, no.6, pp.2662-2671, Jun. 2012.

[44] S. D. Targonski, and D. M. Pozar, Dual-band and dual polarized printed antenna element," *Elect. Lett.*, Vol. 34, No. 23, pp. 2193-2194, 1998.

[45] R. J. Pokuls, Uher, and D. M. Pozar, Dual-frequency and dual- polarization microstrip antennas for SAR applications," *IEEE Trans. Antennas Propagat.*, Vol. 46, No. 9, pp. 1289-1296, 1998.

[46] R. Chair, A. A. Kishk and K. F. Lee, "Wideband dual polarized dielectric resonator antennas at X-band", *Antennas and Propagation Society International Symposium, IEEE*, Vol. 4B, pp. 214 – 217, 2005.

[47] G. Almpanis, C. Fumeaux and R. Vahldieck, "Dual Mode Slot Coupled Cylindrical Dielectric Resonator Antenna," *IEEE Antennas and Propagation Society International Symposium*, pp. 2511-2514, 2006.

[48] K. M. Lee, A. T. S. Wang, and R. S. Chu, "Dual-band, dual-polarization, interleaved cross-dipole and cavity-backed disc elements phased array antenna", *Antennas and Propagation Society International Symposium*, IEEE, 1997 Digest, Vol. 2, pp. 694 – 697, 1997.

[49] B. Huang, Y. Yao and Z. Feng, "A Novel Wide Beam Dual-band Dual-Polarization Stacked Microstrip - Dielectric Antenna", *International Conference on Microwave and Millimeter Wave Technology, ICMMT '07*, pp. 1 – 4, 2007.

[50] S. H. Hsu, Y. J. Ren, and K. Chang, "A dual-polarized planar-array antenna for s-band and x-band airborne applications," *IEEE Antennas and Propagation Magazine*, vol. 51, pp. 70–78, Aug. 2009.

[51] L. Juan, F. Guang, and Y. Lin, "Design of a dual-polarized wideband short backfire antenna with high gain," *IET Microwave Antennas Propag.*, vol. 7, no. 9, pp. 735–740, 2013.

[52] R. G. Vaughan, "Polarization diversity in mobile communications," *IEEE Trans. Veh. Technol.*, vol. 39, no. 3, pp. 177–186, Aug. 1990.

[53] J. J. A. Lempiainen and J. K. Laiho-Steffens, "The performance of polarization diversity schemes at a base station in small/micro cells at 1800 MHz," *IEEE Trans. Veh. Technol.*, vol. 47, no. 3, pp. 1087–1092, Aug. 1998.

[54] B. Lindmark, "A dual polarized dual band microstrip antenna for wireless communications," in *Proc. IEEE Aerospace Conf.*, pp. 333–338, 1998.

[55] K. L. Wong, H. C. Tung, and T. W. Chiou, "Broadband dual-polarized aperture-coupled patch antennas withmodified H-shaped coupling slots," *IEEE Trans. Antennas Propag.*, vol. 50, no. 2, pp. 188–191, Feb. 2002.

[56] M. Barba, "A high-isolation, wideband and dual-linear polarization patch antenna," *IEEE Trans. Antennas Propag.*, vol. 56, no. 5, pp. 1472–1476, May. 2008.

[57] H. Wong, K. L. Lau, and K. M. Luk, "Design of dual-polarized L-probe patch antenna arrays with high isolation," *IEEE Trans. Antennas Propag.*, vol. 52, no. 1, pp. 45–52, Jan. 2004.

[58] T. W. Chiou and K. L. Wong, "A compact dual-band dual-polarized patch antenna for 900/1800-MHz cellular systems," *IEEE Trans. Antennas Propag.*, vol. 51, no. 8, pp. 1936–1940, Aug. 2003.

[59] A. Petosa, R. K. Mongia, A. Ittipiboon, and J. S. Wight, "Investigation of various feed structures for linear arrays of dielectric resonator antennas," *IEEE Antennas & Propagation Symposium Digest AP-S 1995*, pp. 1982–1985, 1995.

[60] M. Wyville, A. Petosa, and J. S. Weight, "Dig feed for dra arrays," *IEEE Antennas & Propagation Symposium Digest AP-S 2005*, vol. 2b, pp. 176–179, 2005.

[61] M. Aras, M. Rahim, Z. Rasin, and M. A. Aziz, "An array of dielectric resonator antenna for wireless application," *IEEE International RF and Microwave Conference Proceedings*, pp. 459– 463, Dec. 2008.

[62] A. Al-Zoubi, A. Kishk, and A. Glisson, "A linear rectangular dielectric resonator antenna array fed by dielectric image guide with low cross polarization," *IEEE Transactions on Antennas and Propagation*, vol. 58, pp. 697–705, Mar. 2010.

[63] R. Tian, V. Plicanic, B. K. Lau, and Z. Ying, "A compact six-port dielectric resonator antenna array: Mimo channel measurements and performance analysis," *IEEE Transactions on Antennas and Propagation*, vol. 58, pp. 1369–1379, Apr. 2010.

[64] G. Drossos, Z. Wu, and L. E. Davis, "Four-element planar arrays employing probe-fed cylindrical dielectric resonator antennas," *Microw.Opt. Technol. Lett.*, vol. 18, no. 5, pp. 315–319, 1998.

[65] E. Arnieri, L. Boccia, and G. Amendola, "Ka-band dual-frequency radiator for array applications," *IEEE Antennas and Wireless Propagation Letters*, vol. 8, pp. 894–897, 2009.

[66] T. Denidni and Q. Rao, "Design, analysis and measurement of a new dual-band compact hybrid resonator antenna," *Int J RF Microwave Comput Aided Eng.*, vol. 16, pp. 629–634, 2006.

[67] T. W. Li and J. S. Sun, "Dual-frequency dielectric resonator antenna with inverse t-shape parasitic strip," *IEEE International conference on wireless communications and Applied Computational Electromagnetics*, p. 384387, Apr. 2005.

[68] T. H. Chang and J. F. Kiang, "Dual-band split dielectric resonator antenna," *IEEE Trans. Antennas Propag*., vol. 55, no. 11, pp. 3155-3162, Nov. 2007.

[69] R. K. Chaudhary, K. V. Srivastava, and A. Biswas, "Wideband multi-layer multi-permittivity half-split cylindrical dielectric resonator an-tenna," *Microw. Opt. Technol. Lett.*, vol. 54, no. 11, pp. 2587–2590, Nov. 2012.

[70] P. V. Bijumon, S. K. Menon, M. N. Suma, M. T. Sebastian, and P. Mo-hanan, "Broadband cylindrical dielectric resonator antenna excited by a modified microstrip line," *Electron. Lett.*, vol. 41, no. 7, pp. 385–387, Mar. 2005.

[71] L. K. Hady, D. Kajfez, and A. A. Kishk, "Triple Mode Use of a Single Dielectric Resonator", *IEEE Transactions on Antennas and Propagation*, Vol. 57, pp. 1325-1335, May 2009.

[72] R. Chair, A. A. Kisk, and K. F. Lee, "Comparative study on different feeding techniques for dual polarized dielectric resonator antennas," *IEEE Antennas and Propagation Society Int. Symp*., Albuquerque, NM, USA, pp. 2495-2498, Jul. 2006.

Disseminations

Conference papers

1. A. Panigrahi, Y. Choukiker, S. K. Behera, R. Jyoti, "Square ring dielectric resonator antenna for wideband applications" *3rd International conference on computer communication and informatics,* (ICCCI'14), Coimbatore, 03-05 January 2014.
2. A. Panigrahi, S. K. Behera, "H-shaped slot coupled Dual-Polarized Dielectric Resonator Antenna for C-Band applications", *Global Conference on Communication Technologies,* (GCCT-15), Kanyakumari, 23-24 April 2015.
3. A. Panigrahi, S. K. Behera, "Dual-Linearly Polarized Dielectric Resonator Antenna Array for L and S band Applications", *International Conference on Microwave, Optical and Communication Engineering,* (ICMOCE-15), IIT Bhubaneswar, 18-20 December 2015.

Journal Papers

1. Ayaskanta Panigrahi and S. K. Behera, "High Isolation and Low Cross Polarization Dual-Polarized Dielectric Resonator Antenna for C-Band applications", *International Journal of RF and Microwave Computer Aided Engineering* (Communicated).

2. Ayaskanta Panigrahi, B. Dwivedy, S. K. Behera, "Design of a Dual Linearly Polarized Dielectric Resonator Antenna Array", *Journal of Electromagnetic Wave and Application* (Communicated).